



University of Kentucky
UKnowledge

University of Kentucky Doctoral Dissertations

Graduate School

2006

HIGH ORDER SHOCK CAPTURING SCHEMES FOR HYPERBOLIC CONSERVATION LAWS AND THE APPLICATION IN OPEN CHANNEL FLOWS

Chunfang Chen
University of Kentucky, cchen0@engr.uky.edu

[Right click to open a feedback form in a new tab to let us know how this document benefits you.](#)

Recommended Citation

Chen, Chunfang, "HIGH ORDER SHOCK CAPTURING SCHEMES FOR HYPERBOLIC CONSERVATION LAWS AND THE APPLICATION IN OPEN CHANNEL FLOWS" (2006). *University of Kentucky Doctoral Dissertations*. 314.
https://uknowledge.uky.edu/gradschool_diss/314

This Dissertation is brought to you for free and open access by the Graduate School at UKnowledge. It has been accepted for inclusion in University of Kentucky Doctoral Dissertations by an authorized administrator of UKnowledge. For more information, please contact UKnowledge@lsv.uky.edu.

ABSTRACT OF DISSERTATION

Chunfang Chen

The Graduate School

University of Kentucky

2006

HIGH ORDER SHOCK CAPTURING SCHEMES FOR HYPERBOLIC
CONSERVATION LAWS AND THE APPLICATION IN OPEN
CHANNEL FLOWS

ABSTRACT OF DISSERTATION

A dissertation submitted in partial fulfillment of the
requirements for the degree of Doctor of Philosophy in the
College of Engineering
at the University of Kentucky

By
Chunfang Chen

Lexington, Kentucky

Director: Dr. Scott A. Yost, Associate Professor of Civil Engineering

Lexington, Kentucky

2006

Copyright © Chunfang Chen 2006

ABSTRACT OF DISSERTATION

HIGH ORDER SHOCK CAPTURING SCHEMES FOR HYPERBOLIC CONSERVATION LAWS AND THE APPLICATION IN OPEN CHANNEL FLOWS

Many applications in engineering practice can be described by the hyperbolic partial differential equations (PDEs). Numerical modeling of this type of equations often involves large gradients or shocks, which makes it a challenging task for conventional numerical methods to accurately simulate such systems. Thus developing accurate and efficient shock capturing numerical schemes becomes important for the study of hyperbolic equations.

In this dissertation, a detailed study of the numerical methods for linear and nonlinear unsteady hyperbolic equations was carried out. A new finite difference shock capturing scheme of finite volume style was developed. This scheme is based on the high order Padé type compact central finite difference method with the weighted essentially non-oscillatory (WENO) reconstruction to eliminate non-physical oscillations near the discontinuities while maintain stable solution in the smooth areas. The unconditionally stable semi-implicit Crank-Nicolson (CN) scheme is used for time integration.

The theoretical development was conducted based on one-dimensional homogeneous scalar equation and system equations. Discussions were also extended to include source terms and to deal with problems of higher dimension. For the treatment of source terms, Strang splitting was used. For multi-dimensional equations, the δ -form Douglas-Gunn alternating direction implicit (ADI) method was employed. To compare the performance of the scheme with ENO type interpolation, the current numerical framework was also applied using ENO reconstruction.

The numerical schemes were tested on 1-D and 2-D benchmark problems, as well as published experimental results. The simulated results show the capability of the proposed scheme to resolve discontinuities while maintaining accuracy in smooth regions. Comparisons with the experimental results validate the method for dam break problems. It is concluded that the proposed scheme is a useful tool for solving hyperbolic equations in general, and from engineering application perspective it provides a new way of modeling open channel flows.

KEYWORDS: Essentially Non-Oscillatory Scheme, Weight Essentially Non-Oscillatory Scheme, Compact Scheme, Hyperbolic Conservation Laws, Shallow Water Equations

Chunfang Chen

05/26/2006

HIGH ORDER SHOCK CAPTURING SCHEMES FOR HYPERBOLIC
CONSERVATION LAWS AND THE APPLICATION IN OPEN
CHANNEL FLOWS

By

Chunfang Chen

Scott A. Yost

Director of Dissertation

Kamyar Mahboub

Director of Graduate Studies

05/26/2006

RULES FOR THE USE OF DISSERTATIONS

Unpublished dissertations submitted for the Doctor's degree and deposited in the University of Kentucky Library are as a rule open for inspection, but are to be used only with due regard to the rights of the authors. Bibliographical references may be noted, but quotations or summaries of parts may be published only with the permission of the author, and with the usual scholarly acknowledgments.

Extensive copying or publication of the dissertation in whole or in part also requires the consent of the Dean of the Graduate School of the University of Kentucky.

A library that borrows this dissertation for use by its patrons is expected to secure the signature of each user.

Name

Date

DISSERTATION

Chunfang Chen

The Graduate School

University of Kentucky

2006

HIGH ORDER SHOCK CAPTURING SCHEMES FOR HYPERBOLIC
CONSERVATION LAWS AND THE APPLICATION IN OPEN
CHANNEL FLOWS

DISSERTATION

A dissertation submitted in partial fulfillment of the
requirements for the degree of Doctor of Philosophy in the
College of Engineering
at the University of Kentucky

By
Chunfang Chen

Lexington, Kentucky

Director: Dr. Scott A. Yost, Associate Professor of Civil Engineering

Lexington, Kentucky

2006

Copyright © Chunfang Chen 2006

ACKNOWLEDGMENTS

I am grateful to my family, friends, colleagues and those who have provided encouragement and help throughout my study and pursue of the doctoral degree. Special thanks go to my advisor, Dr. Scott A. Yost, for his continuous support, insightful advice, and encouragement in the Ph.D program. I am also indebted to Dr. Seongjai Kim and Dr. George P. Huang for their valuable input into my research and this dissertation. Also I would express my sincere thanks to Dr. Tate Tsang, Dr. Lindell Ormsbee, Dr. Srinivasa Lingireddy, and Dr. James Fox for their continuous service on the advisory committee. I also thank Dr. J. D. Jacob for his comments on the dissertation. The support from the Department of Civil Engineering at the University of Kentucky is also greatly acknowledged. Finally, I want to thank my husband, Xiaodong Lian, without whom, I could not have accomplished this endeavor.

TABLE OF CONTENTS

Acknowledgements	iii
List of Tables	vii
List of Figures	viii
Chapter 1. Introduction	1
1.1 Background.....	1
1.2 Related Work	2
1.3 Organization of Dissertation.....	6
Chapter 2. Literature Review - Shock Capturing Methods	8
2.1 Shock Capturing Methods.....	9
2.2 High Resolution Schemes.....	13
2.3 ENO and WENO Schemes	16
2.4 Compact Scheme	17
2.5 Time Discretization Method	19
2.6 Shock Capturing Schemes for Shallow Water Equations.....	20
Chapter 3. Hyperbolic Conservation Laws and Shallow Water Equations	22
3.1 Hyperbolic Conservation Laws.....	22
3.2 Discontinuous Solution.....	24
3.3 Riemann Problem.....	25
3.4 Godunov Scheme	29
3.5 Hyperbolic Scalar Equation	30
3.6 Hyperbolic System Equations.....	31
3.6.1 System Characteristics	31
3.6.2 Solution Structure	33

3.6.3 Approximate Riemann Solver.....	35
3.7 Shallow Water Equations.....	38
3.7.1 Governing Equation.....	38
3.7.2 Characteristic Speeds.....	40
3.7.3 Roe’s Approximate Riemann Solver for Shallow Water Equations.....	41
Chapter 4. High Resolution Numerical Scheme	45
4.1 High Order Reconstruction.....	45
4.1.1 ENO Scheme.....	46
4.1.2 WENO Scheme.....	50
4.1.3 ENO/WENO Scheme for Hyperbolic System Equations.....	54
4.2 Compact Finite Difference Scheme.....	55
4.3 Boundary Conditions.....	57
4.4 Time Discretization.....	58
Chapter 5. Numerical Results of One-dimensional Homogeneous Problems.....	60
5.1 Linear Scalar Case – Convection Equation.....	60
5.2 Non-linear Scalar Case – Burger’s Equation.....	65
5.3 Hyperbolic System Equations – Homogeneous Shallow Water Equations.....	68
5.3.1 One-dimensional Horizontal Case – Wet Bed.....	68
5.3.2 One-dimensional Horizontal Case – Dry Bed.....	71
5.4 Dam Break Experiment.....	73
Chapter 6. Numerical Schemes for Non-homogeneous System Equations and Two-dimension Extension	76
6.1 Source Terms Treatment.....	76
6.1.1 Strang Splitting.....	77
6.2 Alternating Direction Implicit (ADI) Scheme.....	79
6.2.1 Douglas-Gunn ADI.....	79
6.2.2 Douglas-Gunn ADI for 2-D Homogeneous Hyperbolic Equations.....	81
6.2.3 δ -form Douglas-Gunn ADI.....	83

6.3 Two-dimensional Shallow Water Equations Extension	84
6.3.1 Characteristics of 2-D Shallow Water Equations	84
6.3.2 Implementation of the Approximate Riemann Solver	86
Chapter7. Numerical Results of Non-homogeneous Problems and Two- dimension Extension	88
7.1 One-dimensional Shallow Water Equations with Source Terms.....	88
7.2 Two-dimensional Linear Scalar Case – Gaussian Profile.....	92
7.3 Two-dimensional Nonlinear Scalar Case – Burger’s Equation	96
7.4 Two-dimensional Dam Break – Wet Bed, Frictional	98
7.5 Two-dimensional Dam Break Experiment	104
Chapter 8. Conclusions and Future Work	109
Appendices	113
Appendix A: Some Flux Schemes and High Resolution Methods	113
Appendix B: Fourth Order WENO Scheme	117
Appendix C: Optimal Weights for WENO Scheme	119
References	120
Vita.....	131

LIST OF TABLES

Table 5-1. Convergence test – 1-D linear advection equation.....	62
Table 5-2. Convergence test – 1-D Burger’s equation	67
Table 5-3. Convergence test – 1-D homogeneous shallow water equations (wet bed, frictionless).....	71
Table 7-1. Convergence test – 1-D non-homogeneous shallow water equations (wet bed, frictional).....	91
Table 7-2. Convergence test – 1-D non-homogeneous shallow water equations (dry bed, frictional).....	92
Table 7-3. Convergence test – 2-D non-homogeneous shallow water equations (wet bed, frictional).....	103
Table 7-4. Location of stage gauges	104

LIST OF FIGURES

Figure 3-1. Illustration of the initial data for the Riemann problem.....	25
Figure 3-2. Characteristics of shock wave.....	26
Figure 3-3. Characteristics of rarefaction wave.....	27
Figure 3-4. Characteristics of contact discontinuity.....	27
Figure 3-5. Characteristic of two waves.....	34
Figure 3-6. Characteristic of nonlinear waves.....	34
Figure 3-7. Wave structure of shallow water equations.....	40
Figure 4-1. Stencil candidates of interpolation polynomial of fourth order reconstruction.....	48
Figure 5-1. Linear advection equation.....	61
Figure 5-2 (a). Linear hyperbolic scalar equation – case 1.....	64
Figure 5-2 (b). Linear hyperbolic scalar equation – case 2.....	64
Figure 5-3. 1-D Burger’s equation - initial condition.....	66
Figure 5-4. Nonlinear scalar case – 1-D Burger’s equation.....	66
Figure 5-5. 1-D dam break – water depth profile (wet bed, frictionless).....	69
Figure 5-6. 1-D dam break – water depth profile (dry bed, frictionless).....	72
Figure 5-7. Comparison of 1-D dam break solutions for a WES experiment, $x=70.1m$	74
Figure 5-8. Comparison of 1-D dam break solutions for a WES experiment, $x=85.4m$	74
Figure 7-1. 1-D dam break – water depth profile (wet bed, frictional).....	89
Figure 7-2. 1-D dam break – water depth profile (dry bed, frictional).....	90
Figure 7-3. Gaussian rotation - initial profile.....	94
Figure 7-4. Gaussian profile after one cycle of rotation – ENO-Padé.....	94
Figure 7-5. Gaussian profile after one cycle of rotation – WENO-Padé.....	95
Figure 7-6. Comparison of the plane at $x=14.6$ with the exact solution.....	95
Figure 7-7. 2-D Burger’s equation – ENO-Padé.....	97
Figure 7-8. 2-D Burger’s equation – WENO-Padé.....	97
Figure 7-9. 2-D Burger’s equation plane comparison at $x=0$	98

Figure 7-10. Water depth of 2-D dam break – ENO-Padé (wet bed, frictional)	100
Figure 7-11. Water depth of 2-D dam break – WENO-Padé (wet bed, frictional).....	100
Figure 7-12. Velocity contour of 2-D dam break – WENO-Padé (wet bed, frictional).....	101
Figure 7-13. 2-D dam break – water depth profile comparison of the central line (wet bed, frictional).....	102
Figure 7-14. 2-D dam break experiment – plane view of the domain and location of stage gauges	105
Figure 7-15. Comparison of stage hydrograph at gauge -5A.....	106
Figure 7-16. Comparison of stage hydrographs at gauge C.....	106
Figure 7-17. Comparison of stage hydrographs at gauge 4	107
Figure 7-18. Comparison of stage hydrographs at gauge 0	107
Figure 7-19. Comparison of stage hydrographs at gauge 8A	108

Notations

a, b, c, α, β	parameters for Padé scheme
a_w	wave velocity
A	Jacobian matrix
\tilde{A}	approximate Jacobian matrix
c	celerity
E	flux vector in y -direction
f	scalar flux
F	flux vector in x -direction
g	acceleration due to gravity
G	homogeneity satisfying matrix
h	water depth
l	left state
N	number of grids
q	scalar conservative variable
Q	vector of conservative variables
r	right state
R	right eigenmatrix
R^{-1}	inverse right eigenmatrix
s	speed of discontinuity
S	source or sink term
S_{fx}	bottom friction in x -direction
S_{fy}	bottom friction in y -direction
t	time variable
T	time length of integration
u	depth averaged velocity in x -direction
v	depth averaged velocity in y -direction
z	vertical level
Z_x	bed slope in x -direction

Z_y	bed slope in y -direction
λ	eigenvalue
Λ	diagonal matrix consisting of the eigenvalues
α_i, ω_i	nonlinear weights of WENO scheme
β_i	smoothness indicator of WENO interpolation stencil
γ_i	linear weights of WENO scheme
Δx	grid spacing in x -direction
Δy	grid spacing in y -direction
Δt	grid spacing in time

Abbreviations

ADI	Alternating Direction Implicit
CFL	Courant-Friedrichs-Levy condition
CN	Crank-Nicolson method
DG	Discontinuous Galerkin method
ENO	Essentially Non-Oscillatory
FCT	Flux Corrected Transport
FEM	Finite Element Method
FVM	Finite Volume Method
MUSCL	Monotone Upstream-centered Schemes for Conservation Laws
PDE	Partial Differential Equation
RANS	Reynolds-Averaged Navier-Stokes equations
RD	Residual Distribution method
RKDG	Runge-Kutta Discontinuous Galerkin method
SWE	Shallow Water Equations
TV	Total Variation
TVD	Total Variation Diminishing
WENO	Weighted Essentially Non-Oscillatory

Chapter 1

Introduction

1.1 Background

As more water resources projects are appearing in engineering practice such as flood control, sediment management in rivers and lakes, water quality monitoring, and coastal circulation modeling, etc., the study of free surface flow is receiving increasing attention. Mathematical modeling of rivers and estuaries is an essential part in carrying out those projects as it provides a predictive tool in evaluating the effectiveness of those projects. Since modeling such systems usually involves large temporal and spatial scales, generally, numerical techniques have to be relied on for solutions.

Many real-life problems in hydraulic engineering involve flows that change abruptly with time. A typical example is the dam break problem. The failures of dams or levees have occurred in many parts of the world and can be disastrous in terms of damages to human lives and properties. As the occurrence of such event is devastating, it is of significance to accurately predict the consequences of such phenomena. Considering the failure of a dam, people are usually concern about the magnitude of the resultant waves, the speed of the wave front, and the amount of water that will be flooded to the nearby plains. Accurate prediction of the spatial and temporal evolution of the flood after a dam failure is crucial in hydraulic structure design and important for practitioners in making

decisions as to what measures can be taken against such event. In addition, accurate forecast of flood consequences can help the administrations to assess public safety and provide accurate damage estimation.

1.2 Related Work

In modeling rivers and open channel flows, the well known non-hydrostatic, three-dimensional incompressible Navier-Stokes equations are often used. The merit of this model is that it can predict flows at realistic Reynolds numbers in complex geometries. However, although being physically based, the Navier-Stokes equations are difficult to solve problems with large spatial and temporal scales due to the high computation cost. Therefore people introduced certain simplifications to this system. By averaging the flows over time, one obtains the so called Reynolds-Averaged Navier-Stokes equations (RANS), whereby the effects of turbulence are related to the mean flow. The RANS model has been widely used in fluid simulations, but it is still computationally demanding. Sometimes in the situations where the flow has a far larger scale in the longitudinal direction than that in the vertical direction, the component of momentum in the vertical direction is negligible. Therefore, by integration over depth, the Navier-Stokes equation can be simplified to two-dimensional shallow water equations. This model adequately describes the hydrodynamics of a river or a channel where the water depth is relatively low compared to the scales in the longitudinal directions. Mathematically, the shallow water equations are time-dependent, nonlinear partial differential equations (PDEs) of hyperbolic type. This type of equations also arise in many other engineering models such

as the Euler equation of aerodynamics, the Hamilton-Jacobi equation of electronics and the Maxwell equations of electromagnetic fields.

It is well known that the hyperbolic system accepts both smooth as well as discontinuous solutions. A discontinuous solution, also referred to as shock, is characterized by large gradients in the solution quantities such as velocity, density, depth or pressure. Even with smooth initial conditions, discontinuities may develop within finite time. In solving hyperbolic equations with the presence of discontinuities, traditional numerical methods usually yield large errors by either generating nonphysical oscillations or producing numerical diffusions [52]. Hence there is high motivation to develop shock capturing methods.

In the past few decades, a large number of shock capturing schemes of first or second order have been proposed [12, 32, 36, 39, 84]. Recently, increasing research efforts have focused on developing high order numerical methods for shocks. Those high order methods are attractive to problems with long computational time or with high order accuracy requirement. Although such schemes slightly increase the computational complexity, they can achieve comparable results with a coarser spatial resolution. Among those, one class of the methods is the high order essentially non-oscillatory (ENO) scheme [38] and the weighted essentially non-oscillatory (WENO) scheme [57]. Both schemes have demonstrated very promising shock capturing capabilities. Because they can achieve user defined high order accuracy while avoid spurious oscillations, these schemes have been widely used for shock capturing. However, drawback still exists with these schemes that waves of small amplitude might be damped. On the other hand, the

compact schemes, a family of high order schemes, are known to be able to capture weak turbulence and aero acoustic waves [22]. However, when it is applied to problems containing discontinuities, non-physical oscillations may be generated. Based on those facts, the attempt of using a hybrid of ENO/WENO algorithm with the compact scheme seem to provide a way by which shock-turbulence interactions can be efficiently computed since such a scheme combines the advantages of high order compact scheme that can give good approximations for smooth regions and the ENO/WENO scheme that can well represent large gradients near discontinuities.

The idea of hybrid scheme was proposed by Adams *et al.* [4] and adopted by Wang [87], in which coupling of the compact scheme and the ENO scheme was carried out by pre-computing the node-based flux derivatives using the ENO scheme. Those algorithms have been successfully applied to the direct numerical simulation (DNS) of a turbulent compression ramp flow [3] and the simulation of compressible and incompressible flows in aerodynamics [87]. Similar ideas but with different approaches, usually involving the switch between one sub-scheme to another, are also proposed [20, 21, 48]. A recent paper by Pirozzoli [61] employed the hybrid compact-WENO scheme, which used the explicit formulation for the approximation of fluxes. To the best knowledge of the author, no research has been reported following a hybrid idea of using compact scheme with WENO type interpolation for implicit point-wise derivative evaluations Hence, it will be a valuable practice to develop a new hybrid scheme based on compact scheme with WENO reconstruction for flux derivatives using implicit method.

Besides the desire to develop a new hybrid scheme, there are also some other concerns that motivate the current research. First, of those hybrid schemes developed, most use flux splitting method, by which the numerical flux functions are evaluated in a component by component manner. Although this approach is quite simple and efficient, its resolution power is not as good as the characteristic decomposition approach, and it can cause excessive smearing of the shear waves [65]. In this work, a characteristic based approach is used, which couples the Roe type approximate Riemann solver to solve system of conservation laws. This method is expected to provide an efficient approach for solving hyperbolic equation, especially the system equations. Secondly, although the hybrid idea has been applied in aerodynamic applications and simulations successfully, it is still new to hydraulic engineering fields. Therefore, introducing and exploring such algorithm is expected to contribute by providing a new tool for modeling rivers and open channel flows. Furthermore, since the ENO scheme and the WENO scheme are being increasingly recognized and used, comparison of the performances of these two schemes in the context of hybrid schemes would be a valuable practice in a comparative evaluation of schemes.

In this dissertation, the behavior of linear and nonlinear hyperbolic equations are investigated, with the focus given on deriving a better high order shock capturing scheme with a WENO-type interpolation for point-wise derivatives based on the characteristic approach. The new compact-WENO scheme, together with the compact-ENO scheme, will be applied to a number of benchmark test problems, particularly for modeling open channel flows. It is expected that this method will provide a new approach for solving

hyperbolic equations, in general, and make an efficient tool for hydraulic engineering simulations.

1.3 Organization of Dissertation

Two schemes are studied in this dissertation, namely the ENO-*Padé* scheme and the WENO-*Padé* scheme. Theoretical background of numerical wave modeling under the condition of abrupt change in the flow condition is provided. The core part of the presentation is devoted to scheme development and implementations. To evaluate the performance, numerical experiments are conducted and the simulated results are presented.

The dissertation is organized as follows. Chapter 2 presents a literature review of the numerical techniques for hyperbolic conservation laws. Numerical difficulties with the traditional numerical methods are discussed. The state-of-the-art shock capturing numerical methods are introduced. Then a survey on the applications of shock capturing schemes for shallow water equations is given. Chapter 3 presents the theory of hyperbolic conservation laws, including the relevance of the Rankine-Hugoniot discontinuous condition and the Riemann problem. The focus is given on the well known Godunov scheme with Roe type approximate Riemann solver. Then, the shallow water equations are introduced, with the general characteristic approach for solutions outlined. In Chapter 4, the complete numerical scheme is formulated, including a detailed discussion of the semi-implicit time discretization method. The implementation of two types of boundary conditions is provided. Chapter 5 contains the numerical experiments on a number of

one-dimensional benchmark test cases. For each case, details of model setup are given. The results of the ENO-Padé and the WENO-Padé scheme are compared against the available analytical solutions to disclose their predictive capabilities. Those schemes are also quantitatively evaluated through the error analysis and convergence test. Model validations are carried out by running a field simulation and comparing with the measured data. In Chapter 6, the algorithm is extended to include source terms and to deal with two-dimensional problems. Operator splitting technique and the δ -form Douglas-Gunn Alternating Direction Implicit (ADI) algorithm [24] are used for such extensions. Chapter 7 presents the numerical experiments for the extensions given in Chapter 6 on non-homogeneous and two-dimensional hyperbolic equations. Experiment details are given and the results comparisons and discussions are also provided. In Chapter 8, a summary of the present work is provided. Conclusions are formulated with an outlook for future research described.

Chapter 2

Literature Review - Shock Capturing Methods

The general one-dimensional hyperbolic equation, also known as hyperbolic conservation laws, can be written as:

$$\frac{\partial Q}{\partial t} + \frac{\partial F}{\partial x} = 0 \quad (2.1)$$

where Q is the vector of conservative variables to be advected and F is the flux vector, which is usually a function of Q . If the vector consists of a single conservative variable q , then Eq. 2.1 becomes a scalar hyperbolic equation denoted by

$$\frac{\partial q}{\partial t} + \frac{\partial f}{\partial x} = 0 \quad (2.2)$$

where f is the scalar flux corresponding to the variable q .

As mentioned in Chapter 1, the above type of PDEs may involve shocks in the solutions, which usually can not be captured by traditional finite difference methods. Therefore, much research effort has been made in developing special numerical techniques to deal with shocks. Such shock capturing methods have the property of tracking the discontinuities while maintaining the accuracy and stability in smooth regions. In this chapter, a literature review is carried out on classical and recent shock capturing methods for hyperbolic equations. Then focus is given on a review of the high order schemes including the ENO scheme, the WENO scheme, and the compact Padé

scheme. Finally an overview of the shock capturing methods for shallow water equations is provided.

2.1 Shock Capturing Methods

Due to the numerical challenges posed by the presence of shocks or discontinuities in the solution of hyperbolic equations with a general form given in Eq. 2.1, research have been conducted on developing numerical methods that can track discontinuities without significant oscillations as well as can provide accurate approximation to smooth areas. In the past few decades, a number of shock-capturing methods have been developed for solving hyperbolic conservation laws.

Traditional shock capturing schemes use first or second order finite difference methods. Among the first order schemes, an important family is the upwind methods. In such methods, the spatial derivatives are discretized in a way that is consistent with the direction of the wave propagation, thus this class of method is more physically sound. The most popular upwind scheme is the Godunov scheme [27]. In this method, the solution is represented by a series of piecewise constant states, which provides a close representation of the true solution near discontinuities. The solution of this method is evolved from considering the nonlinear interaction between piecewise constants, which, if viewed individually, constitutes a problem called Riemann problem. To solve the Riemann problem, different approaches, either exact [32] or approximate [25, 37, 66, 74, 78] have been proposed. Due to the high computational cost of the exact solver, most numerical methods use approximate solvers. In those methods, solution to the Riemann

problem is based on the characteristics of the Jacobian matrix of the system. Among those, the Osher scheme [25] determines the direction of the flux by choosing the sign of the eigenvalues. The Roe scheme [74], also referred to as flux difference splitting scheme, approximates the Jacobian matrix using an average of the state variables calculated from either side of the Riemann interfacial values. The HLL scheme [37], unlike the other Riemann solvers, considers only the left and the right characteristics and expresses the middle region in terms of the interfacial values. The HLLC flux scheme [78], an improved variant of the HLL flux, contains the middle (contact) wave in the Riemann problem solution. In the flux vector splitting approach [74], the flux is split into two parts with the upwind direction automatically determined based on the sign of the flux. Among those methods discussed above, the Roe scheme is the most widely used approach as a shock capturing operator. So it is selected in this work for the calculation of fluxes. Details of this method, and the related Godunov scheme, are presented in Chapter 3.

The upwind schemes, even though being robust and stable in solving discontinuities, are only first order accurate, also strong diffusion can cause significant smearing in the solutions. Additionally, if the conservation laws are nonlinear, the waves contain components that propagate in either direction. In such situation, the direction has to be identified a priori, which makes the numerical methods become more complex. However, because of its obvious advantages, this type of methods has been widely used, and later improvements have lead to many high resolution schemes. The improved schemes either employ higher order interpolation functions or they post-process the Riemann solutions before averaging to find the updated solution.

Besides the first order methods, there is a class of second order methods, such as the Lax-Wendroff scheme [50], the Beam Warming scheme [8], and the McCormack scheme [91]. Those second order schemes do not require the explicit knowledge of the characteristic of the system, and have the advantage of being non-dissipative. However, they are prone to generating spurious oscillations across discontinuities in the solutions [53, 92]. It is known that the conventional finite difference methods of second order accuracy based on fixed stencil interpolation always introduce spurious oscillations in the vicinity of large gradients. If the numerical oscillations are too large, then the numerical scheme becomes insufficient to resolve the solutions.

Usually, the finite difference method requires structured (mostly Cartesian or Non-Cartesian via a coordinate transformation) grids, which make it inflexible to be applied to irregular domains. Whereas, the finite volume method (FVM), which is based on the integration of the governing equation over non-overlapping cells, has the advantage over the finite difference method that it has the flexibility to be applied to both structured and unstructured meshes of any geometrical shape of elementary cells for space discretization. Another advantage of FVM consists in the guarantee of conservation of physical properties by the integral formulation. As the FVM method is becoming a widely used modeling strategy, the number of papers describing this method is large [35, 44, 54, 55, 63]. The finite volume method is usually cast in staggered grid formulations on which shock capturing methods can be designed by solving a series of one dimensional Riemann problems on the boundary of each cell. Using FVM, evaluation of the numerical flux functions at the edge of each cell is required to update the cell averages. This can be achieved by extracting information on point values from the cell averages, for which high

order approximations can be used. The drawback of FVM is found in applications that require an accuracy of higher than second order. In addition, FVM space discretizations are not suited for the construction of implicit methods because the computation of the average of the source couples the cells and makes an implicit treatment of the source less efficient [62]. Since the finite volume and the finite difference methods are equivalent in 1-D, often, depending on the type of discretization and grid used, they are applied mixed [86], whereby the conservative variables are stored at the nodes of the mesh, while the fluxes are stored at the center of the control volume. Considering such attractive features, in this work a finite volume style high order finite difference numerical method is used.

Besides the finite difference and the finite volume methods, shock capturing methods also includes the finite element approach. A popular one is the Discontinuous Galerkin (DG) Finite Element Method (FVM) [15, 64], in which a higher order piecewise continuous polynomial representation is used in a weighted residual finite element approach. Cockburn and Shu [17] introduced the first Runge-Kutta DG (RKDG) method, which uses an explicit Total Variation Diminishing (TVD) second-order Runge-Kutta discretization and modifies the slope limiter to maintain the formal accuracy of the scheme at the extrema. Another approach is the Residual Distribution method (RD) [1, 2, 19], which allows upwinding by using a continuous, eventually high order, finite element representation. Although more physically based, the finite element methods are computationally expensive in nature, thus are not suitable for a lot of simulations involving large temporal and spatial scales.

2.2 High Resolution Schemes

In the past several decades, attempts to devise numerical methods that can accurately capture shocks have led to the development of many high resolution schemes. “High resolution methods” refers to the method that is at least second order accurate on smooth solutions and non-oscillatory at discontinuities [52].

In order to develop a numerical method of higher order, non-oscillatory, and capable of capturing shocks, it is necessary to introduce a definition for oscillation. Generally a measure of oscillation is the total variation (TV) given by

$$TV(Q^n) = \sum_{i=-\infty}^{\infty} |Q_i^n - Q_{i-1}^n| \quad (2.3)$$

Here TV is the summation of the variation between two consecutive points for all the points in the domain, Q_i^n is the approximated value of point i at time level n . It is easy to see from Eq. 2.3 that oscillations in the computed result will increase the total variation. Any numerical scheme for which the total variation of the solution decreases with time is called Total Variation Diminishing (TVD) scheme. Therefore, if a scheme is TVD, it implies that $TV(Q^n) \leq TV(Q^{n+1})$ is satisfied, and thus oscillations are avoided.

The feature of the TVD requirement makes it possible to derive higher-order accurate methods. Many high order schemes have been proposed based on this principle, among which, a common one is to add artificial diffusion. In this approach, the artificial diffusion is tuned to introduce enough dissipation near discontinuities but made small enough to be negligible in smooth regions. An example of artificial diffusion method is

the McCormack scheme, in which numerical viscosity is added to reduce the oscillations [28]. However, the difficulty with this approach is that it is hard to determine the amount of dissipation needed without causing unnecessary smearing.

For this reason, the high-resolution methods developed more recently have used more direct approaches to impose the nonoscillatory requirement. One approach is to use limiters to the flux. The flux limiter works by imposing constraint to the gradient of the flux function. Such approach is developed to overcome the drawback of those high order methods that are accurate in smooth regions but behave poorly near discontinuities. The idea behind this approach is to combine high order flux with low order flux via the limiter such that high order scheme is used in smooth regions, while switching to low order method near discontinuities. Using non-linear limiters during the estimation of conserved quantities at the cell interface, the oscillations that would have led to a local extreme could be suppressed. Depending on how to select the limiter, different methods are obtained. One of the earliest attempts is the Flux Corrected Transport (FCT) scheme of Boris and Book [12]. It stems from the upwind method but is modified to create a higher order scheme in smooth regions, which then is reduced to a more robust first order algorithm near discontinuities by adding some anti-diffusion flux. The FCT scheme, although being high order in smooth area, gives artificial diffusion at region with large gradient, and is basically of first order accuracy in that location. Yee [94] extended the FCT scheme where the TVD property is maintained at discontinuities while second order accuracy is achieved in smooth regions. Different choices of limiters include the Superbee limiter of Roe [67], a smoother limiter by van Leer [83], the Woodward limiter [18], the Minmod limiter [18], and the Monotone Upstream-centered Schemes for

Conservation Laws (MUSCL) of van Leer [18], etc. Among them, the MUSCL scheme is the most widely applied. It uses a linear reconstruction to process the Riemann solutions to achieve second order accuracy. However, the slope of the piecewise linear distribution is limited [91], thus unless smooth interpolation is used near discontinuities, oscillation will be introduced. Details of the above limiters are given in Appendix A.

The above discussed schemes, although capable of suppressing spurious oscillations, in some cases, may result in diffusion due to the over-suppressing. Although TVD conditions have been applied in many schemes, they are known to degenerate to first order accuracy at local maximum and minimum points. Additionally, the process by which the low order and high order methods are combined owes little to the nonlinear processes associated with real flow discontinuities. Therefore the numerical solution can often exhibit unphysical behavior [56].

To remedy such problems and to produce globally higher-order accuracy, Harten and Osher [39] developed the essentially non-oscillatory (ENO) scheme which allows the loss of the amplitude at one time step to be gained at another [38]. Later, Liu and Osher [57] proposed the weighted essentially non-oscillatory (WENO) scheme for improvement. ENO/WENO spatial operator is able to achieve user defined order of accuracy in smooth regions with monotone shock transition. The major advantages with these schemes include no oscillation raised near large gradients and ease in higher-order extensions. Of these two schemes, the ENO scheme has been widely applied to solve hyperbolic equations; while the WENO scheme, although not as popular, is gaining increasing attention. Literature survey shows that comparison of the performances of these two

schemes has been rarely reported. Therefore, it is well worth to explore the evaluation and comparison of these two schemes to get a better understanding of their applicability and effectiveness in solving hyperbolic equations.

2.3 ENO and WENO Schemes

The ENO scheme was initially proposed by Harten *et al.* [39] in the finite volume framework, in which the cell reconstructions are approximated by a high order essentially non-oscillatory interpolation of a cell average function. The basic idea of this method is that by shifting among all candidates, a “smoothest” stencil can be selected that yields non-oscillatory behavior with uniformly high order accuracy. In the original finite volume formulation, nonlinear reconstruction of the point values is computed from the cell-average that serves to compute the numerical fluxes. Such formulations are effective for one-dimensional problems but become fairly expensive while extending to higher dimensions because of the complexities in computing point values from cell-averaged solutions. To overcome this difficulty, Shu and Osher [73] proposed the finite difference ENO method. By this method, the computation of numerical fluxes can be performed in a dimension splitting fashion. In contrast to the piecewise linear cell reconstruction, which are second order accuracy at most, the ENO scheme can construct a polynomial that is accurate to a higher order.

The WENO scheme was propose by Liu and Osher [57], in which they pointed out that the ENO interpolation of choosing the smoothest stencil overshoots the smooth regions. The first WENO scheme is constructed based on the finite volume ENO scheme

by taking a convex combination of the ENO approximation candidates with properly chosen weights. Later, Jiang and Shu [47] employed the finite difference approach and constructed the improved third and fifth order WENO scheme. They also outlined a general framework for the design of the smoothness indicators and nonlinear weights.

Both the ENO and the WENO schemes are built upon the idea of adaptive stencils in the reconstruction procedure, and can automatically achieve high-order accuracy and non-oscillatory property near discontinuities by making adjustments according to local smoothness. These two schemes have demonstrated very good shock-capturing capabilities. However, they are usually not optimal for computing turbulent flows or for aero acoustics applications because they exhibit poor resolution qualities in high field gradient [87] compared to the linear compact schemes. Attempts to improve the properties include the work of Wang [88] and Weirs *et al.* [90], in which the requirement for the formal order of accuracy of the scheme to achieve better resolution properties at high frequencies is relaxed.

2.4 Compact Scheme

The compact schemes are a family of central type finite difference methods that involve two or three grid points and treat the function and its derivatives as unknowns at the grid nodes. The basic idea of those schemes is to optimize the coefficients of the compact scheme to improve their resolution properties in order to resolve with high accuracy waves whose wavelength is small with respect to the computational grid.

Generally the central methods do not explicitly require the provision of wave propagation information, and thus are easy to understand and implement. Among the central compact schemes, the Padé scheme is a family of high order implicit schemes. It is inherently non-dissipative and is more accurate compared to the explicit schemes. Lele [51] introduced a series of higher-order compact schemes that are the generalization of the Padé scheme. It gives the freedom in choosing mesh geometry, and offers a computationally efficient finite difference form by solving tridiagonal matrix as apposed to the more complex coefficient matrix resulted from other methods. These useful features make it particularly applicable for the simulation of waves with high frequency. Like the other compact schemes, the Padé scheme is accurate in smooth regions with spectral-like resolution, but has been found to cause oscillations when applied directly to flow with discontinuities. To suppress the spurious oscillation and the nonlinear instability, Cockburn and Shu [16] developed the nonlinearly stable compact schemes for shock calculations, which used a limiter to stabilize the compact scheme. In the work of Tolstykh [77] and Zhuang [100], upwind compact scheme was used for which careful design is needed to introduce the appropriate amount of dissipation.

It is recognized from the above discussion that the compact scheme and the shock capturing ENO/WENO scheme have mutual advantages and deficiencies. Thus they naturally give rise to an alternative that combines these two ideas to form a hybrid scheme. In such hybrid scheme, the non-oscillatory reconstruction is employed to prevent oscillations from the discontinuity regions and the compact scheme is used to provide numerical accuracy in the smooth areas outside the shocks. Adams and Shariff [4]

proposed the hybrid compact-ENO scheme, which couples a non-conservative compact upwind scheme with a shock-capturing ENO scheme that is turned on only around discontinuities. Deng and Maekawa [20] developed nonlinear compact schemes based on an adaptive mechanism of selection among different compact stencils and the interpolation is carried out based on the smoothness properties of the function. Pirozzoli [61] derived a hybrid compact-WENO scheme in which a conservative compact scheme is coupled with the WENO scheme. Ren [65] later improved Pirozzoli's work by using the weighted average of two sub-schemes based on characteristic decomposition. Wang [87] combined the Padé compact finite difference scheme with the ENO interpolation for solving compressible and incompressible Navier-Stokes equations. Being successfully applied in aerodynamic modeling, this hybrid scheme has not appeared in other engineering fields, especially, the hydraulic engineering applications. So it is valuable to introduce this model to a wider spectrum of real world applications. Also, investigation of hybrid schemes composing high order compact differencing with the ENO/WENO interpolation would be a significant contribution to the study of hyperbolic equations. In this research, a new scheme based on the hybrid idea is developed which uses the WENO scheme with compact finite difference scheme to solve hyperbolic equations.

2.5 Time Discretization Method

Time integration methods make vast use of explicit methods, mostly two step predictor-corrector or Runge-Kutta, and are common place. However, a well known limitation with the explicit schemes is the restriction to small time step governed by the Courant-Friedrichs-Levy (CFL) condition to maintain stabilities. Usually the CFL

condition is more stringent than what is needed for time accuracy. The Crank-Nicolson (CN) method, a semi-implicit time evolution scheme, on the other hand, is known to be unconditionally stable and allows for larger temporal integration step. But due to its high programming complexity, this method has not become popular in high resolution schemes to solve hyperbolic equations, especially the system equations. With its obvious advantage, this dissertation uses the CN scheme as the time integration method.

2.6 Shock Capturing Schemes for Shallow Water Equations

Since the primary application of this work is to resolve open channel flow problems by solving the shallow water equations, it is necessary to conduct a literature survey of the shock capturing numerical methods for solving this particular class of PDEs.

Fennema and Chaudhry [28], Yost [97] applied the FCT scheme to open channel flows. Fair results were obtained but with quite bit of dissipation. Nujic [59], Yang [93] and Yost [96] used the ENO scheme for solving one-dimensional dam break problem. Zoppou and Roberts [102] used second-order approximate Riemann weighted average flux scheme with a van Leer type limiter to solve dam break problems. Cao [14] used the weighted average flux method in conjunction with the HLLC approximate Riemann solver and the Superbee limiter to study dam-break hydraulics over an erodible sediment bed.

Besides one-dimensional applications, the 2-D shallow water equations have also been investigated by researchers. Zhao *et al.* [98] reported the implementation of an

approximate Riemann solver with the Osher scheme in finite volume, and later extended that work by including flux-vector splitting and flux difference splitting [99]. Tseng [81] used a class of Roe, TVD and ENO scheme to simulate two-dimensional rapidly varied open channel flow. His results demonstrated that these schemes are accurate, robust and highly stable even in flows with strong gradients. Sanders [69] proposed a Godunov-type finite volume scheme to achieve a nonoscillatory and second-order accurate solution. Jha, Akiyama, and Ura [45] used first-order accurate Roe's numerical flux with Harten and Hyman's entropy condition and a second-order accurate Lax-Wendroff scheme to solve two-dimensional flood flows. Gottardi and Venutelli [33] used second order central-type scheme in a three-step Runge-Kutta time stepping scheme for two-dimensional shallow water flows. In this scheme, the reconstruction is performed in the middle cell such that no approximate Riemann solver is needed. Wang, He and Ni [85] used TVD scheme with an optimum-selected limiter to evaluate the flux at element interfaces and utilized a two-step Runge-Kutta method for integration of the conservative shallow water equations on arbitrary quadrilateral meshes. Schwanenberg and Harms [70] used Runge-Kutta discontinuous Galerkin finite-element method to solve 2-D shallow water equations.

In this dissertation, the proposed numerical schemes are investigated for solving 1-D and 2-D shallow water equations. For 2-D equations, the operator splitting techniques and the treatment of source terms are thoroughly studied. Then the Crank Nicolson-ADI method with improved order of accuracy is discussed. Finally, the schemes are tested for the ideal and benchmark 1-D and 2-D dam break problems.

Chapter 3

Hyperbolic Conservation Laws and Shallow

Water Equations

In this chapter hyperbolic conservation laws and the commonly used numerical methods for this type of PDEs are discussed. The presentation begins with discontinuous solution and associated properties, followed by the definition of Riemann problem and an outline of its solution procedure. Then the Godunov scheme is presented for scalar and system hyperbolic equations. Finally the shallow water equations are introduced in this chapter.

3.1 Hyperbolic Conservation Laws

Considering the hyperbolic equations given by Eq 2.1 and Eq. 2.2, assume a uniform mesh is used on the x - t plane with staggered grid. The staggered grid is known to be more attractive than the nonstaggered grid as it gives sharper resolution for the same cell size [57]. The grid is defined as

$$x_i = i\Delta x, \quad i = 1, 2, \dots, N; \quad t^n = n\Delta t, \quad n = 1, 2, \dots \quad (3.1)$$

where Δx and Δt denote the grid spacing in space and time, i is the index of the nodes, N is the total number of nodes. The cell for x_i , denoted by I_i , is bounded by the boundaries

$x_{i-\frac{1}{2}}$ and $x_{i+\frac{1}{2}}$. In such cell-centered configuration, the interfaces are located at

$i = \frac{1}{2}, \frac{3}{2}, \dots, N + \frac{1}{2}$ and the boundaries are located at the points $i = \frac{1}{2}$ and $i = N + \frac{1}{2}$.

As is known, the main characteristic of hyperbolic PDEs is that they admit smooth as well as discontinuous solutions. If the mechanism of wave propagation leads to the formation of shocks, discontinuity will be present in the solution. From mathematics point of view, the conservation laws for hyperbolic PDEs can be expressed in differential or integral form. For the former one, smoothness in the solution is generally assumed. But if a problem contains discontinuities, the derivatives in the governing equations become undefined. To circumvent this problem, the more fundamental integral form should be considered because it requires less smoothness of the solution across the discontinuity.

Consider the hyperbolic scalar equation given in Eq. 2.2. Integration on the computational cell $\Omega_i = [x_{i-\frac{1}{2}}, x_{i+\frac{1}{2}}]$ over the time interval $\tau^n = [t^n, t^{n+1}]$ gives

$$\int (q(x, t^{n+1}) - q(x, t^n)) dx = - \int [f(q(x_{i+\frac{1}{2}}, t)) - f(q(x_{i-\frac{1}{2}}, t))] dt \quad (3.2)$$

Written in difference form, Eq. 3.2 becomes

$$\frac{q_i^{n+1} - q_i^n}{\Delta t} = - \frac{(f(q_{i+\frac{1}{2}}^n) - f(q_{i-\frac{1}{2}}^n))}{\Delta x} \quad (3.3)$$

where q_i^n is the spatial average over the cell Ω_i and is given as

$$q_i^n = \frac{1}{\Delta x} \int_{x_{i-\frac{1}{2}}}^{x_{i+\frac{1}{2}}} q(x, t^n) dx \quad (3.4)$$

and $f_{i+\frac{1}{2}}^n$ is the time-averaged fluxes at the boundaries over a time-step t^n

$$f_{i+\frac{1}{2}}^n = \frac{1}{\Delta t} \int_{t^n}^{t^{n+1}} q(x_{i+\frac{1}{2}}, t) dt \quad (3.5)$$

Usually the evaluation of $f_{i+\frac{1}{2}}^n$ depends on a few neighboring points,

$$f_{i+\frac{1}{2}}^n = f(u_{i-k+1}^n, \dots, u_i^n, u_{i+1}^n, \dots, u_{i+k}^n) \quad (3.6)$$

Eq. 3.3 is the basic form of hyperbolic conservative laws, which states that the rate of change in the conservative variable q in a cell is equal to the difference in the fluxes f entering the cell.

3.2 Discontinuous Solution

For hyperbolic equation, a solution that satisfies the integral form of the equation is often referred to as ‘weak solution’. If a discontinuity exists in the domain, by integrating over the discontinuity, the following condition, known as the Rankine-Hugoniot condition, is satisfied:

$$f_r - f_l = s(q_r - q_l) \quad (3.7)$$

where s is the moving speed of discontinuity given by

$$s = \frac{f(q_l) - f(q_r)}{q_l - q_r} \quad (3.8)$$

For a hyperbolic system to admit discontinuous solutions, the governing equations must be formulated in integral form and must satisfy the Rankine-Hugoniot condition.

It should be noted that even though the integral form allows less regularity than the differential form, not all solutions are viable solutions to the physical problem because weak solutions are not unique. Usually, an additional physical-based condition must be posed to single out the real solution. Such condition is called “entropy condition”, which states that the solution must be the vanishing viscosity solution, i.e. the limiting solution of the viscous equation as the viscous coefficient $\varepsilon \rightarrow 0$.

3.3 Riemann Problem

In dealing with discontinuities, a special type of problem is considered, known as the Riemann problem. It describes two constant states initially separated by a discontinuity.

For Eq. 2.2, the Riemann problem is defined as:

$$\frac{\partial q}{\partial t} + \lambda \frac{\partial q}{\partial x} = 0$$

$$q(x,0) = \begin{cases} q_l & x < 0 \\ q_r & x > 0 \end{cases} \quad (3.9)$$

where λ is the speed of the propagation, l and r denote the left and right side of a discontinuity as depicted in Figure 3-1.

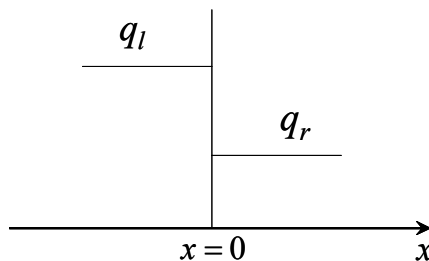


Figure 3-1 Illustration of the initial data for the Riemann problem

On the $x-t$ plane, the solution to the Riemann problem consists of similarity solutions. At time t , the initial discontinuity at $x=0$ is expected to propagate a distance d . It is easy to see that the initial discontinuity propagates with the speed λ . On the characteristic curve plane, the left characteristic curves, where the solution takes on the value of q_l , are separated from the right characteristic curves, where the solution takes on the value of q_r . Depending on the values of q_l and q_r , the solution may be of the following forms:

1) $q_l < q_r$, the characteristic curves on both sides of the wave go into the shock wave and the two states q_l and q_r are connected through a single jump, thus forming a shock wave. The unique weak solution in this case is

$$q(x,t) = \begin{cases} q_l & x < st \\ q_r & x > st \end{cases} \quad (3.10)$$

where s is the speed of discontinuity given by Eq. 3.8. Such relationship is represented in Figure 3-2.

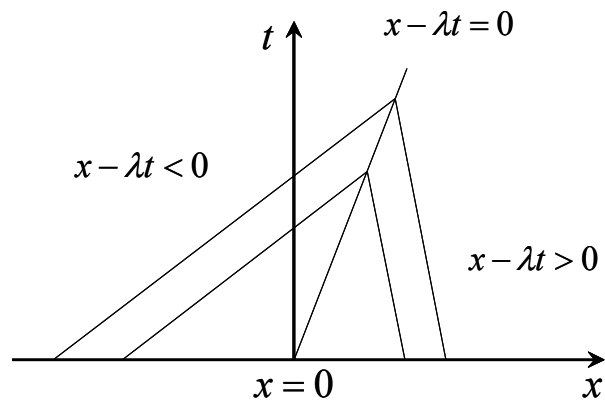


Figure 3-2 Characteristics of shock wave

2) $q_l > q_r$, the speeds of a characteristic family increase from left to right. This corresponds to a rarefied wave for which infinite weak solutions exist. The solution that

satisfies the entropy condition is the weak solution called “rarefaction wave” and is given as

$$q(x,t) = \begin{cases} q_l & x < q_l t \\ \frac{x}{t} & q_l t < x < q_r t \\ q_r & x > q_r t \end{cases} \quad (3.11)$$

In this case, the characteristics on the left and the right of the wave diverge. The two states q_l and q_r are connected through a smooth transition as depicted in Figure 3-3.

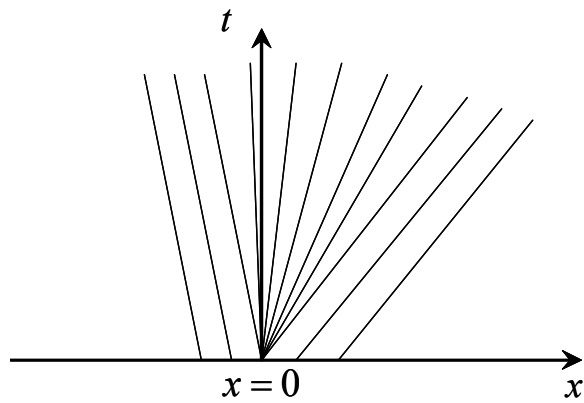


Figure 3-3 Characteristics of rarefaction wave

3) $q_l = q_r$, the characteristics are parallel and the two states are connected through a single jump discontinuity referred to as contact discontinuity. The characteristic curve is depicted in Figure 3-4.

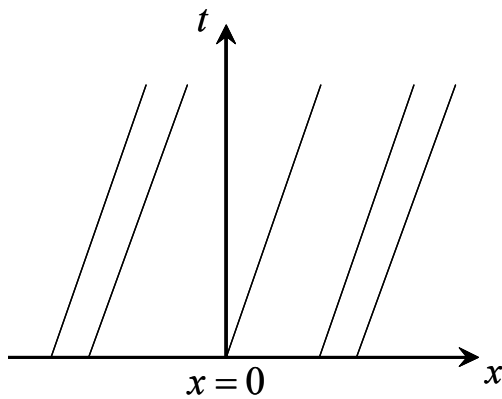


Figure 3-4 Characteristics of contact discontinuity

A Riemann solution may be of any particular characteristic family depending on the initial condition. On the $x-t$ plane, since the characteristic curve must be unique for any point, the characteristic speeds of a Riemann problem could be connected to the outside solution through a shock, a rarefaction or a contact discontinuity as needed. Transition between two characteristics can be viewed as waves emanating from the initial discontinuity because the solution only varies across the transition. For system equations, since more than one characteristic curves are consisted, the solution is a combination of those characteristic families and therefore contains multiple transitions. The Riemann solution for system equations will be discussed in Section 3.6.2.

For general hyperbolic equation, if a discontinuity in the solution is characterized by the left and the right side values, the relevance of the Riemann problem can be seen by assuming a piece-wise constant solution of a cell average in each computational cell $[x_{i-\frac{1}{2}}, x_{i+\frac{1}{2}}]$. The two states $q_l = q_{i-1}$ and $q_r = q_{i+1}$ are separated by the discontinuity at the intercell boundary $x_{i+\frac{1}{2}}$. Thereby a local Riemann problem can be defined with the initial condition given as

$$q(x, t^n) = \begin{cases} q_l & x < x_{i+\frac{1}{2}} \\ q_r & x > x_{i+\frac{1}{2}} \end{cases} \quad (3.12)$$

The local Riemann problem can be solved exactly by solving the nonlinear flux function, which leads to fairly high computational cost. An alternative is to solve the local Riemann problem in an approximate approach, which will be discussed in Section

3.6.3. By this approach, the interfacial value $q_{i+\frac{1}{2}}$ is first approximated, and then the fluxes $f(q_{i\pm\frac{1}{2}})$ can be evaluated by solving the Riemann problem using a conservative method. In Section 3.4, an important conservative method – the Godunov scheme is discussed.

3.4 Godunov Scheme

As mentioned earlier, numerical difficulties arise in hyperbolic type of PDEs, which necessitates special treatments of discontinuities. In dealing with such problems, a numerical method is expected to be conservative, i.e. the variable q in Eq. 2.2 should be conserved. It is recognized that traditional numerical methods based on the general first or second order methods for PDEs can lead to spurious oscillations near a shock wave, or the propagation of waves at wrong speeds. In the classical work of Lax and Wendroff [50], it was found that a conservative numerical method, if convergent, will converge to the weak solution of the conservation laws. Hou and LeFloch [42] proved that if a non-conservative method is used, it converges to the wrong solution if it contains a shock wave. Recall the conservation laws in Eq. 3.3, for a numerical method to be conservative, the fluxes $f_{i\pm\frac{1}{2}}$ must be the true averages of the fluxes across the boundaries over a time step. There are many choices for the computation of $f_{i\pm\frac{1}{2}}$ that give conservative numerical methods. Among them, the Godunov scheme was a successful early attempt and has been shown to be robust and accurate in dealing with the difficulties in the hyperbolic conservation laws.

Consider $f_{i+\frac{1}{2}}$ as an example and note that the same principle applies to $f_{i-\frac{1}{2}}$, in the Godunov scheme, the flux $f_{i+\frac{1}{2}}$ is computed at the interface using the solution $q_{i+\frac{1}{2}}$ obtained at the interface by solving a local Riemann problem described in Section 3.3. This is accomplished first by estimating q_l and q_r via interpolation, the order of which determines the order of accuracy of the scheme. Consider the first order interpolation for instance, a piecewise constant value is used and the state variables are $q_l = q_i$ and $q_r = q_{i+1}$. With the obtained q_l and q_r , the local Riemann problem can be solved using an exact or approximate method. The results from these separate Riemann problems are then averaged to update the solution.

3.5 Hyperbolic Scalar Equation

In this section, the conservation laws for hyperbolic scalar equation given by Eq.2.2 is considered. Two typical examples of this type of PDEs are the linear advection equation, for which $f = au$ with a being a constant, and the inviscid Burger's equation, for which $f = u^2$.

Using first order interpolation, the numerical flux can be computed by

$$f_{i+\frac{1}{2}} = \begin{cases} f(u_i) & a \geq 0 \\ f(u_{i+1}) & a < 0 \end{cases} \quad (3.13)$$

where a , referred as the ‘‘Roe speed’’, is defined by

$$a = \begin{cases} \frac{f(u_{i+1}) - f(u_i)}{u_{i+1} - u_i} & u_i \neq u_{i+1} \\ f'(u_i) & u_i = u_{i+1} \end{cases} \quad (3.14)$$

It is easy to note that the scheme switches sign depending on the sign of a , which is an indicator of the local wave direction. Specifically, the wave propagates from left to right if a is positive, and the reverse if a is negative. This is in fact the first order upwind scheme.

3.6 Hyperbolic System Equations

In the previous section, the hyperbolic theory is discussed for scalar equation. It becomes more complicated when applied to hyperbolic system equations. For the system given by Eq.2.1, if the derivatives of the flux exist, the system can be rewritten as:

$$\frac{\partial Q}{\partial t} + A \frac{\partial Q}{\partial x} = 0 \quad (3.15)$$

where A is the Jacobian matrix $A = \frac{\partial F}{\partial Q}$. This system is hyperbolic if matrix A is diagonalizable and has a complete set of real eigenvalues and eigenvectors. Since the characteristic of the system matrix determines the mathematical character of the governing equations, first it is necessary to discuss the properties of the Jacobian matrix through the characteristic theory.

3.6.1 System Characteristics

Consider the matrix form of the hyperbolic system equations given by Eq. 3.15. If the

vector Q consists of n variables, then the Jacobian matrix A is an $n \times n$ matrix, where λ_i denotes an eigenvalue and r_i denotes the corresponding right eigenvector. If matrix A is diagonalizable, it can be expressed as

$$A = R\Lambda R^{-1} \quad (3.16)$$

where $\Lambda = \text{diag}(\lambda_1, \lambda_2, \dots, \lambda_n)$ is the diagonal matrix consisting of the eigenvalues, R is the right eigenmatrix $R = (r_1, r_2, \dots, r_n)$ made up of the corresponding right eigenvectors.

Define a new variable $V(v_1, v_2, \dots, v_m)$ via the following transformation

$$V = R^{-1}Q \quad (3.17)$$

then substitution of Eq. 3.17 into Eq. 3.15 yields:

$$V_t + \Lambda V_x = 0 \quad (3.18)$$

Here V is called the vector of characteristic variable. Since the matrix Λ is diagonalized, Eq. 3.18 is equivalent to the following:

$$\frac{\partial v_k}{\partial t} + \lambda_k \frac{\partial v_k}{\partial x} = 0, \quad k = 1, 2, \dots, n \quad (3.19)$$

In Eq. 3.19, the system is decoupled into n scalar Riemann problems, each being a linear advection equation of a characteristic variable v_i . Every equation is associated with a particular eigenvalue corresponding to the characteristic speed of the individual wave component, and holds along the characteristic curve $\frac{dx}{dt} = \lambda_i$. Converting to the original variable, the linear scalar equation with constant coefficient has a solution in the form

$$v_k(x, t) = (R^{-1}q_0(x - \lambda_k t)), \quad k = 1, 2, \dots, n \quad (3.20)$$

After solving the n local Riemann problems, the original solution can be found by inverting the changed variable $Q = RV$ and is given by

$$q(x, t) = \sum_{k=1}^n v_k t_k = \sum_{k=1}^n (R^{-1} q_0(x - \lambda_k t))_k t_k \quad (3.21)$$

3.6.2 Solution Structure

In this section discussion is given on the solution structure of system equations. For a linear system, consider a Riemann problem with an initial single discontinuity

$$Q(x, 0) = \begin{cases} Q_l & x < 0 \\ Q_r & x > 0 \end{cases} \quad (3.22)$$

Take a system of two equations for example. Since it has two eigenvalues, the structure of the solution includes two waves emanating from the origin, each for one eigenvalue. Such solution structure results in three states as depicted in Figure 3-5: the original state to the left Q_l , the one to the right Q_r , and a middle state Q_m between the two waves. Among them, the left and the right going waves are two shocks. In the middle region, the state is resulted from the passage of two waves emerging from the origin of the initial discontinuity. With constant initial values, each wave travels from the initial interface at the characteristic velocities λ_1 and λ_2 . Recall the decoupled system given by Eq. 3.19, the initial profile of every characteristic variable simply advects at its characteristic speed. The jump across each propagating discontinuity satisfies the Rankine-Hugoniot condition with each corresponding to an eigenvalue.

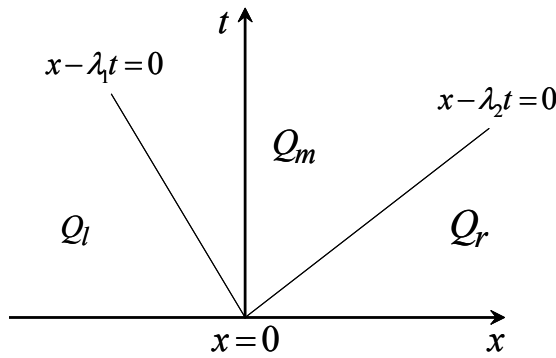


Figure 3-5 Characteristic of two waves

For a nonlinear system, the wave speeds from neighboring cells are usually different, thus another situation may exist in which two states are connected through a smooth transition in a genuinely non-linear field by a rarefaction wave. Therefore, four possible wave patterns may occur for the Riemann problem. The combinations, depicted in Figure 3-6, include (a) two shock waves, (b) two rarefaction waves, (c) left shock with right rarefaction waves, and (d) left rarefaction with right shock waves.

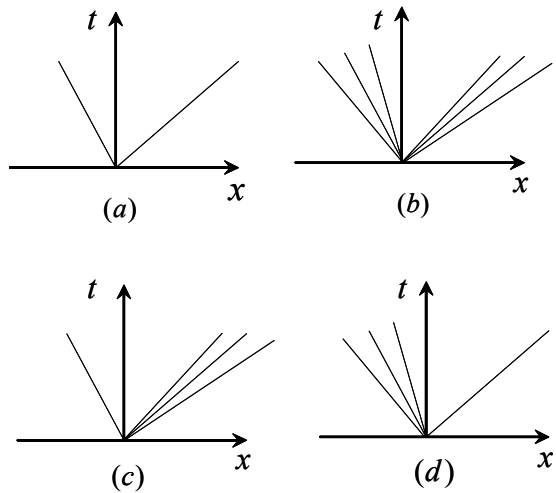


Figure 3-6 Characteristic of nonlinear waves

In this structure, the left and right regions are either shock waves or rarefaction waves. The mid region, under the interaction of the left and right state, forms a shear wave.

3.6.3 Roe's Approximate Riemann Solver

As demonstrated in Section 3.2, the Riemann problem based on the Godunov method for scalar equation is rather straightforward. In the situation of system equations, however, the computation of the flux becomes complex. Solving the Riemann problems exactly involves the solution of nonlinear equations, for which an iterative procedure is always involved, thus resulting in demanding computational expense. Moreover, the possible combinations to connect the states Q_l and Q_r will drastically increase the amount of computations due to the step for determining the solution structures with different patterns. On the other hand, since the cell averaging by the Godunov method already reduces the accuracy, it would be adequate to use an approximate approach rather than the costly exact solver. Such approximate approach is expected to simplify the solution procedure and be more efficient. Generally, the approximate approach involves finding an approximation state \tilde{A} to the Jacobian matrix A that gives the exact solution in the case of a single shock, which can be expressed as:

$$\tilde{A}(Q_r - Q_l) = F(Q_r) - F(Q_l) \quad (3.23)$$

Recall the Rankine-Hugoniot condition given by Eq. 3.7, it can be seen that a single shock is an eigenvector of \tilde{A} . As discussed in Section 2.1, past researches have proposed a number of efficient approximate Riemann solvers [11, 25, 29, 66]. In this work, the most popular and robust Roe's approximate Riemann solver is used.

For a scalar conservation laws, the numerical flux of the Roe scheme is given by Eq. 3.13 and Eq. 3.14. For a system equation, since the Riemann problem is locally defined,

the nonlinear part should be treated in local characteristic fields. This can be achieved by “freezing” the Jacobian matrix of the flux function on the local cells. Thereby the original Riemann problem is replaced by the approximate Riemann problem, which can thus be solved exactly. The solution obtained from such replacing still retains the initial data. The resultant Jacobian matrix is a constant matrix which satisfies the Rankine-Hugoniot condition:

$$F(Q_{i+1}) - F(Q_i) = \tilde{A}_{i+\frac{1}{2}}(Q_{i+1} - Q_i) \quad (3.24)$$

Such intermediate matrix is called the “Roe matrix”. To maintain the conservative as well as the hyperbolic properties, the “Roe matrix” \tilde{A} is required to satisfy the following conditions:

- 1) \tilde{A} has real eigenvalues and a complete set of linearly independent right eigenvectors
- 2) \tilde{A} is consistent with the exact Jacobian matrix

$$\tilde{A}(Q, Q) = A(Q) \quad (3.25)$$

- 3) \tilde{A} ensures conservation across discontinuities

$$F(Q_r) - F(Q_l) = \tilde{A}(Q_r - Q_l) \quad (3.26)$$

The construction of a matrix satisfying Eq. 3.24 through Eq.3.26 can be quite complicated. The values consisted in such matrix are called “Roe average”. It should be noted that there is no unique choice for the average. In the original Roe’s approach, an intermediate parameter vector was introduced where both the conserved variable and the flux were expressed in terms of it. The average was obtained by simply taking the

arithmetic means of the variables. Later, Roe and Pike [68] proposed a simpler method, which avoids constructing the Roe matrix explicitly. In Section 3.7.3, the Roe matrix for the shallow water equations will be discussed.

By approximating $Q(x, t)$ with a piecewise constant function, a local Riemann problem is solved at each time step. This allows for the decomposition of the fluxes at the cell interfaces into waves determined by the eigenvectors of the Jacobian matrix. The Roe's scheme decomposes the Jacobian matrix, as given by Eq. 3.16, and then the Jacobian matrix can be written in terms of the averaging state as:

$$A_{i+\frac{1}{2}} = R_{i+\frac{1}{2}} \Lambda_{i+\frac{1}{2}} R_{i+\frac{1}{2}}^{-1} \quad (3.27)$$

Recall the characteristic theory presented in Section 3.6.1, the decomposition, together with the change of variables, results in a series of linear advection equations with each propagating at a characteristic speed of the corresponding eigenvalue of the ‘‘Roe matrix’’. Instead of treating the equations as individual scalar linear advection equations, one can solve the system as a whole by performing matrix operations. Also it is noticed that the three matrices on the right hand side of Eq. 3.27 are approximations to the interface quantities, and should be evaluated with the ‘averaged’ values.

With the Roe matrix and the Roe average, the interfacial flux can be calculated using the approximate Riemann solver:

$$F_{i+\frac{1}{2}} = \frac{1}{2} \left(F(Q_{i+\frac{1}{2}}^l) + F(Q_{i+\frac{1}{2}}^r) \right) - \frac{1}{2} \left| A_{i+\frac{1}{2}} \right| \left(Q_{i+\frac{1}{2}}^r - Q_{i+\frac{1}{2}}^l \right) \quad (3.28)$$

From the decomposition given in Eq. 3.16, it is easy to verify that the absolute value of the Roe matrix satisfies

$$\left| A_{i+\frac{1}{2}} \right| = R_{i+\frac{1}{2}} \left| \Lambda_{i+\frac{1}{2}} \right| R_{i+\frac{1}{2}}^{-1} \quad (3.29)$$

with the absolute diagonal matrix given by

$$\left| \Lambda_{i+\frac{1}{2}} \right| = \text{diag}(|\lambda_1|_{i+\frac{1}{2}}, \dots, |\lambda_n|_{i+\frac{1}{2}}) \quad (3.30)$$

Eq. 29 and Eq.30 can be substituted into Eq. 28 to calculate $F_{i+\frac{1}{2}}$. It is noted that Eq. 3.28 is in fact the generalized form of the first-order upwind scheme.

3.7 Shallow Water Equations

3.7.1 Governing Equation

The mathematical model of incompressible fluid flow is based on the three-dimensional fully dynamic Navier-Stokes equations. For flows in rivers or open channels of mild slopes, usually the depth of water is far less than that in the longitudinal and latitudinal dimensions, therefore the vertical component of the velocity and the corresponding shear stress are small enough to be neglected. Hence the pressure gradient is independent of the vertical level z , implying a hydrostatic pressure distribution. By assuming incompressible, inviscid and hydrostatic pressure, the shallow water equations can be derived by integrating the Navier-Stokes equations over depth. The general two-dimensional shallow water equations then take the form:

$$h_t + (hu)_x + (hv)_y = 0 \quad (3.31)$$

$$(hu)_t + (hu^2)_x + (huv)_y = -gh(Z_x + S_{fx}) \quad (3.32)$$

$$(hv)_t + (huv)_x + (hv^2)_y = -gh(Z_y + S_{fy}) \quad (3.33)$$

where h is water depth; u is depth averaged velocity in the x -direction; v is depth averaged velocity in the y -direction; g is acceleration due to gravity; Z_x is bed slope in the x -direction; Z_y is bed slope in the y -direction; S_{fx} is bottom friction in the x -direction; S_{fy} is bottom friction in the y -direction. Generally, the bottom friction can be estimated using Manning's formula:

$$S_{fx} = \frac{n^2 u \sqrt{u^2 + v^2}}{h^{4/3}}, S_{fy} = \frac{n^2 v \sqrt{u^2 + v^2}}{h^{4/3}} \quad (3.34)$$

where n is Manning's roughness coefficient.

In this system, Eq. 3.31 represents the conservation of mass by enforcing the balance of total volume of water. Eq. 3.32 and Eq. 3.33 constitute the momentum equations in x - and y -direction, respectively. The shallow water equations can also be written in an equivalent matrix form as:

$$\frac{\partial Q}{\partial t} + \frac{\partial F(Q)}{\partial x} + \frac{\partial E(Q)}{\partial y} = S(Q) \quad (3.35)$$

where Q denotes a vector containing the conservative variables h , u and v ; $F(Q)$ and $E(Q)$ are vectors of the flux tensor and are functions of Q ; $S(Q)$ is the source or sink term. Expressed in terms of the primary variables, the vectors are written as:

$$Q = \begin{pmatrix} h \\ hu \\ hv \end{pmatrix}, F = \begin{pmatrix} hu \\ hu^2 + \frac{1}{2}gh^2 \\ huv \end{pmatrix}, E = \begin{pmatrix} hv \\ huv \\ hv^2 + \frac{1}{2}gh^2 \end{pmatrix}, S = \begin{pmatrix} 0 \\ gh(s_{0x} - s_{fx}) \\ gh(s_{0y} - s_{fy}) \end{pmatrix} \quad (3.36)$$

with $S_{0x} = -Z_x, S_{0y} = -Z_y$.

3.7.2 Characteristic Speeds

Similar to other hyperbolic systems, the shallow water equations may contain shocks in the solution. As discussed earlier, a generalization of the hyperbolic equations that contain shocks is the Riemann problem. Therefore, to study the solution structure of the shallow water equations, it is necessary to look at its characteristic field first. Since this system consists of three equations, it has three distinct eigenvalues λ_1, λ_2 and λ_3 with each associated with one wave. The three eigenvalues form four states Q_l, Q_{*l}, Q_{*r} and Q_r as depicted in Figure 3.7.

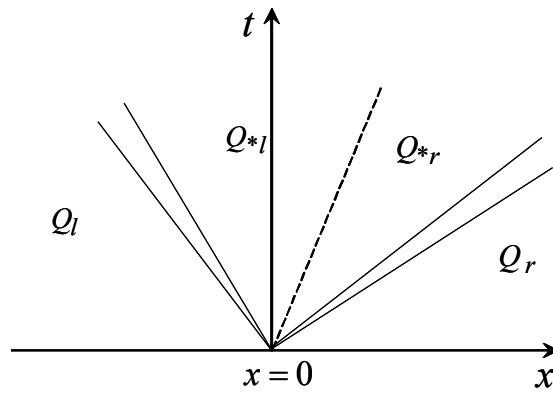


Figure 3-7 Wave structure of shallow water equations

By examining the regions separated by the characteristics, it is found that the following wave possibilities may exist: between the states Q_l and Q_{*l} , the left wave can

be a rarefaction or shock wave; between the states Q_{*l} and Q_{*r} , there is always a shear wave and between Q_{*r} and Q_r , the right wave could be a right rarefaction or shock wave. Notice that the first and the third eigenvalues correspond to that of the one-dimensional shallow water equations, which are shock or rarefaction. The second eigenvalue arises from the latitudinal velocity component v , which only changes across the eigenvalue, while the water depth h and the longitudinal velocity u are not affected. Hence the overall solution structure is a combination of the left and the right shock or rarefaction waves, with a shear wave in the middle.

It is obvious that the directions of the characteristics determine how the wave information is transmitted: if both the left and the right characteristics have the same sign, the information transmits in the positive direction, hence the waves move only in the downstream direction, which corresponds to a supercritical flow; if one characteristic speed is positive and one is negative, the information transmits in both directions representing a subcritical flow, by which the information propagates both upstream and downstream.

3.7.3 Roe's Approximate Riemann Solver for Shallow Water Equations

Based on the discussion of the approximate Riemann solvers in Section 3.6.3 for hyperbolic system equations, this section presents an outline of the Roe's scheme for solving the shallow water equations. Consider the one-dimensional homogeneous shallow water equations

$$\frac{\partial Q}{\partial t} + \frac{\partial F(Q)}{\partial x} = 0 \quad (3.37)$$

$$Q = \begin{pmatrix} h \\ hu \end{pmatrix}, \quad F = \begin{pmatrix} hu \\ hu^2 + \frac{1}{2}gh^2 \end{pmatrix} \quad (3.38)$$

The vector flux F can be linearized with respect to the vector of variables Q through the Jacobian matrix expressed as

$$\frac{\partial F(Q)}{\partial x} = A(Q) \frac{\partial Q}{\partial x} \quad (3.39)$$

Here Eq. 3.39 assumes $F = AQ$. This can be true only if $F_x = AQ_x$. This property is called the homogeneous property of functions. Specifically, the function $F(Q)$ is said to be homogeneous of degree one in the variable Q . Mathematically, if a function $F(Q)$ is homogeneous to degree k in Q , it has the following relation

$$F(\alpha Q) = \alpha^k F(Q) \quad (3.40)$$

First order degree homogeneity is valid for systems such as the Euler equations of aerodynamics. However, this is not true for the shallow water equations. In fact, the shallow water equations are shown to be a homogeneous function of order two [101]. Hence the Jacobian matrix is not applicable in this case. Instead, a matrix G needs to be constructed which satisfies $F = GQ$. In the work of Berger and Stockstill [9], G is shown to be:

$$G = \begin{pmatrix} 0 & 1 \\ -u^2 + gh/2 & 2u \end{pmatrix} \quad (3.41)$$

This matrix has two eigenvalues

$$\lambda_1 = u + c/\sqrt{2}, \lambda_2 = u - c/\sqrt{2} \quad (3.42)$$

They are the two characteristic speeds along which the wave is transmitted. Now the corresponding eigenvectors can be computed. By carrying out a similar procedure as given in Section 3.6.1, the diagonal matrix together with the left and the right matrices can be obtained as:

$$\Lambda = \begin{pmatrix} u + c/\sqrt{2} & 0 \\ 0 & u - c/\sqrt{2} \end{pmatrix} \quad (3.43)$$

$$R = \begin{pmatrix} 1 & 1 \\ u + c/\sqrt{2} & u - c/\sqrt{2} \end{pmatrix} \quad (3.44)$$

$$R^{-1} = \frac{1}{\sqrt{2}c} \begin{pmatrix} -u + c/\sqrt{2} & 1 \\ u + c/\sqrt{2} & -1 \end{pmatrix} \quad (3.45)$$

To keep consistency of the notation throughout the dissertation, the symbol ‘ A ’ and the term ‘Jacobian matrix’ are maintained to denote the homogeneity satisfying matrix G . Note that matrix $A_{i+\frac{1}{2}}$ in Eq. 3.29 requires the evaluation of Eq. 3.43 through Eq. 3.45 at the cell interface $x_{i+\frac{1}{2}}$, which are functions of the Roe average. Roe [66] constructed the averages in terms of the states Q_l and Q_r , which allows for conservative evaluation of flux vector. For the shallow water equations, Roe’s average is given by:

$$\beta = \sqrt{\frac{h_{i+\frac{1}{2}}^r}{h_{i+\frac{1}{2}}^l}}, \quad u_{i+\frac{1}{2}} = \frac{u_{i+\frac{1}{2}}^l + \beta u_{i+\frac{1}{2}}^r}{1 + \beta}, \quad c_{i+\frac{1}{2}} = \sqrt{\frac{1}{2}[(c_{i+\frac{1}{2}}^l)^2 + (c_{i+\frac{1}{2}}^r)^2]} \quad (3.46)$$

where $c = \sqrt{gh}$ is the celerity. The subscripts l and r refer to the left and right states.

This numerical flux, together with the conservative form of the conservation laws, forms the Godunov scheme of first order accuracy. To obtain solutions of high order accuracy, high order difference formulations and flux approximations must be used. That will be discussed in Chapter 4.

Chapter 4

High Resolution Numerical Scheme

In this chapter, a high order non-oscillatory shock capturing finite difference scheme on uniform cell-centered grids is developed. The scheme is based on the high order compact central type Padé scheme with ENO/WENO reconstructions. The semi-implicit Crank-Nicholson scheme is used for temporal discretization. First, the discussion of the numerical scheme is presented for scalar equation, then it is generalized to system equations.

4.1 High Order Reconstruction

Consider the scalar hyperbolic equation given by Eq. 2.2, by performing reconstruction using the information of the conservative variable q at some other locations, accurate information about this variable can be obtained. As stated in Section 3.1, conservative numerical methods are constructed by discretizing the domain into cells featuring piece-wise constant state q_i between the positions of $x_{i-\frac{1}{2}}$ and $x_{i+\frac{1}{2}}$, which result in a series of Riemann problems. For solving these Riemann problems, the Roe's approximate solver has the general form:

$$f_{i+\frac{1}{2}} = f(q_{i+\frac{1}{2}}^r, q_{i+\frac{1}{2}}^l) = \frac{1}{2} \left[f(q_{i+\frac{1}{2}}^r) + f(q_{i+\frac{1}{2}}^l) - \alpha (q_{i+\frac{1}{2}}^r - q_{i+\frac{1}{2}}^l) \right] \quad (4.1)$$

where the superscripts l and r represent the left and the right interfacial states of $x_{i+\frac{1}{2}}$, α is the characteristic velocity. For scalar case, α is the Roe speed given by Eq. 3.14. For system equations, α is the local Jacobian matrix at the cell interface $x_{i+\frac{1}{2}}$. The computation of the flux function for system equations is similar to that for scalar equation. Difference lies only in that the evaluation of the Roe flux for system equations requires the computation of the absolute value of the Jacobian matrix.

Using high order approximations for those terms of the interfacial quantities on the right side of Eq. 4.1, high order approximation to the flux $f_{i+\frac{1}{2}}$ can be achieved. In this work, the ENO and the WENO scheme are employed to do such interpolation, as discussed below.

4.1.1 ENO Scheme

Generally, to obtain high order accuracy of a function, the interpolation stencil must contain more nodal points as compared to that for a lower order approximation. For a high order interpolation on a stencil of multiple points, if the interpolation function contains discontinuities, such traditional fixed stencil approximation may not be adequate near the discontinuities because large gradient inside the stencil may cause over- or under-shoot of the actual values. This phenomenon is known as ‘‘Gibbs phenomena’’ [79]. Attempt to overcome this problem motivates the usage of an ‘‘adaptive stencil’’. By shifting the stencils across a large gradient region, one expects to avoid those stencils

containing large gradients. The ENO scheme is based on such adaptive stencil idea, in which, stencils composed of an arbitrary number of points can be used for high order approximation. The basic idea of the ENO approximation is to shift the stencil among all candidate stencils and select the one that produces the smoothest reconstruction of the function. The reconstruction procedure is described as follow.

Assume a variable quantity is defined on the staggered grid configuration as described in Section 2.1. A polynomial can be obtained to approximate this quantity on a certain cell $I_i = [x_{i-\frac{1}{2}}, x_{i+\frac{1}{2}}]$ using interpolation. With the designed order of accuracy n , an $n+1$ point stencil is to be used to produce a polynomial $p_i^n(x)$ of degree n . The objective is to find a stencil of $n+1$ consecutive point which contains x_i , such that the interpolation polynomial $f(x)$ from this stencil is the smoothest compared to the other possible stencils. For example, for the left quantities $f_{i+\frac{1}{2}}^l$ and $q_{i+\frac{1}{2}}^l$ in Eq. 4.1 on cell I_i , the procedure to compute such a polynomial consists of choosing a stencil with k points to the left and $n+1-k$ to the right of $x_{i+\frac{1}{2}}$. Then the available stencils of an n th-order interpolation consists of the following consecutive stencils $[x_{i-n}, x_{i-n+1}, \dots, x_i]$, $[x_{i-n+1}, x_{i-n+2}, \dots, x_{i+1}]$, \dots , and $[x_i, x_{i+1}, \dots, x_{i+n}]$, from which one stencil is to be selected. This stencil group determines a total of n different n th-order polynomials. By shifting stencils, the discontinuous cell that may exist can be avoided. Figure 4-1 illustrates the stencil group of a fourth order interpolation for the left quantities as an example.

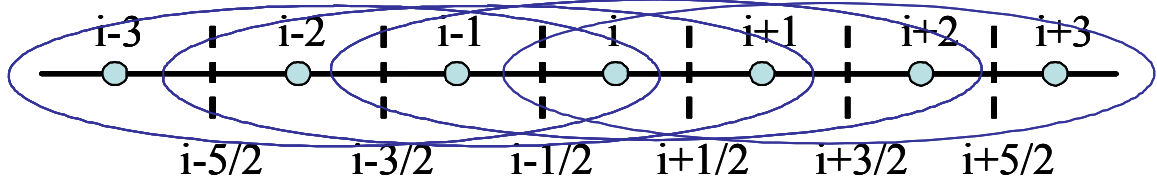


Figure 4-1 Stencil candidates of interpolation polynomial of fourth order reconstruction

To achieve this effect, Newton interpolation polynomial is considered. Newton's interpolation uses divided difference to construct the polynomial. In Newton method, the zero order degree polynomial is defined as $P^0(x_i) = f(x_i)$ for $i = 0, 1, \dots, n$. Given the following substitution $f[x_i] = f(x_i)$, the divided difference of a function is defined as:

$$\begin{aligned}
 f[x_0, x_1] &= \frac{f[x_1] - f[x_0]}{x_1 - x_0} \\
 f[x_0, x_1, x_2] &= \frac{f[x_1, x_2] - f[x_0, x_1]}{x_2 - x_0} \\
 &\vdots \\
 f[x_0, x_1, \dots, x_n] &= \frac{f[x_1, x_2, \dots, x_n] - f[x_0, x_1, \dots, x_{n-1}]}{x_n - x_0}
 \end{aligned} \tag{4.2}$$

Then an n th degree interpolation polynomial can be expressed using Newton divided difference as:

$$\begin{aligned}
 P^n(x) &= f(x_0) + (x - x_0)f[x_0, x_1] + (x - x_0)(x - x_1)f[x_0, x_1, x_2] + \dots \\
 &+ (x - x_0) \cdots (x - x_{n-1})f[x_0, x_1, \dots, x_n]
 \end{aligned} \tag{4.3}$$

The advantage of Newton method is that the order of the polynomial can be increased from n to $n+1$ by simply adding one term. More importantly, the divided difference has the following property as long as the function is smooth on the stencil:

$$f[x_i, \dots, x_{i+j}] = \frac{f^{(j)}(\xi)}{j!}, \quad \xi \in [x_i, x_{i+j}] \quad (4.4)$$

If there is discontinuity at some point inside the stencil, it is easy to verify that

$$f[x_i, \dots, x_{i+j}] = o\left(\frac{1}{\Delta x^j}\right) \quad (4.5)$$

This property indicates that the divided difference can be used as a measure of smoothness of the function inside the stencil.

Note that the interfacial flux $f_{i+\frac{1}{2}}$ in Eq. 4.1 also involves the approximations of the quantities on the right of the interface $x_{i+\frac{1}{2}}$, i.e. $f_{i+\frac{1}{2}}^r$ and $q_{i+\frac{1}{2}}^r$. For these two quantities, a similar procedure can be followed as for $f_{i+\frac{1}{2}}^l$ and $q_{i+\frac{1}{2}}^l$. The only difference lies in the candidate stencils for the interpolations. It is easy to understand that the stencil group should be one point right shifted from the left stencil group, i.e. it includes the stencils of $[x_{i-n+1}, x_{i-n+2}, \dots, x_{i+1}]$, $[x_{i-n+2}, x_{i-n+3}, \dots, x_{i+2}]$, \dots , and $[x_{i+1}, x_{i+2}, \dots, x_{i+n+1}]$.

From the procedure described above, it is obvious that the minimum number of points in a stencil for interpolation should be two. To find an n -point stencil, a series of steps should be performed in the selecting process, starting from two points and adding one

into the stencil at each step. The steps can be carried out as follows. Starting from a stencil $[x_i, x_{i+1}]$, the first order interpolation polynomial can be obtained as:

$$f_{i+\frac{1}{2}}(x) = f[x_i] + f[x_i, x_{i+1}](x - x_i) \quad (4.5)$$

For the next step, there are only two possibilities for a second order polynomial: add either the left neighbor point x_{i-1} or the right neighbor point x_{i+2} to expand the stencil. To decide which one to be included, the two corresponding divided differences, which serve as the indicator of the relative smoothness of the two polynomials, should be compared. The smoother one, represented by a smaller absolute value, is then selected. Repeated this procedure until the number of nodes is reached for the polynomial. The resultant stencil is thus used for the reconstruction.

In performing ENO reconstructions, it is possible that an adaptation in the smooth region may occur due to the trivial round off errors of the solution near zero, and thus changing the stencils. Such adaptation is thought to be unnecessary. To remedy this problem, a ‘biased’ stencil can be used. Typically this bias might be a central or one node upwind to start the shift. The basic idea is to stay as close as possible to the preferred stencil unless an alternative stencil is a factor of b ($b > 1$) better in smoothness.

4.1.2 WENO Scheme

As indicated in previous section, the ENO interpolation is uniformly high order accurate. However, some improvements can be made for it. In the ENO scheme, an n^{th} order interpolation stencil covers $2n-1$ cells, but with only one cell being actually used. It

is expected that if all these $2n-1$ cells are used, a $(2n-1)^{th}$ order of accuracy can be achieved. In addition, the selection procedure of the ENO scheme needs a lot of “if” branches, which results in high computational cost and is less efficient.

Based on these facts, the WENO scheme was developed. Instead of using only one optimal stencil as the ENO scheme does, the WENO scheme uses a convex combination of all the possible stencils with a properly selected weight for each individual stencil. The weights, denoted as ω_r , are designed to adapt to the relative smoothness of the candidate stencils. If the function f has discontinuities in one or more of the stencils, the corresponding weight(s) ω_r is essentially 0, implying that its effect on the reconstruction is minimized. The way of selecting the weights reflects the contribution of each stencil according to their smoothness, and ensures that the reconstructions are built from those stencils without discontinuities. With a stencil group of k available candidate stencils, the selected weights by the WENO scheme are superposed in a way such that the maximal accuracy can be achieved and the spurious oscillations are prevented. In doing so, the WENO scheme emulates to the ENO scheme near the discontinuities while evolves to central schemes in smooth regions.

The general form of the weights of the WENO scheme is given as

$$\omega_r = \frac{\alpha_r}{\sum_{i=1}^k \alpha_i}, \quad r=1, \dots, k \quad (4.6)$$

with

$$\alpha_r = \frac{\gamma_r}{(\varepsilon + \beta_r)^2} \quad (4.7)$$

The constants γ_r depend on the particular quantity that must be reconstructed with high order accuracy, and β_r is the smoothness indicator of the stencil. The stencil is biased to the smooth stencil, thus avoiding the oscillations. If the function is smooth within a stencil, then the smooth indicator is order of two ($\beta_r = O(\Delta x^2)$). If discontinuity exists in the stencil, the smooth indicator is basically order of one. Here a small value of ε is used to avoid division by 0. In this work, ε is set with a value of 10^{-6} . Obviously the weights should satisfy the following relationship for consistency:

$$\omega_r \geq 0, \quad \sum_{r=1}^k \omega_r = 1 \quad (4.8)$$

Consider an n^{th} order reconstruction about the cell I_i , a total of $2n+1$ points are contained in the candidate stencils. In smooth regions, a stencil formed by these $2n+1$ points could be used since the reconstructed functions are smooth regardless of the stencil selected, therefore, an order of accuracy of $2n+1$ can be obtained. Hence, the accuracy is improved in smooth areas.

For WENO type reconstruction, third and fourth order formulations have been well formulated and are widely used. In the current work, third order is selected based on the accuracy and efficiency considerations for the applications in this work. The third order scheme is described below. Details of the fourth order scheme are given in Appendix B.

For third order WENO scheme, the numerical flux $f_{i+\frac{1}{2}}$ is defined as follows:

$$f_{i+\frac{1}{2}} = \omega_1 f_{i+\frac{1}{2}}^{(1)} + \omega_2 f_{i+\frac{1}{2}}^{(2)} + \omega_3 f_{i+\frac{1}{2}}^{(3)} \quad (4.9)$$

where $f_{i+\frac{1}{2}}^{(p)}$ are the three third order fluxes on three different stencils, and are given as:

$$f_{i+\frac{1}{2}}^{(1)} = \frac{1}{3}f_{i-2} - \frac{7}{6}f_{i-1} + \frac{11}{6}f_i \quad (4.10)$$

$$f_{i+\frac{1}{2}}^{(2)} = -\frac{1}{6}f_{i-1} + \frac{5}{6}f_i + \frac{1}{3}f_{i+1} \quad (4.11)$$

$$f_{i+\frac{1}{2}}^{(3)} = \frac{1}{3}f_i + \frac{5}{6}f_{i+1} - \frac{1}{6}f_{i+2} \quad (4.12)$$

The nonlinear weights ω_i are given by

$$\omega_i = \frac{\alpha_i}{\sum_{i=1}^3 \alpha_i}, \quad i = 1, 2, 3 \quad (4.13)$$

with α_i determined by

$$\alpha_i = \frac{\gamma_i}{(\varepsilon + \beta_i)^2} \quad (4.14)$$

Values for the three linear weights are [21]:

$$\gamma_1 = \frac{3}{10}, \quad \gamma_2 = \frac{3}{5}, \quad \gamma_3 = \frac{1}{10} \quad (4.15)$$

A complete table of the optimal linear weights up to seventh order is given in Appendix C.

The smoothness indicator β_i is computed with the following formula:

$$\beta_1 = \frac{13}{12}(f_i - 2f_{i+1} + f_{i+2})^2 + \frac{1}{4}(3f_i - 4f_{i+1} + f_{i+2})^2 \quad (4.16)$$

$$\beta_2 = \frac{13}{12}(f_{i-1} - 2f_i + f_{i+1})^2 + \frac{1}{4}(f_{i-1} - f_{i+1})^2 \quad (4.17)$$

$$\beta_3 = \frac{13}{12}(f_{i-2} - 2f_{i-1} + f_i)^2 + \frac{1}{4}(f_{i-2} - 4f_{i-1} + 3f_i)^2 \quad (4.18)$$

It should be noted that the optimal stencil has a one point upwind bias (to the left), which is suitable for the upwind flow with a moving direction from left to right. If the flow has a reverse direction, the corresponding symmetric formulation should be used.

4.1.3 ENO/WENO Scheme for Hyperbolic System Equations

The high order reconstructions presented in Section 4.1.1 and Section 4.1.2 are based on hyperbolic scalar equation. In the case of system equations, the approximate Riemann solver given by Eq. 3.28 can be used to build the interfacial flux $F_{i+\frac{1}{2}}$. The conservative variables $Q_{i+\frac{1}{2}}^l$ and $Q_{i+\frac{1}{2}}^r$ are first approximated by the ENO/WENO reconstruction in a component-wise manner, then the fluxes $F(Q_{i+\frac{1}{2}}^l)$ and $F(Q_{i+\frac{1}{2}}^r)$ can be evaluated with the approximations obtained.

For nonlinear hyperbolic system, as mentioned earlier, the approximate Riemann solver should be carried out on local characteristic fields. This corresponds to finding an average state $Q_{i+\frac{1}{2}}$, i.e. the Roe averages, on which the three components $R_{i+\frac{1}{2}}$, $R_{i+\frac{1}{2}}^{-1}$ and $|\lambda_i|_{i+\frac{1}{2}}$ (Eq. 3.43 - Eq. 3.45) for the Jacobian matrix $A_{i+\frac{1}{2}}$ are computed. Note that the

Roe averages are also functions of the approximations of the left and the right conservative variables $Q_{i+\frac{1}{2}}^l$ and $Q_{i+\frac{1}{2}}^r$.

Using characteristic approach, the procedure for solving system equations can be summarized as follows:

- 1) Perform the scalar ENO/WENO procedure for each component of the variable vector at point i to obtain the left and the right approximations.
- 2) Compute an average state using the Roe average with the results obtained from step 1).
- 3) Compute the eigenvalues and the associated eigenmatrices to obtain the absolute

approximate Jacobian matrix $\left| A_{i+\frac{1}{2}} \right|$ using Eq. 3.29.

- 4) Substitute the quantities into Eq. 3.28 and calculate the flux.

4.2 Compact Finite Difference Scheme

Notice that the conservative form given in Eq. 3.3 for the derivative of the flux is only first order. In this work, a higher order compact finite difference formulation is used that provides consistency with high order non-oscillatory reconstructions of the interfacial values, thus results in an overall high order scheme.

The compact scheme is a family of high order finite difference methods, which has been successfully applied in aerodynamic applications. Different from the traditional

finite difference method, in which the derivatives of a function with given nodes are approximated as a linear combination of the nodal values, the compact scheme instead approximates the derivatives using all the nodal values. Such approximation provides a better representation of the shorter length scales. Because of its ability to achieve high order accuracy as well as its stable property, this method is selected for finite difference discretization in this dissertation. In this section, the properties of high order compact schemes are reviewed first, and then the formulations for the shallow water equations are derived.

The compact scheme is central type finite difference scheme. The word “compact” means it can be written in a diagonal form. The advantage of such diagonal form is that the resultant linear system can be solved by tridiagonal solver. As a central scheme, it also has the advantage over upwind scheme that the knowledge of the characteristic structure of the system is not required. Moreover, compact formulation based on a staggered grid can give sharper resolution of the same cell size.

The Padé scheme is a compact finite difference scheme developed by Lele [51]. The basic idea is to write the derivatives at each nodal point using a Taylor expansion. Then by checking the error terms with the user defined order of accuracy and omitting the higher order terms, a diagonal form can be obtained. The advantage of this procedure is that it can achieve arbitrary high order of accuracy.

On the staggered grid described in Section 2.1, the compact Padé approximation to the derivative of the flux F_i' is given by solving the following system equations

$$\beta F'_{i-2} + \alpha F'_{i-1} + F'_i + \alpha F'_{i+1} + \beta F'_{i+2} = c \frac{F_{i+5/2} - F_{i-5/2}}{5\Delta x} + b \frac{F_{i+1/2} + F_{i-1/2}}{3\Delta x} + a \frac{F_{i+1/2} - F_{i-1/2}}{\Delta x} \quad (4.19)$$

where a , b , c , α and β are parameters to be decided by matching the Taylor series expansions with a certain order of accuracy specified. The first unmatched term determines the truncation error and thus the intended order of accuracy. It is easy to prove [51], with the values of $a = \frac{12}{11}$, $b = 0$, $c = 0$, $\alpha = \frac{1}{22}$, and $\beta = 0$, a fourth order approximation results. In this work, the fourth order scheme is used. The resultant linear system can be solved by the popular tridiagonal matrix solution method - Thomas Algorithm.

4.3 Boundary Conditions

Depending on the physical process and the characteristics of the domain, different boundary conditions can be enforced. Two types of boundary conditions are commonly used in simulating waves, namely the periodic boundary condition and the non-periodic boundary condition. For periodic boundary, a cyclic pattern is assumed in the propagation of variables. In dealing with boundaries of this type, Eq. 4.19 can be directly applied with as many ghost points on both sides as needed. Non-periodic boundary, on the other hand, is often applied in reflective or solid boundaries, which is usually described by the Dirichlet or Neumann boundary conditions. In the case of non-periodic boundary condition, methods of one order lower in accuracy can be used on the boundaries, whereas the approximations to the interior points will not be affected. For

the compact scheme used in this work, a one-sided formulation with reduced order of accuracy is given as:

$$F'_1 + \alpha_1 F'_2 = \frac{1}{h} \left(a_1 F_{1/2} + b_1 F_{3/2} + c_1 F_{5/2} \right) \quad (4.20)$$

$$\alpha_2 F'_{N-1} + F'_N = \frac{1}{h} \left(c_2 F_{N-3/2} + b_2 F_{N-1/2} + a_2 F_{N+1/2} \right) \quad (4.21)$$

With the selection of the following parameters [87], a third order scheme is formed:

$$\alpha_1 = -1, \quad a_1 = -1, \quad b_1 = 2, \quad c_1 = -1, \quad \alpha_2 = -1, \quad a_2 = 1, \quad b_2 = -2, \quad c_2 = 1 \quad (4.22)$$

For ENO/WENO reconstruction, if a periodic boundary is specified, the interpolation can be performed using the imaginary exterior points extended from the interior points. While in the case of non-periodic boundary, the interpolation has to be limited to the available nodes within the computational domain. Besides the above two types of boundaries, solid boundary and open boundary are often seen in solving shallow water equations problems. These two types of boundary conditions will be used in the numerical tests of this work.

4.4 Time Discretization

Explicit schemes are often used for time integration in shock-capturing models. Although mathematically simple to implement, the explicit schemes are subject to the common Courant-Friedrichs-Levy (CFL) condition restriction. Thus small step size is generally required. In this work, the semi-implicit Crank-Nicholson method is employed for time discretization. For linear problems, such semi-implicit methods are not restricted

by the CFL condition. In addition, the standard Crank-Nicholson method is known to be non-dissipative, though it can be oscillatory. With the usage of non-oscillatory shock-capturing scheme for spatial discretization, it is expected that the drawback of this temporal discretization scheme can be compensated.

Let Δt be the time step and $t^n = \Delta t n$ at time level n . When applied to Eq. 2.2, the Crank-Nicholson method reads:

$$\frac{q^{n+1} - q^n}{\Delta t} + \frac{1}{2}(f^{n+1} + f^n)_x = 0 \quad (4.23)$$

For time level $n+1$, employ a deferred iterative solution algorithm

$$(q^{n+1})^{m+1} = (q^{n+1})^m + (\Delta q^{n+1})^m \quad (4.24)$$

Then q can be updated at each iteration by the formulation

$$(q^{n+1})^{m+1} = q^n - \frac{\Delta t}{2} \left((f^{n+1})_x^{m+1} + (f^n)_x \right) \quad (4.25)$$

Eq. 4.25 is then substituted into Eq. 4.24 to yield

$$(q^{n+1})^m + (\Delta q^{n+1})^m = q^n - \frac{\Delta t}{2} \left[(f(q + \Delta q)^{n+1})_x^m + (f^n)_x \right] \quad (4.26)$$

The correction Δq is solved iteratively until a predetermined small value of tolerance ε is reached, and then one can move to the next time level.

In this chapter, theoretical development of the proposed numerical scheme is carried out. The framework of the scheme is formulated. The presentation herein is revolved around one-dimensional equations. In Chapter 5, these schemes will be tested on one-dimensional scalar and system problems.

Chapter 5

Numerical Results of One-dimensional Homogeneous Problems

In this chapter, numerical experiments are conducted on the ENO-Padé and the WENO-Padé schemes developed in Chapter 4. The results are presented and the performances of these two schemes are compared to illustrate their shock capturing capabilities. Third order ENO and WENO interpolations are used for all the numerical tests.

5.1 Linear Scalar Case - Convection Equation

The first problem considered is a linear advection equation [76], also known as one-way wave equation, with an initial condition of sine curve:

$$u_t + a_w u_x = 0, \quad -1 \leq x \leq 1 \quad (5.1)$$

$$u(x,0) = \sin(\pi x) \quad (5.2)$$

where a_w is the wave velocity (here a constant value of 1 is used). A periodic boundary condition is used with the period of 2. A spatial interval of $\Delta x=0.02$ and a temporal interval of $\Delta t=0.01$ are used.

As discussed in Chapter 3, for linear convection equation of Eq. 5.1, the analytical solution is given as $u(x,t) = u_0(x - at)$. This form of solution implies that the linear convection equation simply translates the wave at the prescribed constant speed in the direction of the velocity, while the initial shape does not change with time. By integrating the governing equation for $T=10$, the numerical results of both schemes are illustrated in Figure 5-1. The exact solution is also provided in the same figure.

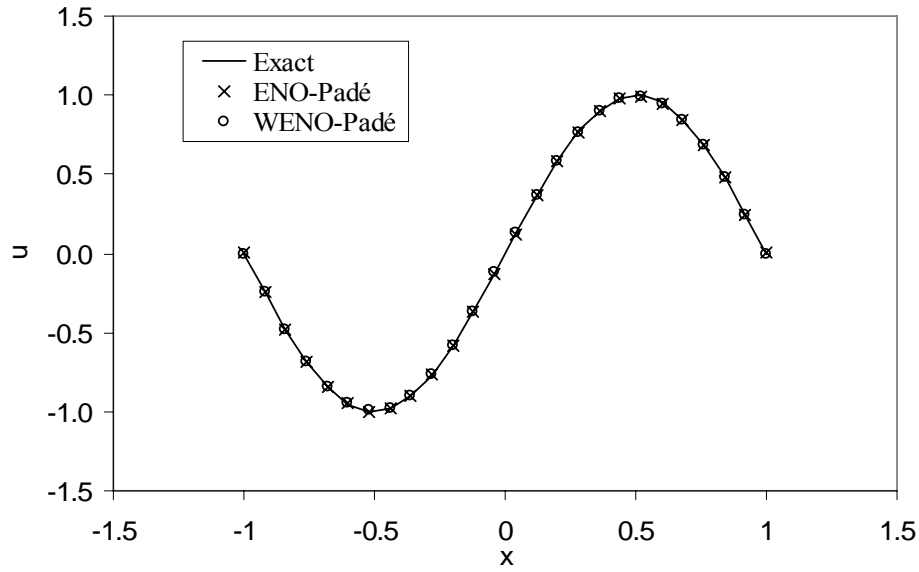


Figure 5-1 Linear advection equation

From Figure 5-1, it is seen that both schemes show good approximations to the exact solution with no oscillation or dissipation observed and no phase difference present. To assess the performances of these two models in a more quantitative way, an accuracy test was conducted with a set of grids $N=25, 50, 100$. For each Δx , the L_1 norm is computed by

$$\text{Error}_N(L_1) = \sum_{i=1}^N \frac{|u_i - u_i^{ext}|}{N} \quad (5.3)$$

where u_i is the model predicted value, u_i^{ext} is the analytical solution, N is the number of nodal points.

Based on the error, a convergence rate is derived, which can be used to verify the order of convergence of a numerical scheme. The formula for the convergence rate is given by

$$\text{Convergence rate} = \log_2 \left(\frac{\text{error}_N}{\text{error}_{2N}} \right) \quad (5.4)$$

With the quantitative measures defined above, results of these two schemes are reported in Table 5-1. The computed convergence rates show that both schemes converge at orders of three or greater, implying the achievement of full order of accuracy by them for problems with smooth solutions. The results also verify the formal order of accuracy of these two models from their derivations. Meanwhile, a comparison of the errors indicates a better performance of the WENO-*Padé* scheme in this case. As the grid size decreases, the WENO-*Padé* scheme produces more accurate results as apposed to the ENO-*Padé* scheme of the same resolution.

Table 5-1 Convergence test - 1-D linear advection equation

N	Δx	ENO- <i>Padé</i>		WENO- <i>Padé</i>	
		L ₁ norm	Convergence rate	L ₁ norm	Convergence rate
25	0.08	0.002515		0.00566	
50	0.04	0.00032	2.97	0.00041	3.79
100	0.02	3E-05	3.41	1.2e-05	5.09

The second test consists of the cases originally proposed in [73] by Harten *et al.* for linear hyperbolic equation Eq. 5.1 with the initial discontinuous conditions

$$u(x,0) = \begin{cases} 1, & -0.2 \leq x \leq 0.2 \\ 0, & \textit{otherwise} \end{cases} \quad (5.5)$$

and

$$u(x,0) = \begin{cases} -x \sin(\frac{3}{2}\pi x^2), & -1 \leq x < -\frac{1}{3} \\ |\sin(2\pi x)|, & |x| \leq \frac{1}{3} \\ 1 - \sin(3\pi x)/6, & \frac{1}{3} < x < 1 \end{cases} \quad (5.6)$$

These two cases have also been employed by many other works to evaluate the capabilities of numerical schemes in handling solution that consists of smooth regions as well as discontinuities. For both cases a periodic boundary condition is enforced at $x=\pm 1$. The spatial and temporal resolutions of $\Delta x=0.02$ and $\Delta t=0.01$, as employed in Test 1, are also used.

In the first case, two contact discontinuities exist in the initial condition. It is of particular interest to see how the discontinuities evolve with time. The governing equation was integrated to $T=3$. The computed results by these two schemes are shown in Figure 5-2 (a). From inspection, it is seen that no oscillation arises in the vicinity of the contact discontinuities. In smooth regions, accurate approximations are achieved to the true solution. However, in regions near the discontinuities, smear of the sharp turns are observed in both methods. A possible explanation would be that the choice of the starting point of the stencil near the shocks may cause such diffusive effect. Comparing these two methods, the WENO-*Padé* scheme gives better overall approximation than the ENO-*Padé* scheme, especially near the sharp corners.

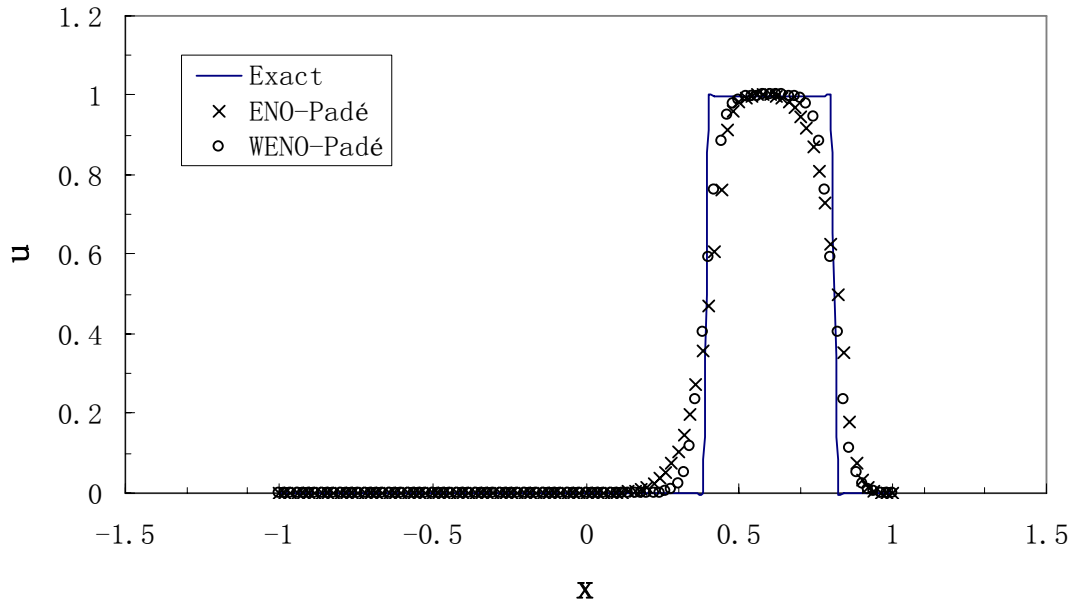


Figure 5-2 (a) Linear hyperbolic scalar equation – case 1

The second case was integrated for $T=2$, and the results are shown in Figure 5-2 (b) together with the analytical solution.

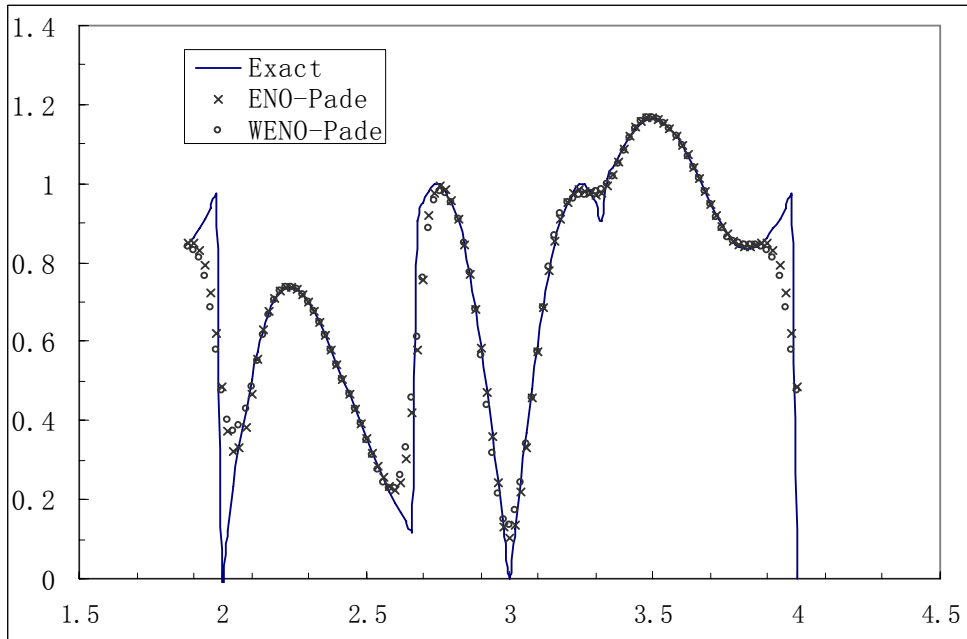


Fig 5-2 (b) Linear hyperbolic scalar equation – case 2

One can see from the above figure that the numerical models provide accurate solutions in the smooth regions, and are capable of capturing the discontinuities without observable oscillations. However, small amount of smear exist in the solutions near the sharp corners. These two schemes demonstrate similar behaviors except at local extrema, where the WENO-Padé scheme shows slightly better approximations. From this test case it is found that the schemes can not achieve full order of accuracy at local extrema, but with somewhat degenerate results. A possible solution to deal with it is to use adaptive grids by which the grids near the extrema can be refined. This subject is discussed in Chapter 8.

5.2 Non-linear Scalar Case - Burger's Equation

The test in this section investigates the performance of the numerical schemes in dealing with nonlinear scalar hyperbolic equations. A typical example of the nonlinear scalar hyperbolic equation is the inviscid Burger's equation. As Burger's equation is the simplified form of the Navier-Stokes equations but still retains many characteristics of it, studying the properties of Burger's equation is helpful in understanding the behaviors of the Navier-Stokes equations. Therefore, this equation has been widely used as benchmark problem for the validation of shock capturing numerical methods [5, 6, 61, 71, 72, 76]. The test case selected in this study is used by Shu *et al.* [72], for which the analytical solution was included. The problem is defined on the domain $[-1,1]$, with a periodic boundary condition of period of 2:

$$u_t + (u^2 / 2)_x = 0, \quad -1 \leq x \leq 1 \quad (5.7)$$

The initial condition is a sine curve, as illustrated in Figure 5-3:

$$u(x,0) = \frac{1}{4} + \frac{1}{2} \sin \pi x \quad (5.8)$$

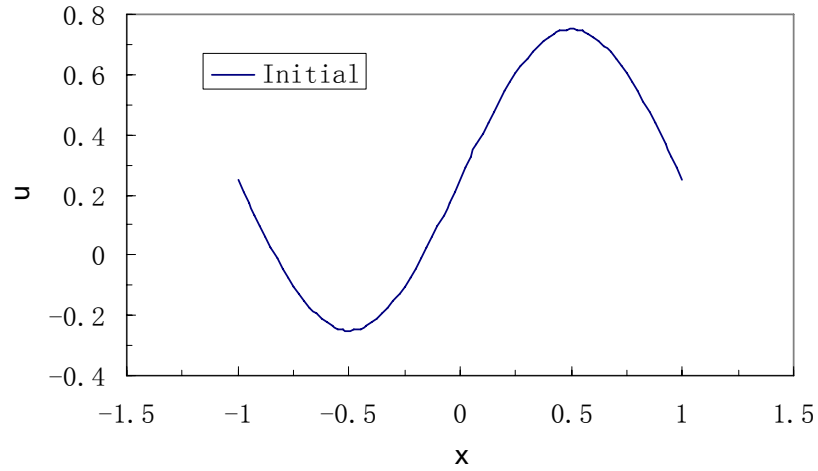


Figure 5-3 1-D Burger's equation – initial condition

Figure 5-4 shows the numerical results together with the true solution at $T = 2/\pi$.

The numerical solution has been obtained by considering a uniformly spaced grid of $\Delta x = 0.025$ and a constant time step of $\Delta t = 0.005$.

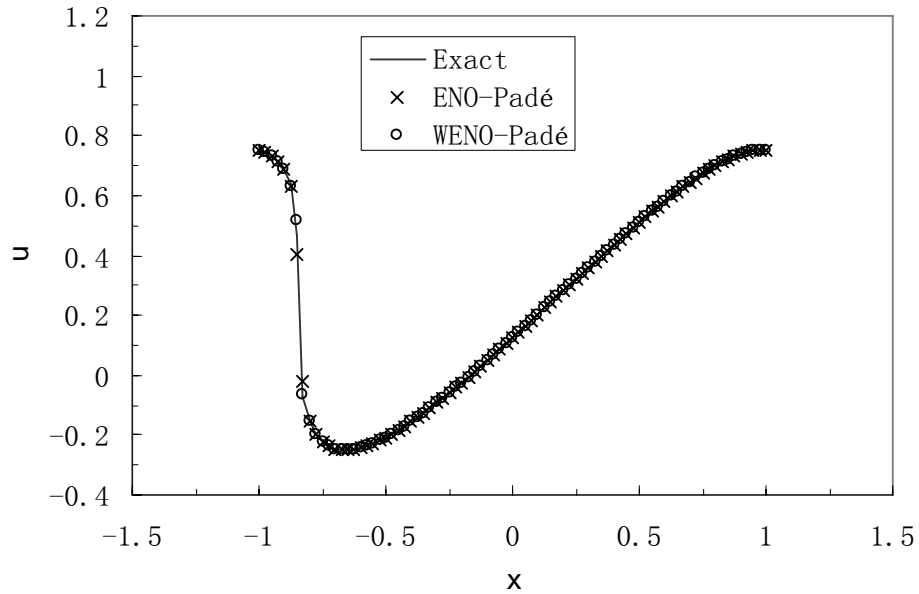


Figure 5-4 Nonlinear scalar case – 1-D Burger's equation

From Figure 5-4, one can see that the solution consists of a steepening wave initially propagating to the right, and then at time T it develops into a moving shock. This is purely a nonlinear phenomenon regardless of how smooth the initial condition is. In general, good agreement between the numerical solutions and the analytical solution is obtained. This figure gives evidence of the capability of these two schemes to compute discontinuous solution without observable oscillations. In order to better appreciate the difference between the schemes, a grid convergence test was performed and the results are reported in Table 5-2.

Table 5-2 Convergence test – 1-D Burger’s equation

N	Δx	ENO- <i>Padé</i>		WENO- <i>Padé</i>	
		L_1 error	Convergence rate	L_1 error	Convergence rate
20	0.1	0.009434		0.011455	
40	0.05	0.0004184	1.17	0.005174	1.15
80	0.025	0.001932	1.11	0.001931	1.42
160	0.0125	0.000792	1.29	0.00085	1.18

It shows a convergence rate of slightly more than unity of both methods for this nonlinear case. It should be noted that the rate of convergence reported here is the overall convergence rate. For nonlinear cases one usually obtains better convergence away from the shock, while degradation is normally observed near the shock because when considering the nonlinear conservation laws, the characteristics point into the shock. According to linear theory, dissipative schemes reduce errors propagating backwards against the direction of characteristics. Thus, it is reasonable to expect locally large errors at the shock to stay in a layer near the shock [26].

5.3 Hyperbolic System Equations – Homogeneous Shallow Water Equations

In this section, the application of the numerical schemes to system conservation laws is presented. The numerical methods are applied to simulate dam break problems by solving the homogeneous shallow water equations. Dam break problem can be described by the scenario where a solid wall, separating upstream water in a channel on one side from the downstream water or dry land on the other side, experiences an instantaneous collapse and leads to flood through the breach. The resultant flood develops a wave front that propagates at a certain speed.

Note that the numerical schemes presented in Chapter 4 are based on hyperbolic scalar equation. For system equations, basically two approaches can be used to implement these schemes. One is to apply the numerical scheme to each individual equation in the system. Such approach is conceptually straight forward, but may not be applicable for cases where the variables are highly coupled. The other is to employ the approximate Riemann solvers and apply the schemes in a component-wise fashion. This approach is more efficient in dealing with system equations because it treats the system in matrix form regardless of the complexity of the relationship between the variables. In this work, the second approach is selected for solving the shallow water equations.

5.3.1 One-dimensional Horizontal Case - Wet Bed

The first application studied is a one-dimensional problem which has the analytical solution given by Stoker [75]. In this problem, a unit width, horizontal channel of $1000m$

long is assumed. A dam is located at $x=500m$ separating the upstream and the downstream water of $10m$ and $2m$ in depth, respectively. Initially, the water is at rest on both sides. At time $t=0$, the dam is removed instantaneously (i.e., a complete dam break). Open boundaries are assumed at the upstream and the downstream ends. The grid size of $\Delta x = 5m$ and the time step of $\Delta t = 1s$ are used. Since this test is selected to validate the numerical schemes for homogeneous system, frictionless bed is assumed. The simulation was performed for $T=30s$ after the break. Figure 5-5 shows the water level profiles of the two schemes, together with the analytical solution for comparison.

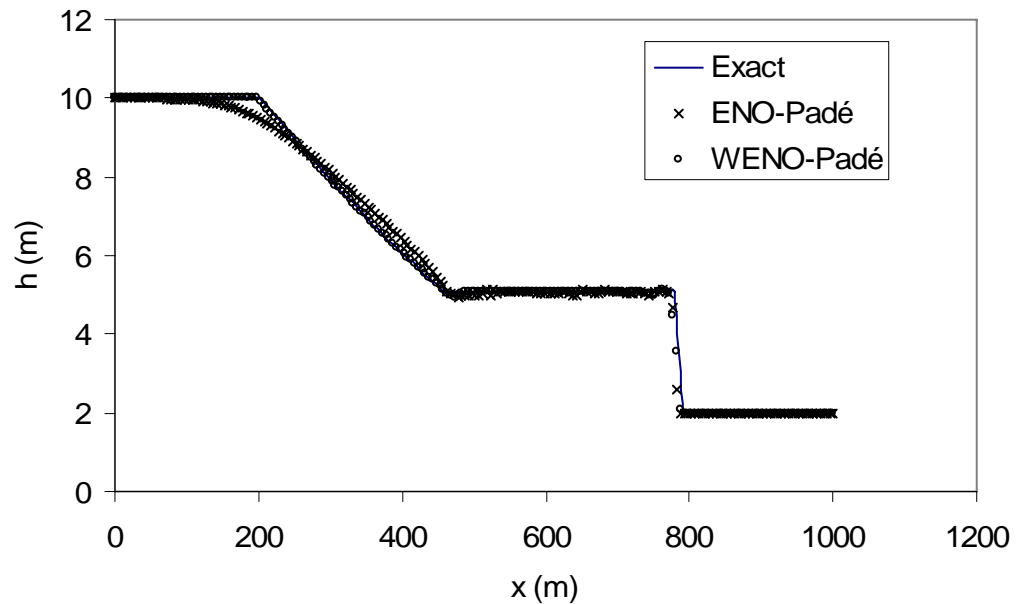


Figure 5-5 1-D dam break – water depth profile (wet bed, frictionless)

In this case the water level experiences a transition from subcritical flow to supercritical flow. A new discontinuous depression is formed and propagates upstream thus reducing the water depth, while the positive surge wave moves downstream. The height of the wave near the dam remains invariable. As observed from Figure 5-5, both schemes demonstrate good approximations to the shock fronts, with only slight diffusion

behind the shock. No oscillation is present in the profiles. In regions near the rarefaction wave, the WENO-Padé scheme produces apparently better approximation than the ENO-Padé scheme. The figure shows a good transition between subcritical flow and supercritical flow by the WENO-Padé scheme, meanwhile, the rarefaction wave is also well represented. The profiles computed by the ENO-Padé scheme, however, show noticeable smearing near the rarefaction region.

In order to further verify the results from observations, an accuracy test was conducted. The simulation was run with the grid sizes of $N=100, 200, 400, 800$. Table 5-3 reports the L_1 norm and the convergence rate for water depth and velocity of these two methods. Inspection of the results shows a roughly 0.7 order of convergence for the ENO-Padé scheme and first order convergence rate for the WENO-Padé scheme in both water level and velocity. These quantitative evaluations are basically consistent with the profiles depicted in Figure 5-5. It should be noted that in this test, similar to that of Section 5.2, all points in the numerical solution were used to measure the errors, including the points near the shock and the rarefaction waves, which lead to relatively larger error. Additionally, the degraded performance of the numerical results can be attributed to the families of characteristics intersecting the shock. It is possible for the large error near the shock to propagate out into the entire post-shock region by following a characteristic which emerges from the shock. Although below the theoretical convergence order, the numerical convergence rate nevertheless confirms that the construction of high order schemes with the combination of the ENO/WENO scheme and the compact approach is reasonable. Comparing the performances of these two models,

the error of the WENO-*Padé* scheme is nearly four to five times less than that of the ENO-*Padé* solution.

Table 5-3 Convergence test – 1-D homogeneous shallow water equations
(wet bed, frictionless)

ENO- <i>Padé</i>					
N	Δx	L_1 error (depth)	Convergence rate	L_1 error (velocity)	Convergence rate
100	10	1.66E-01		2.15E-01	
200	5	0.102659	0.70	0.13194	0.70
400	2.5	0.061311	0.74	0.076895	0.78
800	1.25	0.038615	0.67	0.049295	0.64
WENO- <i>Padé</i>					
N	Δx	L_1 error (depth)	Convergence rate	L_1 error (velocity)	Convergence rate
100	10	6.31E-02		8.39E-02	
200	5	0.027904	1.17	0.037978	1.14
400	2.5	0.013789	1.01	0.018404	1.04
800	1.25	0.007339	0.91	0.009969	0.88

5.3.2 One-dimensional Horizontal Case - Dry Bed

The numerical test presented above was based on a wet bed assumption, in which the downstream water level is comparable to that of the upstream. Sometimes there may exist another scenario, known as “dry bed” problem, in which the downstream flow has far lower water level than the upstream. In the extreme, the downstream water depth is absolutely zero. When solving the “dry bed” situation, numerical schemes usually face extra challenges in that a mixed-flow regime (i.e. supercritical and subcritical flows coexist) occurs for flow in horizontal, frictionless channels when the ratio of downstream depth to upstream depth is smaller than 0.138 [40]. This flow regime poses a special difficulty to the numerical schemes. Under a dry bed condition in extreme, the moving

boundary (dry/wetting) of a zero water depth is numerically difficult to handle. To deal with this difficulty, a common practice in numerical computations is to assume a minimum water depth or discharge on the dry bed. Such assumption is adopted in this test case. In the downstream, a water depth of $0.02m$ is assumed. The same grid sizes as for the wet bed case above with $\Delta x = 5m$ and $\Delta t = 1s$ are used. The numerical solution at $T=30s$ is shown in Figure 5-6.

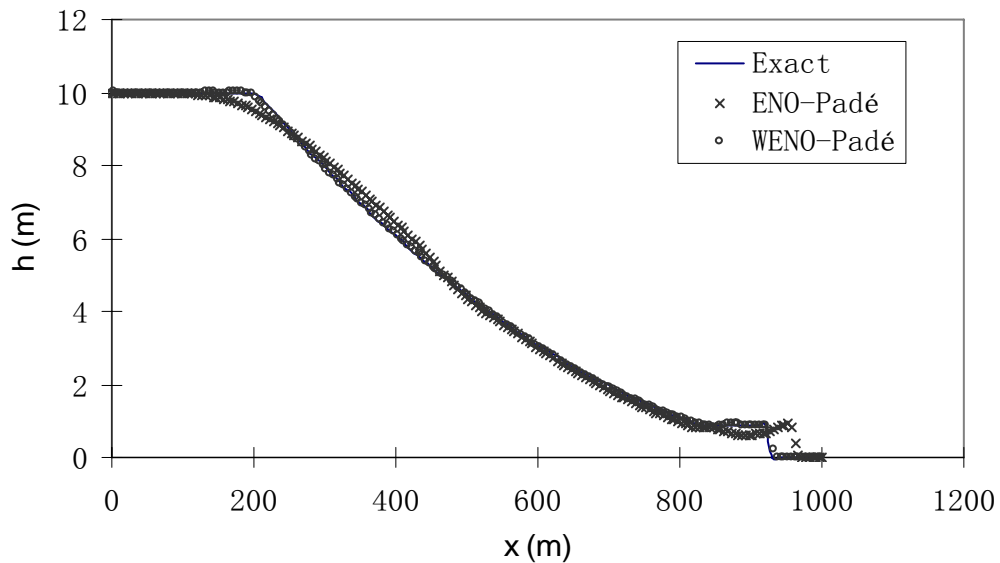


Figure 5-6 1-D dam break – water depth profile (dry bed, frictionless)

As can be seen from Figure 5-6, the WENO-Padé scheme closely tracks the shock front without causing noticeable oscillations. Also it shows accurate approximation to the transition and the rarefaction wave. The ENO-Padé scheme, however, displays relatively larger error near the shock and a damped solution in the transition.

Comparisons of the wave motion for the wet bed and dry bed cases show that when a wet bed is considered, the wave height near the dam and the new reflection wave

spreading upstream almost remain invariable. In the case of dry bed, however, it is obvious that the wave height and the wave speed change with time. The results show good approximation by the WENO-Padé scheme in capturing the shock front and the rarefaction waves for both cases, which implies that this scheme can provide better predictions for 1-D dam break simulations.

5.4 Dam Break Experiment

The test cases of dam break problems conducted above compare only simulation results with analytic solutions of idealized dam-break flows. In order to demonstrate the capability of the proposed model to describe a real dam-break situation, the model was applied to a physical laboratory experiment carried out at the Waterway Experiment Station (WES), U.S. Corps of Engineers in 1960 [89]. This experiment has been used by many authors such as Tseng [82], Bradford [13], and Hsu [43]. The experiments were conducted in a rectangular channel of $122m$ long, $1.22m$ wide with a bottom slope of 0.005 , and the Manning's roughness coefficient of 0.009 . The dam is located halfway along the channel. The water depth upstream of the dam was $0.305m$, and the downstream water depth was zero (dry bed).

The flow domain was discretized into 122 grids with uniform distribution. A constant time step of $\Delta t=0.1$ is used. An initial downstream water depth of $0.00005m$ is assumed. Figure 5-7 (a) and (b) show the simulated results and the experimental data at downstream distances of $x=70.1m$ and $x=85.4m$, respectively.

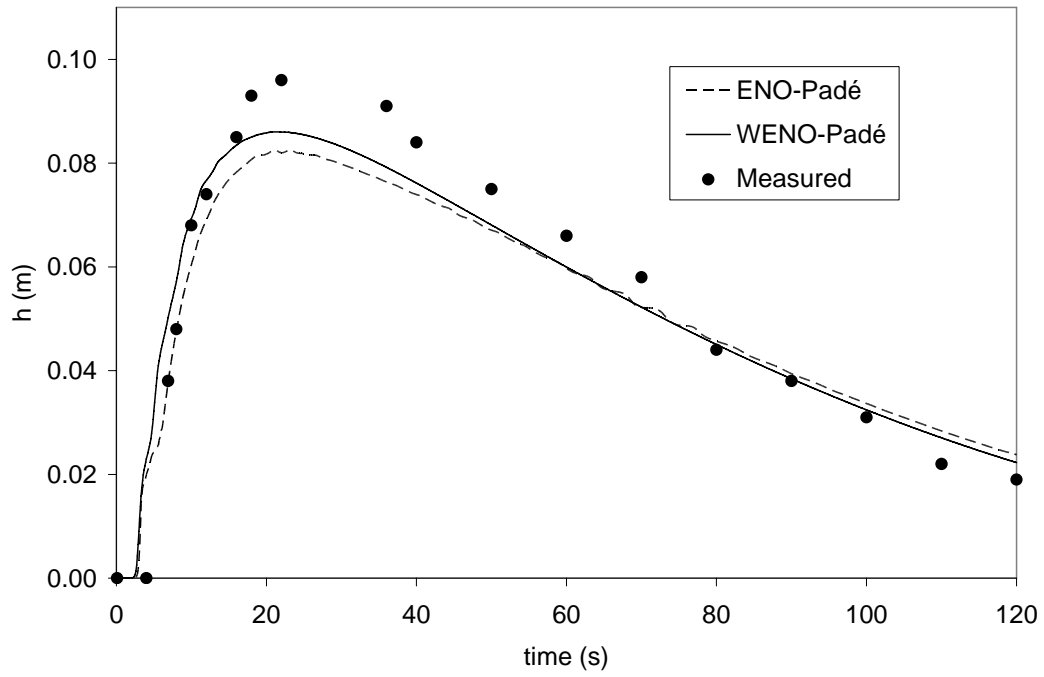


Figure 5-7 Comparison of 1-D dam break solutions for a WES experiment, $x=70.1m$

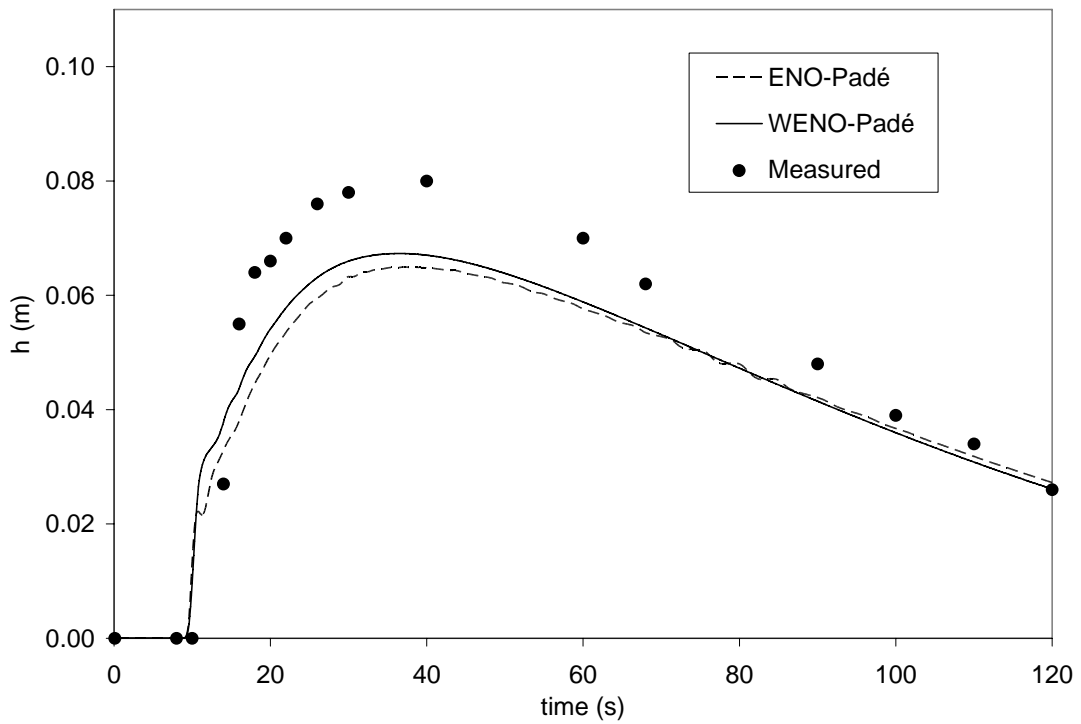


Figure 5-8 Comparison of 1-D dam break solutions for a WES experiment, $x = 85.4m$

One can see that the simulated water depth, in general, match with the values determined from measurements, with better agreement obtained in the lower to mid range of water depth. In the higher water depth regime, both models show under-predicted results. This can be caused by the highly turbulent process, for which, the 1-D shallow water equations are not adequate to describe the physical process. Comparing these two schemes, the WENO-*Padé* scheme gives slightly better approximations than the ENO-*Padé* scheme, especially in the high water depth range. The overall performances of these two models show that they are capable of simulating dam-break flows.

In summary, the numerical experiments presented in this chapter have demonstrated the capabilities of the numerical schemes in solving one-dimensional homogeneous hyperbolic equations. Comparing these two schemes, the WENO-*Padé* scheme shows superior predicting capabilities to the ENO-*Padé* scheme in terms of accuracy and rate of convergence, especially when applied to a system case – the shallow water equations. In Chapter 7, the numerical experiments are extended to solve non-homogeneous hyperbolic equations and to deal with multidimensional problems.

Chapter 6

Numerical Schemes for Non-homogeneous System Equations and Two-dimension Extension

The numerical schemes discussed so far are designed for one-dimensional homogeneous equations. In real world applications of open channel flows, bottom topography is usually varied, and the frictional effects are often not negligible. Those effects add source terms to the governing equations. Another practical issue is that in many simulations, the use of multi-dimensional models is necessary due to the complexity of the flow. In such situations, two- or three-dimensional models have to be resorted to provide more physically based description of the problem so that the realistic nature and properties of the flow can be captured. With this regard, this chapter extends the numerical schemes developed in Chapter 4 to two-space dimensions and to include the source terms.

6.1 Source Terms Treatment

In the past decades, high resolution shock-capturing schemes have been successfully applied in solving homogeneous shallow water equations. However, shallow water equations with source terms, such as irregular bed topography, bottom roughness, etc. give rise to non-homogeneous system, for which, the study is not mature yet.

In dealing with non-homogeneous problems, currently, three approaches are often used, namely, the point-wise approach [31], the upwind discretization approach [10, 31], and the fractional step approach [49]. Among them, the point-wise explicit evaluation is the simplest, by which the source terms are directly evaluated at grid points. However, problems may arise when the source term contains spatial derivatives. In such situation, upwind method is usually employed to discretize the source terms. In using this method, care must be taken to retain only the conservative variables when the flux splitting is performed. The fractional step method, on the other hand, works by separating the homogeneous part from the source terms. At each time step, one first solves the homogeneous system and then an ordinary differential equation associated with the source terms. This approach is easy to implement because the numerical techniques outlined in previous chapters for the homogeneous equations can be used directly, and the ordinary differential equations can be solved by the Euler method. In this study, the fraction step method is selected for solving non-homogeneous hyperbolic equations.

6.1.1 Strang Splitting

Strang splitting is a popular operator splitting technique. Using this technique, the system equations can be treated as augmented homogeneous problem, which is followed by the solution of an ordinary differential equation that describes the effect of the source terms. Since the focus of this chapter is to develop numerical methods for two-dimensional shallow water equations with source terms, the discussion of operator splitting is thus based on the derivation of this particular system. It is noted that this method can be generalized to other hyperbolic systems.

Recall the general form of 2-D shallow water equations given by Eq. 3.35, performing Strang Splitting, this system can be transformed into the following two augmented equations:

$$\frac{\partial Q}{\partial t} + \frac{\partial F(Q)}{\partial x} + \frac{\partial E(Q)}{\partial y} = 0 \quad (6.1)$$

$$\frac{\partial Q}{\partial t} = S(Q) \quad (6.2)$$

For solving each equation above, freedom is allowed in choosing the numerical operators. Generally, one may use the best scheme for each sub-problem. Notice that Eq. 6.1 is the homogeneous hyperbolic conservation laws defined in two dimensions. It can be solved by any shock capturing method. Eq. 6.2 is an ordinary differential equation and can be integrated using the standard implicit backward Euler scheme, which offers the advantage of numerical stability. Therefore, the overall solution procedure of this system can be given by the following three steps:

- 1) Integrate Eq. 6.2 over n to obtain Q^*
- 2) Solve Eq. 6.1 over Δt to get Q^{**}
- 3) Solve Eq. 6.2 over $\Delta t/2$ again to calculate Q^{n+1}

As mentioned above, step 1) is to find the solution of a two-dimensional homogeneous system. Solving such system with implicit schemes usually involves solving a large banded matrix. Clearly, if one could factor the space difference operators into separate spatial variables, then instead of having to solve a complex matrix problem, one would have only to solve block-tridiagonal systems using the efficient tridiagonal solver. In the past few decades, a number of numerical procedures, such as the ADI, LOD,

AOS and AFI schemes [7, 24, 41, 58, 60] have been formulated. These methods approximate the solutions of multidimensional problems by treating the spatial variables separately in a cyclic fashion, thus can achieve significant improvement in efficiency. Among those, the alternative direction implicit (ADI) approach has been used widely with success. Because of its applicability to a wide variety of problems, this method is selected for the current research. In Section 6.2, the ADI method is presented in general; then in Section 6.2.1, a detailed description is given to one family of the ADI methods – the Douglas-Gunn ADI [23], which is employed in this work.

6.2 Alternating Direction Implicit (ADI) Scheme

The idea of using alternative directions is to split the problem into one-dimensional problems. At every time step, one direction is solved using an implicit numerical approximation, and then direction alternates for the other. The ADI schemes thus developed are based upon the original ADI concept of Peaceman and Rachford [60], and Douglas and Gunn [23], which is proved to be unconditionally stable by Fourier analysis. The implicit method results in a tridiagonal matrix system, which can be solved easily by the Thomas algorithm.

6.2.1 Douglas-Gunn ADI

In this work, the Douglas-Gunn ADI scheme is used to solve two-dimensional homogeneous problems given by Eq. 6.1, which are resulted from step splitting operation of two-dimensional non-homogeneous equation. It should be noted that the splitting

errors of the ADI method is of the same order as the spatial and temporal discretization parameters for the underlying method. For this work, in particular, the ENO-Padé and the WENO-Padé schemes are the methods used for spatial discretization and the Douglas-Gunn ADI scheme with the standard Crank-Nicolson time differencing is used for time integration. According to Douglas and Kim [24], the two level right hand side differencing can reduce the splitting error from $O(\Delta t^2)$ to $O(\Delta t^3)$ for ADI schemes, so this differencing strategy is employed in the current work.

To distinguish the notation of general partial differential equations from that of the hyperbolic equations discussed earlier, here w is used to represent the variable(s) to be solved in the governing equation. Consider a multidimensional problem that has the discretized form from a finite difference approximation

$$w_i + Aw = f \quad (6.3)$$

where $A = A_1 + A_2 + \dots + A_m$, A_i is the finite difference operator in the x_i direction, and m is the spatial dimension of the problem. Applying the Crank-Nicolson time discretization method to Eq. 6.1 gives

$$\frac{w^{n+1} - w^n}{\Delta t} + \frac{1}{2}(w^{n+1} + w^n) = \frac{1}{2}(f^{n+1} + f^n) \quad (6.4)$$

Then splitting of Eq. 6.4 by Douglas-Gunn ADI algorithm gives:

$$\left(1 + \frac{\Delta t}{2} A_k\right) w^{n,1} = \left(1 - \frac{\Delta t}{2} A_1 - k \sum_{i=2}^m A_i\right) w^n + \frac{\Delta t}{2} (f^{n+1} + f^n) \quad (6.5)$$

$$\left(1 + \frac{\Delta t}{2} A_k\right) w^{n,k} = w^{n,k-1} + \frac{\Delta t}{2} A_k w^n \quad k = 2, \dots, m \quad (6.6)$$

$$w^{n+1} = w^{n,m} \quad (6.7)$$

The intermediate values $w^{n,1}, \dots, w^{n,m-1}$ can be eliminated by recursively solving Eq. 6.6. As seen from Eq. 6.5 and Eq. 6.6, for each $i=1, \dots, m$, a tridiagonal system corresponding to A_i is solved to obtain the intermediate values.

6.2.2 Douglas-Gunn ADI for 2-D Homogeneous Hyperbolic Equations

For two-dimensional homogeneous hyperbolic equation given in Eq. 6.1, assume the initial data at time t^n is known. Then with the Crank-Nicholson discretization, Eq. 6.1 can be written as:

$$\frac{Q^{n+1} - Q^n}{\Delta t} = -\frac{1}{2}(A_1^n + A_2^n)Q^n - \frac{1}{2}(A_1^{n+1} + A_2^{n+1})Q^{n+1} \quad (6.8)$$

where $A_1 = \frac{\partial F}{\partial x}$, $A_2 = \frac{\partial E}{\partial y}$ are the operators obtained from finite difference approximation

on the uniform grid over the domain.

Applying fractional steps operation, Eq. 6.8 is replaced with two one-dimensional problems:

$$\left(I + \frac{\Delta t}{2} A_1^{n+1}\right)Q^{n,1} = \left(I - \frac{\Delta t}{2}(A_1^n + A_2^n)\right)Q^n - \frac{\Delta t}{2} A_2^{n+1}Q^n \quad (6.9)$$

$$\left(I + \frac{\Delta t}{2} A_2^{n+1}\right)Q^{n,2} = \left(I - \frac{\Delta t}{2}(A_1^n + A_2^n)\right)Q^n - \frac{\Delta t}{2} A_1^{n+1}Q^{n,1} \quad (6.10)$$

where $Q^{n,2} = Q^{n+1}$. Eq. 6.9 and Eq. 6.10 are the so-called x -sweep and y -sweep equations, representing the x - and y -direction problems, respectively. ADI splitting involves two sub-iterations: the first precedes the fields from time step n to $n+1/2$, and

the second advances the fields from $n+1/2$ to $n+1$. State variables of y -direction remain explicit while the variables in x -direction are calculated. The calculation of these variables uses semi-implicit updating equations along directions, which alternate from one sub-iteration to the next.

The formula of ADI scheme thus developed can be modified in the second sub-iteration to simplify the computation as follow. By subtracting Eq. 6.9 from Eq. 6.10, one obtains

$$(I + \frac{\Delta t}{2} A_2^{n+1})Q^{n+1} = Q^{n,1} + \frac{\Delta t}{2} A_2^{n+1}Q^n \quad (6.11)$$

It is noted that the tridiagonal matrix structure is still maintained in Eq. 6.11. Usually, Eq. 6.9 and Eq. 6.11 are taken as the Douglas-Gunn splitting formula and are used in the actual computations.

Note that in ADI splitting the finite difference operators involve two time levels. The x -direction operator A_1 has levels of A_1^n and A_1^{n+1} corresponding to the spatial derivatives of $\frac{\partial F^n}{\partial x}$ and $\frac{\partial F^{n+1}}{\partial x}$. Of these two derivatives, the explicit term $\frac{\partial F^n}{\partial x}$ can be approximated directly by using the ENO-Padé or the WENO-Padé scheme. While the implicit term $\frac{\partial F^{n+1}}{\partial x}$, which could be highly nonlinear, has to be linearized first. For the y -direction operator A_2 , a similar procedure follows to compute A_2^n and A_2^{n+1} .

In the next section, one will see that the splitting given by Eq 6.9 through Eq. 6.11 can be further simplified by employing the δ -form Douglas-Gunn ADI method.

6.2.3 δ -form Douglas-Gunn ADI

Based on the standard Douglas-Gunn ADI scheme, this section outlines the transformed δ -form of this algorithm. In using δ -form, the correction to a variable is computed instead of the variable itself. At each time level, the residual is updated iteratively until a preset tolerance is reached.

In deriving the δ -form formulations, one first needs to define a correction quantity, δ , for each time step:

$$\delta Q^i = Q^{n,i} - Q^n, \quad i=1, 2 \quad (6.12)$$

In the first step, $(I + \frac{\Delta t}{2} A_1^{n+1})Q^n$ is subtracted from both sides of Eq. 6.9, which gives

$$(I + \frac{\Delta t}{2} A_1^{n+1})\delta Q^{n,1} = -\frac{\Delta t}{2}(A_1^n + A_2^n + A_1^{n+1} + A_2^{n+1})Q^n \quad (6.13)$$

In the second step, Q^n is subtracted from both sides of Eq. 6.11,

$$(I + \frac{\Delta t}{2} A_2^{n+1})\delta Q^{n,2} = Q^{n,1} - Q^n = \delta Q^{n,1} \quad (6.14)$$

Finally, the values at time level $n+1$ can be updated using

$$Q^{n+1} = Q^n + \delta Q^{n,2} \quad (6.15)$$

Note that the tridiagonal form is maintained for both Eq. 6.13 and Eq. 6.14. Therefore, the Thomas Algorithm can be used in an iterative manner. It should be pointed out that

although the derivation of the equations from Eq. 6.9 through Eq. 6.15 is based on a two-dimensional case, it can be generalized to three dimensions in a similar way.

6.3 Two-dimensional Shallow Water Equations Extension

6.3.1 Characteristics of 2-D Shallow Water Equations

In Chapter 3, the approximate Riemann solver for one-dimensional hyperbolic problem was presented in which the Roe matrix was obtained by the characteristic approach. In Chapter 5, the developed schemes were applied to one-dimensional shallow water equations. To succeed in multi-dimensional extensions of this scheme to two-dimensional shallow water equations, a study of the characteristic structure of this system is conducted.

Recall the general form of two-dimensional homogeneous hyperbolic equations as given by Eq. 6.1, in the case of shallow water equations, the Jacobian matrices for the x -direction flux, F , and the y -direction flux, E , are found as:

$$A_1 = \frac{\partial F}{\partial Q} = \begin{bmatrix} 0 & 1 & 0 \\ -u^2 + \frac{gh}{2} & 2u & 0 \\ -uv & v & u \end{bmatrix} \quad (6.16)$$

$$A_2 = \frac{\partial E}{\partial Q} = \begin{bmatrix} 0 & 0 & 1 \\ -uv & v & u \\ -v^2 + \frac{gh}{2} & 0 & 2v \end{bmatrix} \quad (6.17)$$

The eigenvalues of matrix A_I are found to be:

$$\lambda_{A_1}^1 = u + c/\sqrt{2}, \lambda_{A_1}^2 = u - c/\sqrt{2}, \lambda_{A_1}^3 = u \quad (6.18)$$

With the eigenvalues, one can compute the eigenvector corresponding to each eigenvalue. Then the diagonal matrix and the associated left and right eigenmatrices can be written out as:

$$\Lambda_{A_1} = \begin{bmatrix} u + c/\sqrt{2} & 0 & 0 \\ 0 & u - c/\sqrt{2} & 0 \\ 0 & 0 & u \end{bmatrix} \quad (6.19)$$

$$R_{A_1} = \begin{pmatrix} 1/v & 1/v & 0 \\ (u + c/\sqrt{2})/v & (u - c/\sqrt{2})/v & 0 \\ 1 & 1 & 1 \end{pmatrix} \quad (6.20)$$

$$R_{A_1}^{-1} = \begin{pmatrix} (-u + c/\sqrt{2})v/(\sqrt{2}c) & v/(\sqrt{2}c) & 0 \\ (u + c/\sqrt{2})v/(\sqrt{2}c) & -v/(\sqrt{2}c) & 0 \\ -v & 0 & 1 \end{pmatrix} \quad (6.21)$$

Following similar argument, the eigenvalues for matrix A_2 are:

$$\lambda_{A_2}^1 = v, \lambda_{A_2}^2 = v + c/\sqrt{2}, \lambda_{A_2}^3 = v - c/\sqrt{2} \quad (6.22)$$

The diagonal matrix and the eigenmatrices for matrix A_2 are:

$$\Lambda_{A_2} = \begin{pmatrix} v & 0 & 0 \\ 0 & v + c/\sqrt{2} & 0 \\ 0 & 0 & v - c/\sqrt{2} \end{pmatrix} \quad (6.21)$$

$$R_{A_2} = \begin{pmatrix} 0 & 1/u & 0 \\ 1 & 1 & 1 \\ 0 & (v + c/\sqrt{2})/u & (v - c/\sqrt{2})/u \end{pmatrix} \quad (6.22)$$

$$R_{A_2}^{-1} = \begin{pmatrix} -u & 1 & 0 \\ (-v + c/\sqrt{2})u/(\sqrt{2}c) & 0 & u/(\sqrt{2}c) \\ (v + c/\sqrt{2})u/(\sqrt{2}c) & 0 & -u/(\sqrt{2}c) \end{pmatrix} \quad (6.23)$$

Here $c = \sqrt{gh}$ is called the celerity.

6.3.2 Implementation of the Approximate Riemann Solver

To solve the transformed δ -form ADI given in Eq. 6.13 through Eq. 6.15, similar procedure to that utilized for one-dimensional equations can be performed. Specifically, the approximations to the derivatives of fluxes F and E can be computed using the ENO- β -Padé or the WENO- β -Padé scheme as described in Chapter 4. Recall that in those methods, the calculations of the interfacial quantities $Q_{i+\frac{1}{2}}$ and $F_{i+\frac{1}{2}}$ use the approximate Riemann solver with the Roe matrix computed from Roe averages. For two-dimensional problems, the Roe average given by Eq. 3.46 can be applied directly to compute $F_{i+\frac{1}{2}}$. For $E_{i+\frac{1}{2}}$, besides the evaluation of the average state in Eq. 3.46, a new average variable needs to be defined for the intermediate value of v . Having a similar form to $u_{i+\frac{1}{2}}$, the Roe average for $v_{i+\frac{1}{2}}$ is given by Toro [80] as:

$$v_{i+\frac{1}{2}} = \frac{v_{i+\frac{1}{2}}^l + \beta v_{i+\frac{1}{2}}^r}{1 + \beta} \quad (6.24)$$

where β is defined in Eq. 3.46.

Note that when applying the implicit method, the system equations results in the need for solving a block tridiagonal system. For the two-dimensional shallow water equations, the block tridiagonal matrix is made up of 3×3 block unit of dimension N_y , which have to be inverted for x_i ($i = 1, \dots, N_x$) at each time step. Here N_x and N_y are the number of nodal points in the x - and y -direction, respectively. To solve such block tridiagonal system, the Thomas Algorithm can be directly applied with all the algebraic operations

performed on matrix basis rather than on scalars. The only exception is the division operator, for which, matrix inversion should be performed. In this study, the inversion of the 3×3 matrix was calculated directly. Such explicit inverse involves only basic matrix operations, thus helps to improve the efficiency of the implementation.

Chapter 7

Numerical Results of Non-homogeneous Problems and Two-dimension Extension

Based on the discussion of the extensions of the numerical schemes to higher dimensions and the inclusion of source terms presented in Chapter 6, this chapter is devoted to the numerical tests for two-dimensional hyperbolic equations, and 1-D and 2-D problems with source terms.

7.1 One-dimensional Shallow Water Equations with Source Terms

Considering the one-dimensional homogeneous shallow water equations discussed in Chapter 5, a more complete situation is the non-homogeneous case, in which the source terms are included. In general, the source terms take into account the effects caused by bottom frictions, channel slope, and other source/sink factors. In this section, similar tests to those of the homogeneous models were conducted for non-homogeneous models. In order to compare the results, experiments were designed to use a channel that has the same configurations as that used in Chapter 5. The channel is flat, $1000m$ long, and has a

dam located at $x=500m$. Initially the water depths upstream and downstream of the dam are $10m$ and $2m$ with the water being in stationary. At $T=0$ the dam was removed instantaneously. Open boundary is applied at the lower end of the channel. To account for the bottom friction, Manning's equation is used with the roughness coefficient of 0.03 , which is considered to be a reasonable estimation for concrete channel.

Both wet bed and dry bed cases were considered. For the dry bed, a downstream water depth of $0.01m$ was assumed. A grid size of $\Delta x = 5m$ was tested with $\Delta t = 1s$. The stage profiles at $T=30s$ are shown in Figure 7-1 for wet bed. Since the analytical solution for the non-homogeneous equation is not available, that of the homogeneous problem is plotted in the figure for each case to illustrate the effects caused by bottom friction.

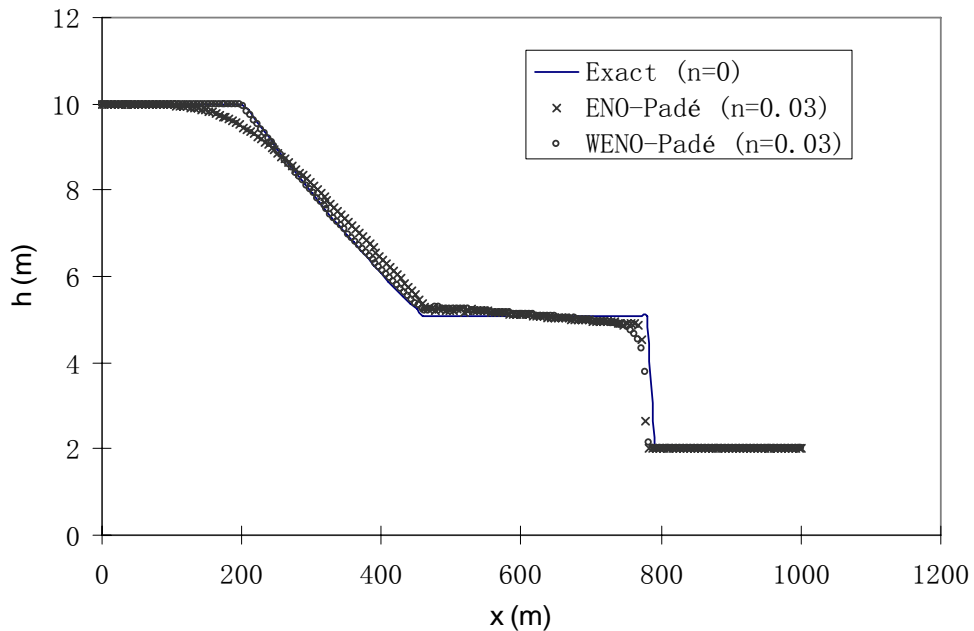


Figure 7-1 1-D dam break – water depth profile (wet bed, frictional)

The stage profiles for the dry bed case are shown in Figure 7-2.

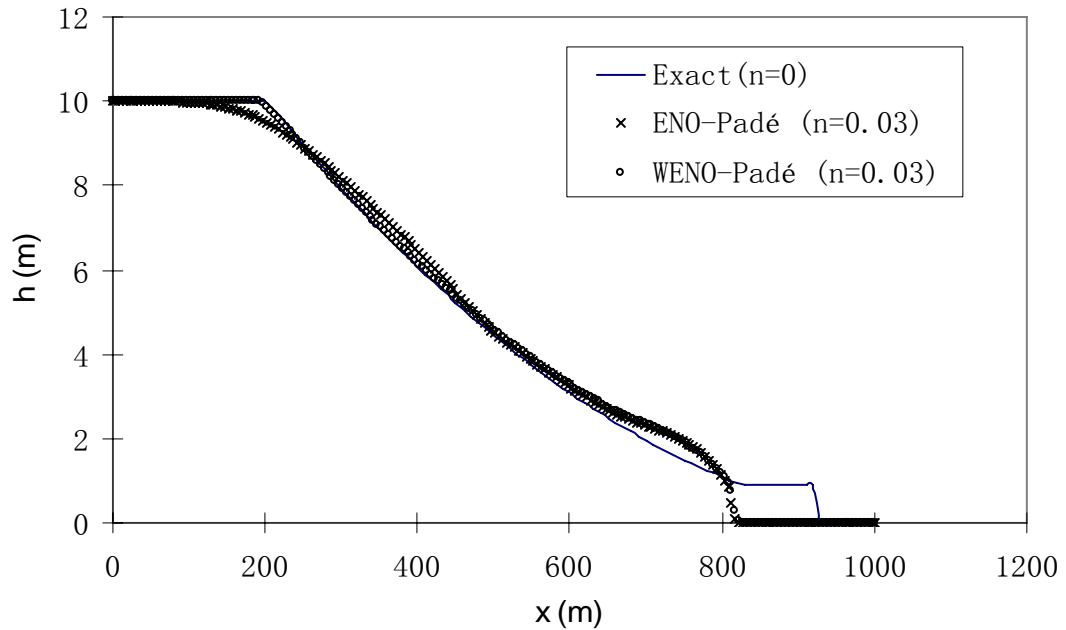


Figure 7-2 1-D dam break – water depth profile (dry bed, frictional)

For both cases, comparing the results of frictional bed with those without friction (see Figure 5-5 and Figure 5-6), it is easy to see that the stages tilt because of the bottom friction. It is also observed from Figure 7-2 that due to the dominance of the frictional force over the advancing wave front, the shock wave merges with the transition into a curved wave, which is then smoothly connected with the rarefaction. Inspection reveals that both schemes are capable of tracking the wave front properly as well as maintain a stable transition of the rarefaction wave. Comparing these two schemes, the WENO-Padé scheme produces sharp corner whereas the ENO-Padé scheme gives relatively larger smear around the corner.

In order to quantitatively assess these two schemes, self-convergence tests were performed. The L_1 error were computed for both water depth and velocity with a series of resolutions $N=100,200,400,800$. It should be noted that this method only provides

information regarding the internal consistency of the numerical method and its intrinsic convergence properties, but does not quantify the solution as compared to the “true” one.

The results are reported in Table 7-1 and Table 7-2, for which L_1 error is computed by

$$\text{Error}_N(L_1) = \sum_{i=1}^N \frac{|u_i^{\Delta x} - u_i^{\Delta x/2}|}{N} \quad (7.1)$$

where $u_i^{\Delta x}$ and $u_i^{\Delta x/2}$ are the model predicted value with the number of nodes N and $2N$,

and the convergence rate is calculated by

$$\text{Convergence rate} = \log_2 \left(\frac{\text{Error}_N}{\text{Error}_{2N}} \right) \quad (7.2)$$

Table 7-1 Convergence test – 1-D non-homogeneous shallow water equations
(wet bed, frictional)

ENO-Padé					
N	Δx	L_1 error (depth)	Convergence rate	L_1 error (velocity)	Convergence rate
100	10				
200	5	8.62E-02		1.18E-01	
400	2.5	0.047765	0.85	0.06249	0.92
800	1.25	0.024939	0.94	0.032079	0.96
WENO-Padé					
N	Δx	L_1 error (depth)	Convergence rate	L_1 error (velocity)	Convergence rate
100	10				
200	5	5.13E-02		6.63E-02	
400	2.5	0.023091	1.15	0.029332	1.18
800	1.25	0.00973	1.24	0.012907	1.18

Table 7-2 Convergence test – 1-D non-homogeneous shallow water equations
(dry bed, frictional)

ENO-Padé					
N	Δx	L_1 error (depth)	Convergence rate	L_1 error (velocity)	Convergence rate
100	10				
200	5	0.063359		0.114282	
400	2.5	0.042403	0.58	0.071197	0.69
800	1.25	0.024013	0.82	0.040499	0.82
WENO-Padé					
N	Δx	L_1 error (depth)	Convergence rate	L_1 error (velocity)	Convergence rate
100	10				
200	5	0.027474		0.061766	
400	2.5	0.014666	0.90	0.029811	1.05
800	1.25	0.006948	1.08	0.01289	1.21

For the wet bed case, the ENO-Padé scheme converges at an order of approximately 0.9 and the WENO-Padé scheme converges at an order of one. Comparison of the L_1 errors shows that the WENO-Padé model is roughly twice more accurate than the ENO-Padé model. From Table 7-2, similar results were observed for the dry bed case, for which the ENO-Padé scheme converges at a slower rate of approximately between 0.6 and 0.8, whereas the WENO-Padé scheme still converges at an order of one. Again, the error of the WENO-Padé method is less than that of the ENO-Padé method.

7.2 Two-dimensional Linear Scalar Case – Gaussian Profile

A two-dimensional linear scalar example used by Wang [87] was tested in this section. It is the rotation of a Gaussian profile given by:

$$\phi(x, y) = \exp\left(-\frac{r^2}{2\sigma^2}\right) \quad (7.3)$$

with

$$r = \sqrt{(x - x_c)^2 + (y - y_c)^2} \quad (7.4)$$

Here (x_c, y_c) is the central point of the Gaussian profile, σ is an adjustable constant. In this test, $\sigma = 1$ is used. The motivation for this test is to investigate the rotation effect on the flow field.

This problem is solved in the spatial domain $[0, 30] \times [0, 30]$ with the initial center of mass located at point $(14.6, 22.5)$. The governing equation for the rotation of scalar in Cartesian coordinate is given by:

$$\frac{\partial \phi}{\partial t} + \frac{\partial u \phi}{\partial x} + \frac{\partial v \phi}{\partial y} = 0 \quad (7.5)$$

with the rotational velocities given by

$$u = -\alpha(y - y_0), v = -\alpha(x - x_0) \quad (7.6)$$

Here α is the constant rotating velocity, which is $\pi/180$ in this case. The coordinate (x_0, y_0) is the rotational axis, and is set to $(14.6, 14.6)$. The velocity rotates in counter-clockwise direction with respect to the center of mass. An infinite open boundary condition is assumed, implying that the rotation of the scalar will not be affected by the outside condition. A uniformly spaced mesh with a grid size of $\Delta x = \Delta y = 0.3$ was used. The numerical integration was carried out by a constant time step of $\Delta t = 0.1$.

A sketch of the initial profile is given in Figure 7-3. Figure 7-4 and Figure 7-5 report the profiles computed by the ENO-Padé scheme and the WENO-Padé scheme after one

cycle of rotation. Good approximations were obtained, both in terms of the magnitude of the crest as well as the position of the cone.

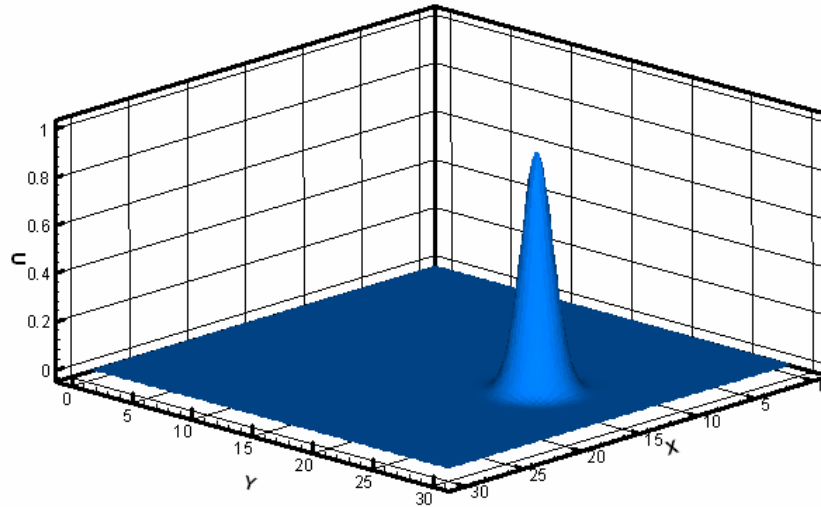


Figure 7-3 Gaussian rotation – initial profile

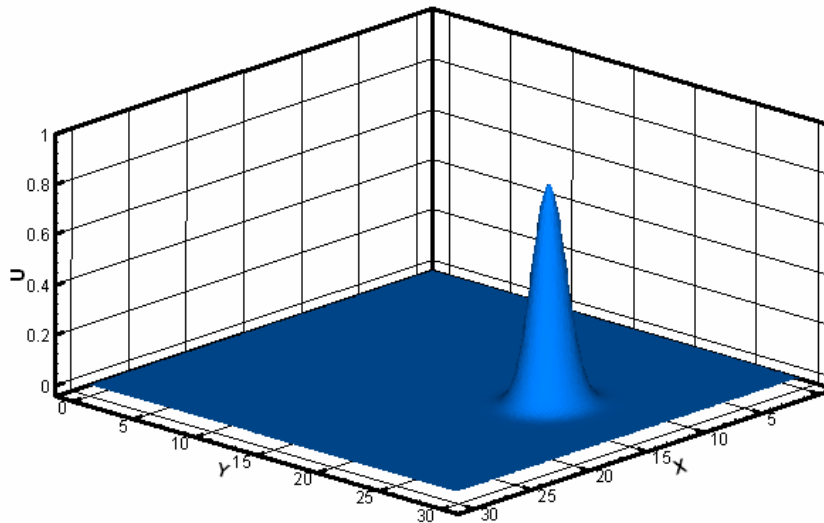


Figure 7-4 Gaussian profile after one cycle of rotation – ENO-Padé

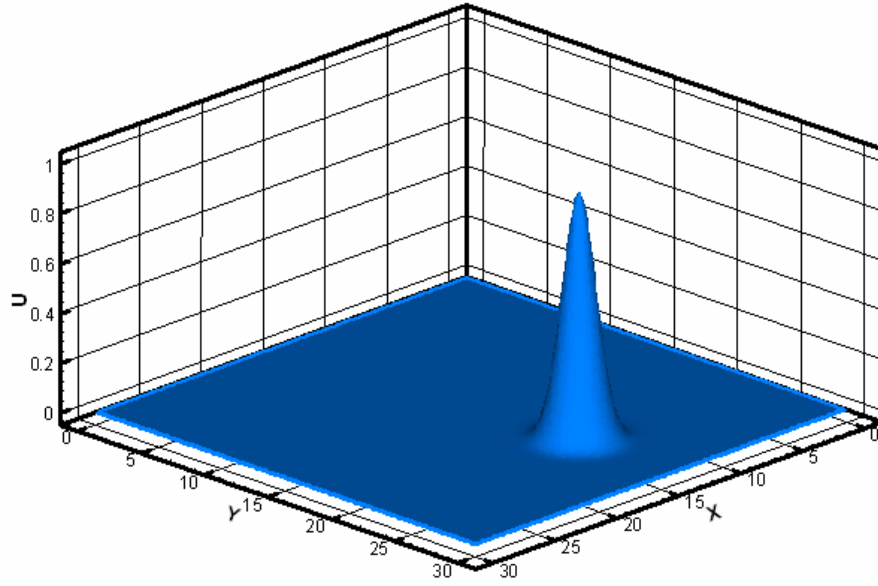


Figure7-5 Gaussian profile after one cycle of rotation – WENO-Padé

To better inspect the results and compare with the analytical solution, a 2-D plane was extracted by cutting a slice through the middle of the cone along $x=14.6$, which depicts the cone shape and the magnitude of the peak. The comparison of the numerical results of these two schemes with the analytical solution is presented in Figure 7-6.

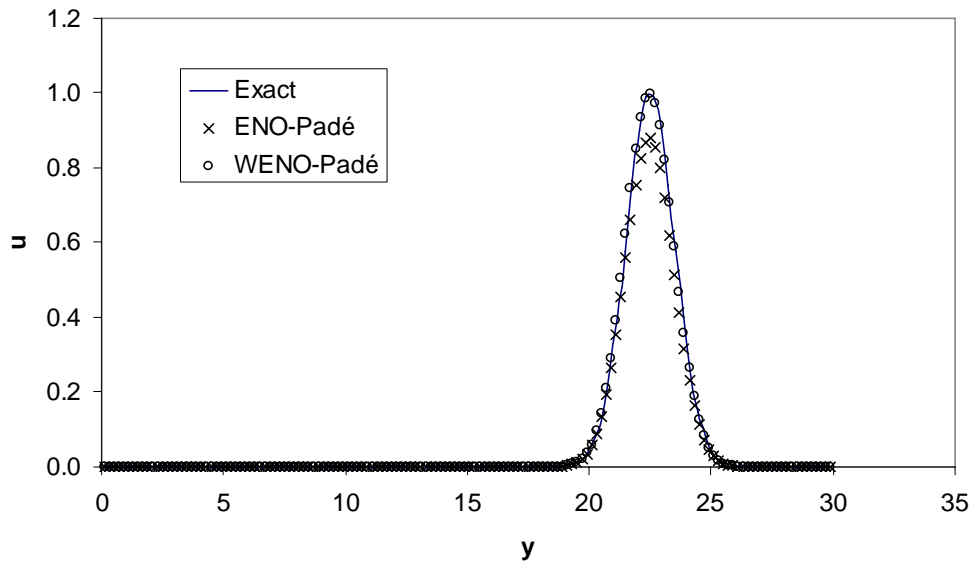


Figure 7-6 Comparison of the plane at $x=14.6$ with the exact solution

In general, the features of the profile are captured by both schemes. Comparison of these two models reveals that the shape of the cone is well preserved by the WENO-Padé scheme, while the ENO-Padé scheme produces relatively larger smear of the peak. The results indicate that the WENO-Padé scheme is more stable than the ENO-Padé scheme for this rotation problem.

7.3 Two-dimensional Nonlinear Scalar Case – Burger’s

Equation

The third test considered is the two-dimensional Burger’s equation used by Shu *et al.* [73]. The problem is defined as

$$u_t + \left(\frac{u^2}{2}\right)_x + \left(\frac{u^2}{2}\right)_y = 0 \quad [-1 \leq x \leq 1, -1 \leq y \leq 1] \quad (7.7)$$

where the initial condition of four constant states given are:

$$u(x, y, 0) = \begin{cases} u_1 & x > 0, y > 0 \\ u_2 & x < 0, y > 0 \\ u_3 & x < 0, y < 0 \\ u_4 & x > 0, y < 0 \end{cases} \quad (7.8)$$

Open boundaries are implemented, i.e. the outside region of the four states are maintained constant as the initial value. A computational grid size of $\Delta x = \Delta y = 0.05$ with a time step of $\Delta t = 0.005$ was used. Starting from the initial state of $(-1, -0.2, 0.5, 0.8)$, integration of Eq. 7.7 over time until $T=1$ gives the results as depicted in Figure 7-7 and Figure 7-8 for the ENO-Padé and the WENO-Padé scheme, respectively.

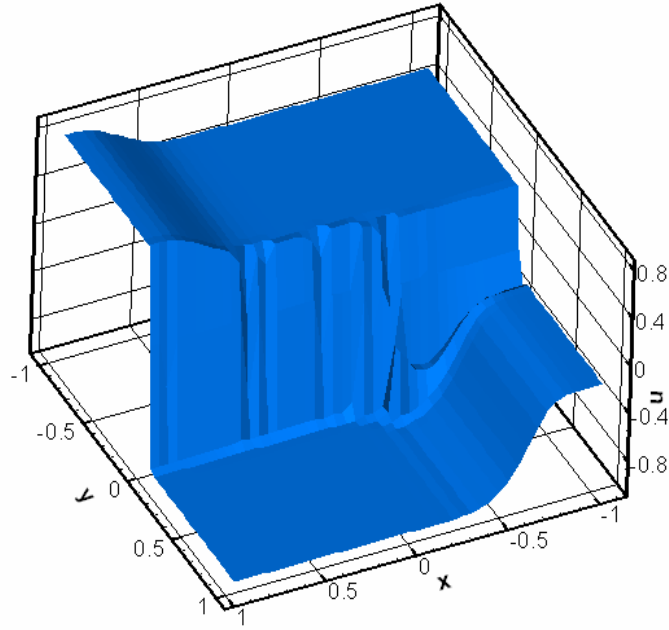


Figure 7-7 2-D Burger's equation – ENO-Padé

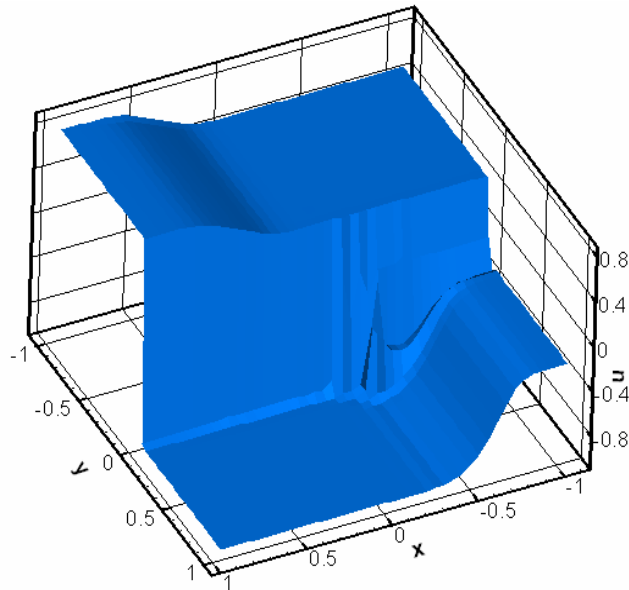


Figure 7-8 2-D Burger's equation – WENO-Padé

It is clearly seen that in the mid region of the domain along the y -axis, a pair of shocks develops. Along the x -axis, rarefaction is formed traveling towards the outside. This test is utilized to illustrate how well these two methods cope with the interaction of

shocks and rarefactions. The results in Figure 7-7 and Figure 7-8 reveal that the shocks were tracked by both schemes. Further assessment was made by cutting slices along the middle of the x -axis through the y -axis. The resultant line graph in the 2-D plane represents the wave profile expanding in the x -direction. The results of both schemes are plotted in Figure 7-9. One can see that well maintained wave profiles are obtained by both models. Comparing these two profiles, the WENO-Padé method keeps “sharper” transitions at the corners than the ENO-Padé method, indicating a better shock capturing capabilities of the WENO-Padé model.

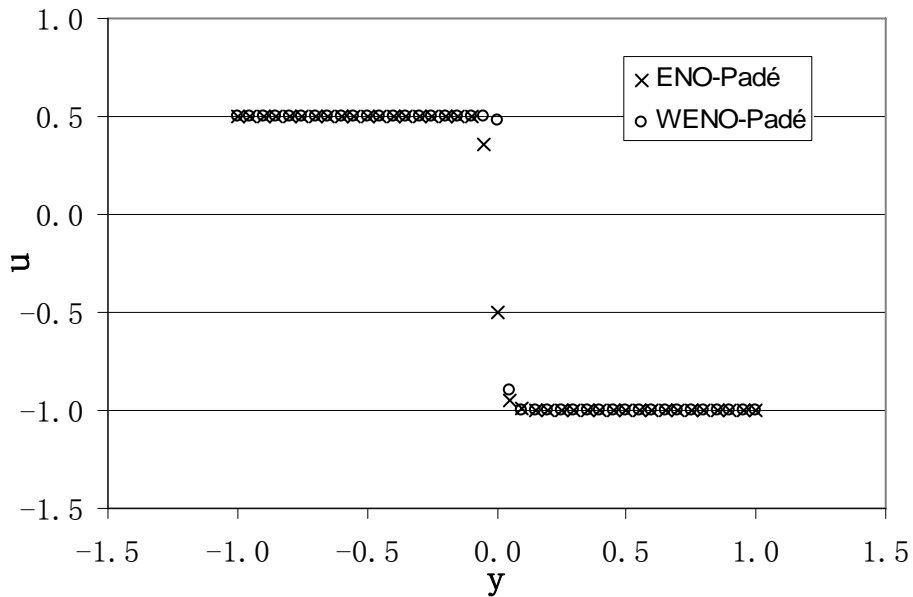


Figure 7-9 2-D Burger's equation plane comparison at $x=0$

7.4 Two-dimensional Dam Break - Wet Bed, Frictional

In this section, experiment was conducted to test the two-dimensional numerical schemes for solving dam break problems analogous to the 1-D problem presented in

Chapter 5. In this test, the computational domain consists of a channel in a $200m \times 200m$ square region with a flat bottom. A dam is located at $x=100m$, parallel to the y -axis across the channel. The initial water depth is $10m$ at the upstream and $5m$ at the downstream of the dam, both being in a stationary state. Along the wall, solid boundary conditions are applied, implying that the normal velocity (perpendicular to the wall) is zero, while the latitudinal velocity on the wall is allowed. Constant water depths are assumed at the upstream and the downstream ends of the channel. The grid sizes are chosen to be $\Delta x = 4m$ and $\Delta y = 4m$. A time step of $\Delta t = 0.1s$ is used. In order to coincide with the grids, a wall thickness equal to the x -direction grid size is assumed for the dam so that the two edges of the dam reside on two consecutive lines of the mesh. In this test, frictional bed is considered, for which Manning's roughness coefficient is set to 0.03 . At $T=0$, the dam instantaneously collapsed resulting in a $75m$ wide breach in the middle of the dam. On the broken of the dam, a bore propagates downstream and spreads laterally. Meanwhile, a rarefaction wave travels towards the upstream.

Simulation of the flood flow is performed to a final time of $T=9$. The simulated water depth profiles of the ENO-*Padé* method and the WENO-*Padé* method are presented in Figure 7-10 and Figure 7-11. It can be seen that both schemes are able to capture the shock front and the backward rarefaction, which is an indication that the models are implemented correctly. A plane view of the velocity contour is also plotted in Figure 7-12 for the WENO-*Padé* scheme to illustrate the magnitude and the direction of the velocity vectors.

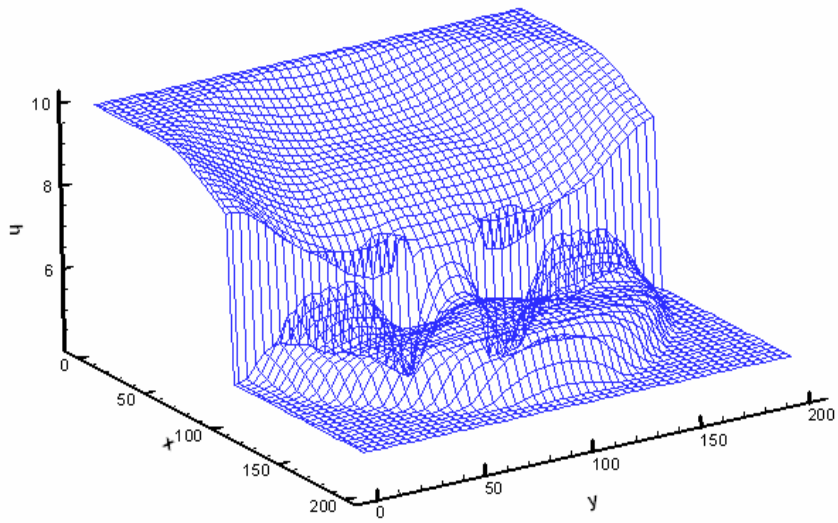


Figure 7-10 Water depth of 2-D dam break - ENO-Padé (wet bed, frictional)

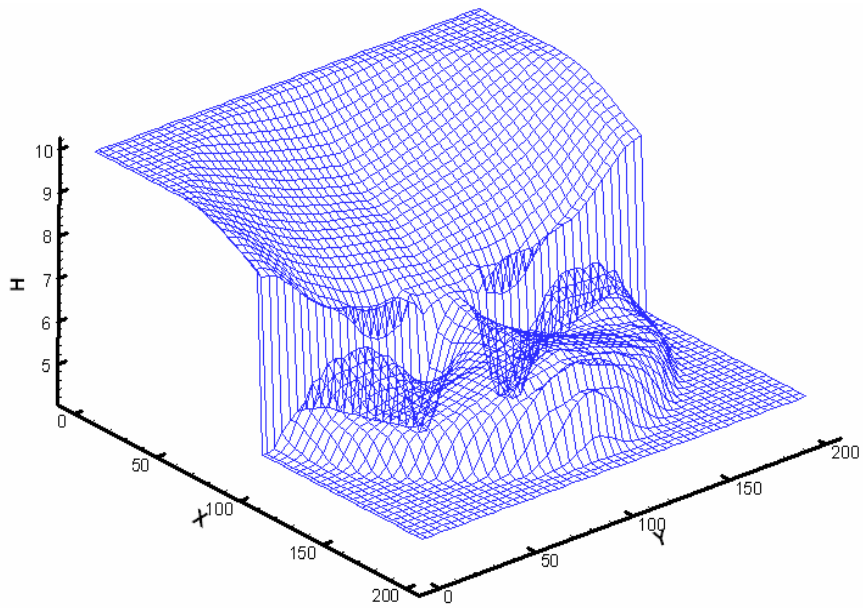


Figure 7-11 Water depth of 2-D dam break – WENO-Padé (wet bed, frictional)

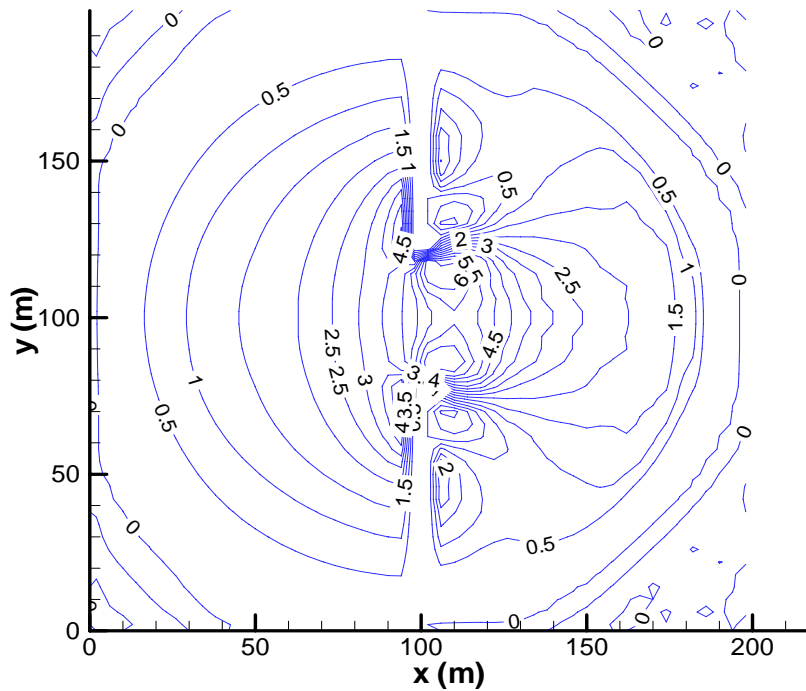


Figure 7-12 Velocity contour of 2-D dam break – WENO-Padé (wet bed, frictional)

A closer inspection was made to compare the performances of these two methods, for which a plane along the centerline of the breach parallel to the x -axis was extracted. Since this plane of centerline represents the main stream of the flow, which consists of the wave front, it adequately reflects the characteristics of the flow propagation. The water depth profile is presented in Figure 7-13. One can see that these two schemes agree well with each other. Both present a profile that is similar to the validated one-dimensional models in Chapter 5, which implies that the two-dimensional ENO-Padé and WENO-Padé scheme are intrinsically correct.

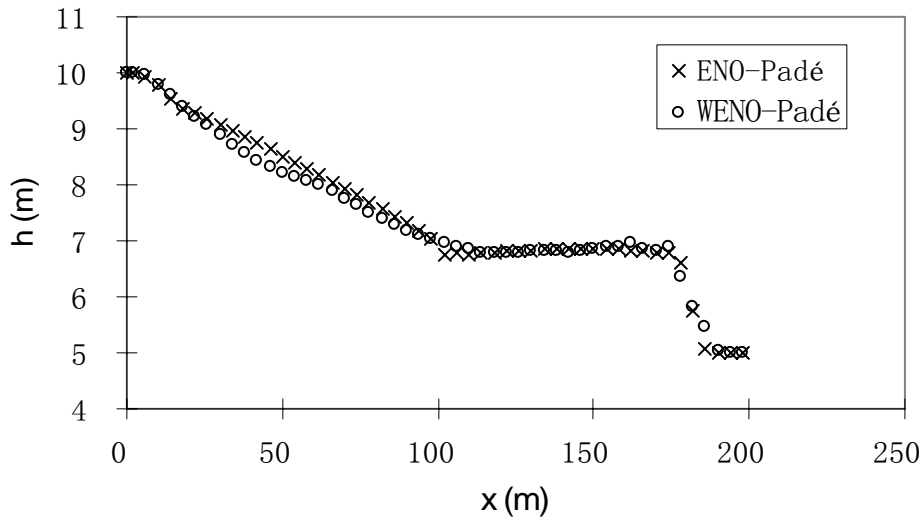


Figure 7-13 2-D dam break – water depth profile comparison of the central line (wet bed, frictional)

In order to further assess the accuracy of these two schemes, self-convergence tests were performed. The L_1 error were computed for water depth (h) and velocity vectors (u and v) with a series of resolutions $N=20,40,80,160$. These values along with the convergence rate are summarized in Table 7-3. One can see from the table that the ENO-Padé scheme converges at less than unity while the WENO-Padé scheme converges at approximate order of one. Comparison of the L_1 errors shows that the error in the prediction of the WENO-Padé model is less than that of the ENO-Padé model and is roughly twice more accurate than the ENO-Padé model.

Table 7-3 Convergence test – 2-D non-homogeneous shallow water equations (wet bed, frictional)

ENO-Padé							
N	$\Delta x (= \Delta y)$	L ₁ error (depth-h)	Convergence rate	L ₁ error (velocity-u)	Convergence rate	L ₁ error (velocity-v)	Convergence rate
20*20	10						
40*40	5	0.18331		0.198273		0.128682	
80*80	2.5	0.099212	0.89	0.118665	0.74	0.089897	0.52
160*160	1.25	0.050276	0.98	0.065183	0.86	0.05502	0.71
WENO-Padé							
N	$\Delta x (= \Delta y)$	L ₁ error (depth-h)	Convergence rate	L ₁ error (velocity-u)	Convergence rate	L ₁ error (velocity-v)	Convergence rate
20*20	10						
40*40	5	0.12501		0.157837		0.108179	
80*80	2.5	0.05971	1.07	0.07653	1.04	0.05649	0.94
160*160	1.25	0.026987	1.15	0.035468	1.11	0.027979	0.98

7.5 Two-dimensional Dam Break Experiment

In this section, the implementation of the two models was validated against the experimental data of flood wave propagation due to a partial dam-break by Fraccarollo and Toro [29], which has been widely tested by many authors [30, 34, 46, 95]. The experimental flume, shown in Figure 7-14, is $3m$ long and $2m$ wide. The area occupied by the reservoir is $1m$ in the x -direction and $2m$ in the y -direction. A breach of $0.4m$ wide is symmetrically centered on the wall. The bottom of the reservoir and floodplain is horizontal. The three flood-plain boundaries are all open. In the selected case, the initial water depth in the reservoir is $0.6m$ and the floodplain is dry. Five stations for measuring stage hydrographs are shown in Figure 7-14 and their coordinates are listed in Table 7-4. In the simulation, model velocities normal to closed boundary are taken equal to zero. To ensure numerical stability of the schemes, a water depth of $0.001m$ is assumed for the flood plain. The computational domain is discretized into rectangular cells with $\Delta x=0.1m$, $\Delta y=0.1$ m. Similar to the 1-D case, a wall of $0.1m$ in thick is assumed to allow the two sides of the wall residing on the grids so that the solid boundary can be easily implemented.

Table 7-4 Location of stage gauges

Stations	-5A	C	4	0	8A
X(m)	0.18	0.48	1.00	1.00	1.722
Y(m)	1.00	0.40	1.16	1.00	1.00

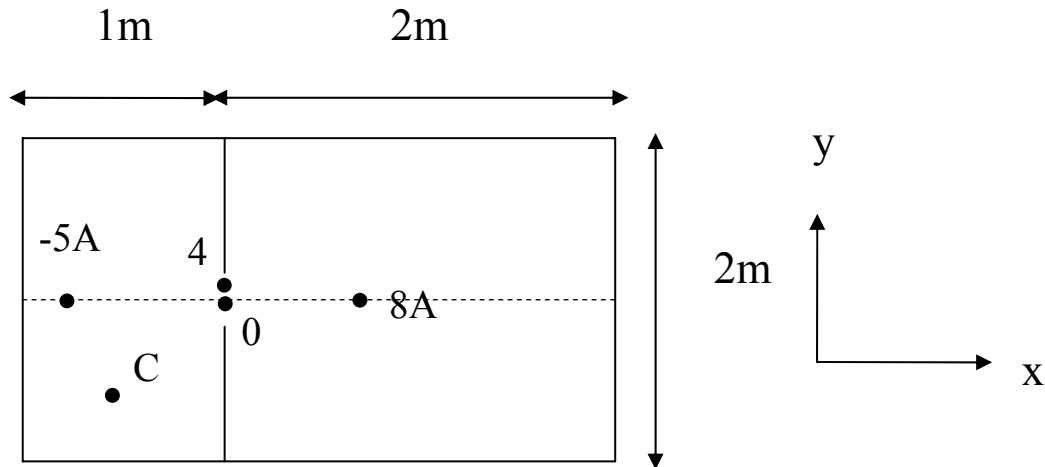


Figure 7-14 2-D dam break experiment – plane view of the domain and location of stage gauges

Figure 7-15 - Figure 7-19 present the observed and the simulated results of water depth by the ENO-Padé and the WENO-Padé method at those five gauges. After the sudden opening of the gate, a surge is formed and propagates over the floodplain. Simultaneously, a strong depression wave occurs in the reservoir and causes the water surface near the gate to descend drastically. In general, reasonable agreement between the measured and the computed results are achieved: the changing pattern of the water depth in the reservoir and in the flood plain developed as the models predicted; the magnitude is basically within the simulated scopes except in the reservoir, where the models somewhat over-predicted the water depth. This can be explained as caused by the effects of the thickness of the wall, which imposed larger sheer stress on the streams flowing through the breach, thus reduced the velocity of the flow. Comparable results are obtained by these two methods.

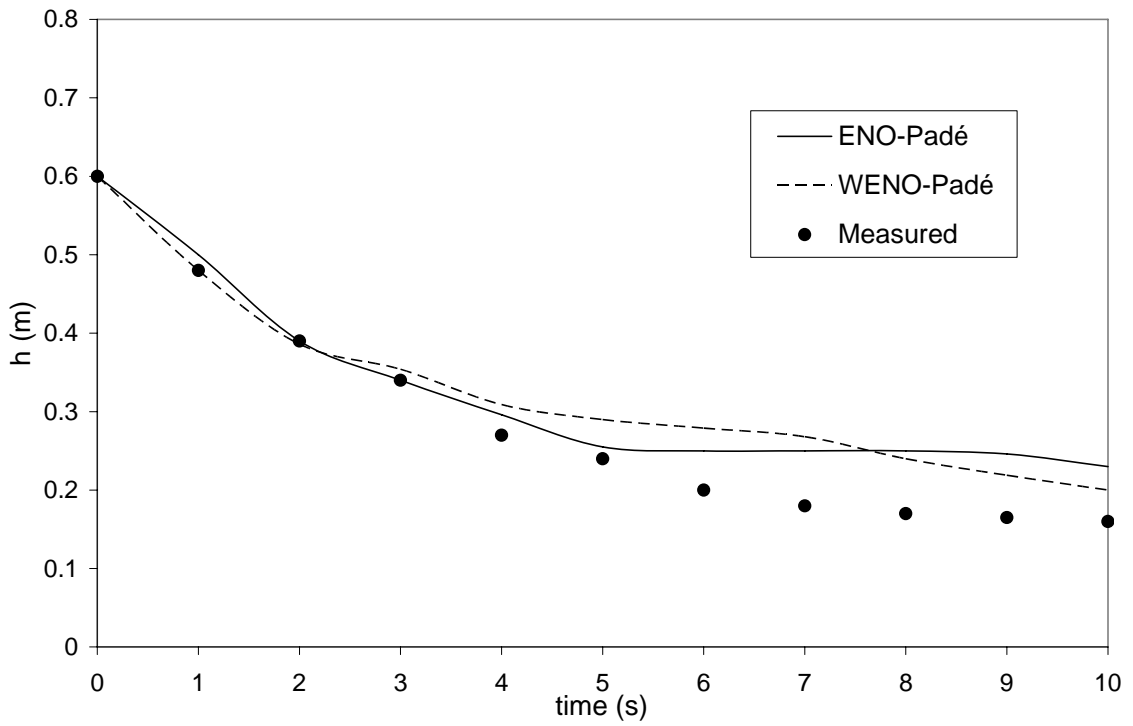


Figure 7-15. Comparison of stage hydrographs at gauge -5A

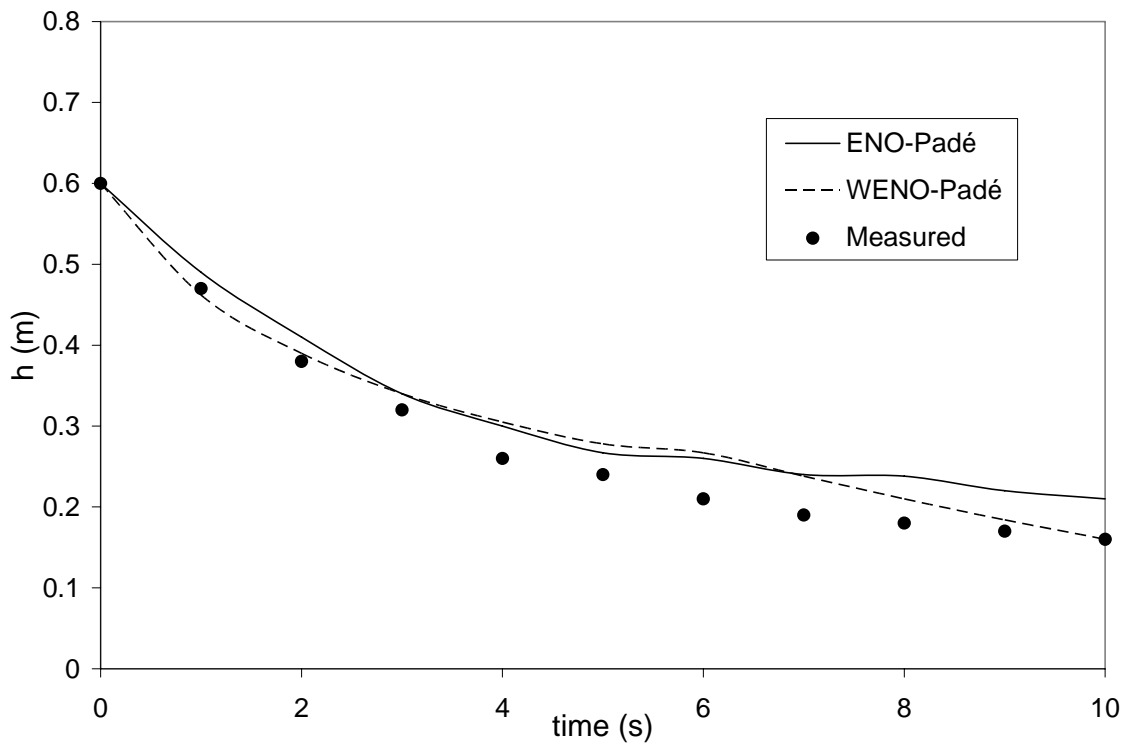


Figure 7-16. Comparison of stage hydrographs at gauge C

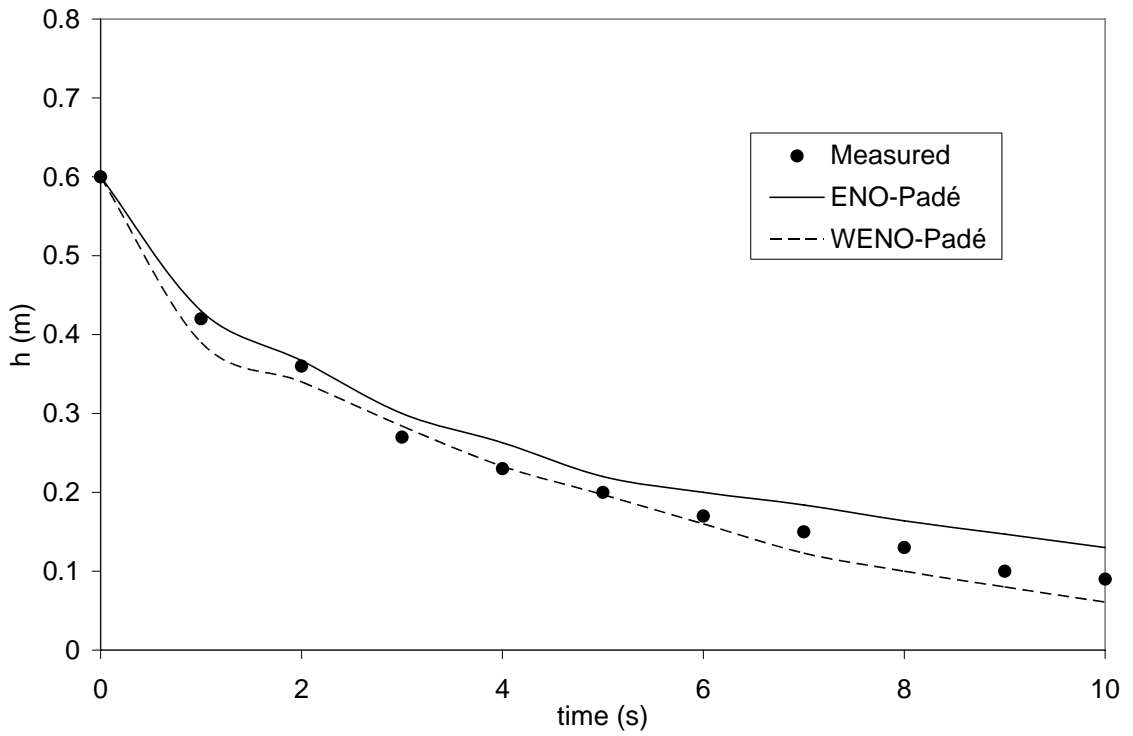


Figure 7-17. Comparison of stage hydrographs at gauge 4

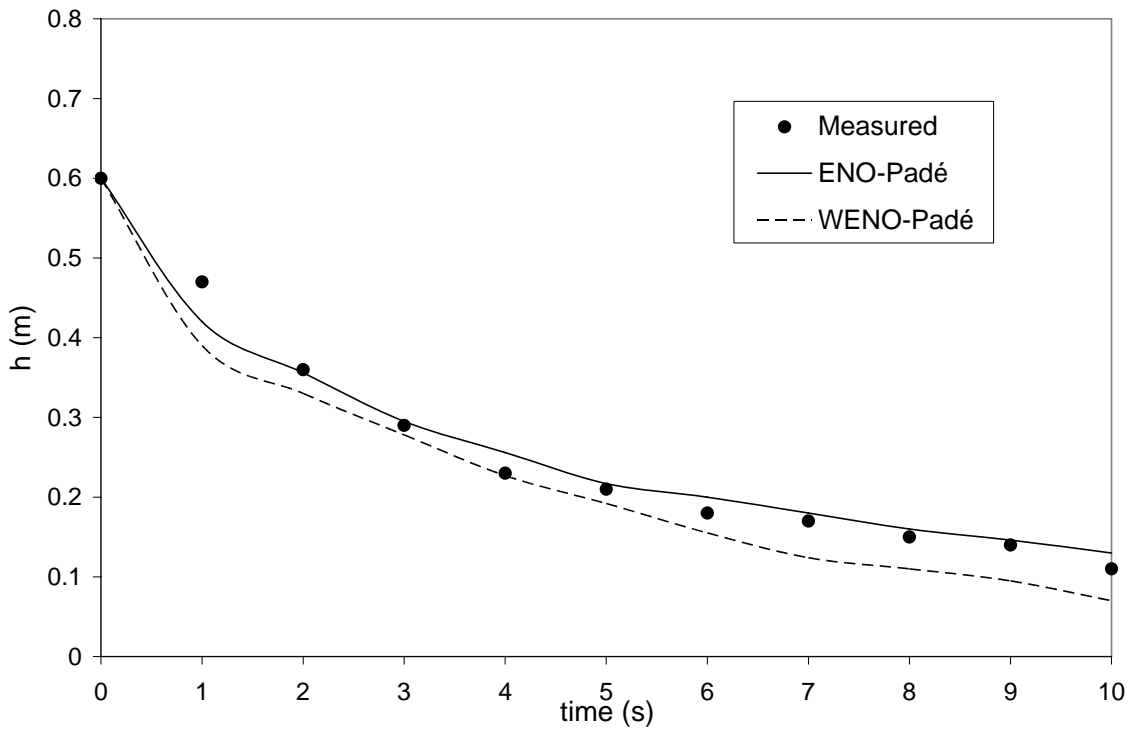


Figure 7-18. Comparison of stage hydrographs at gauge 0

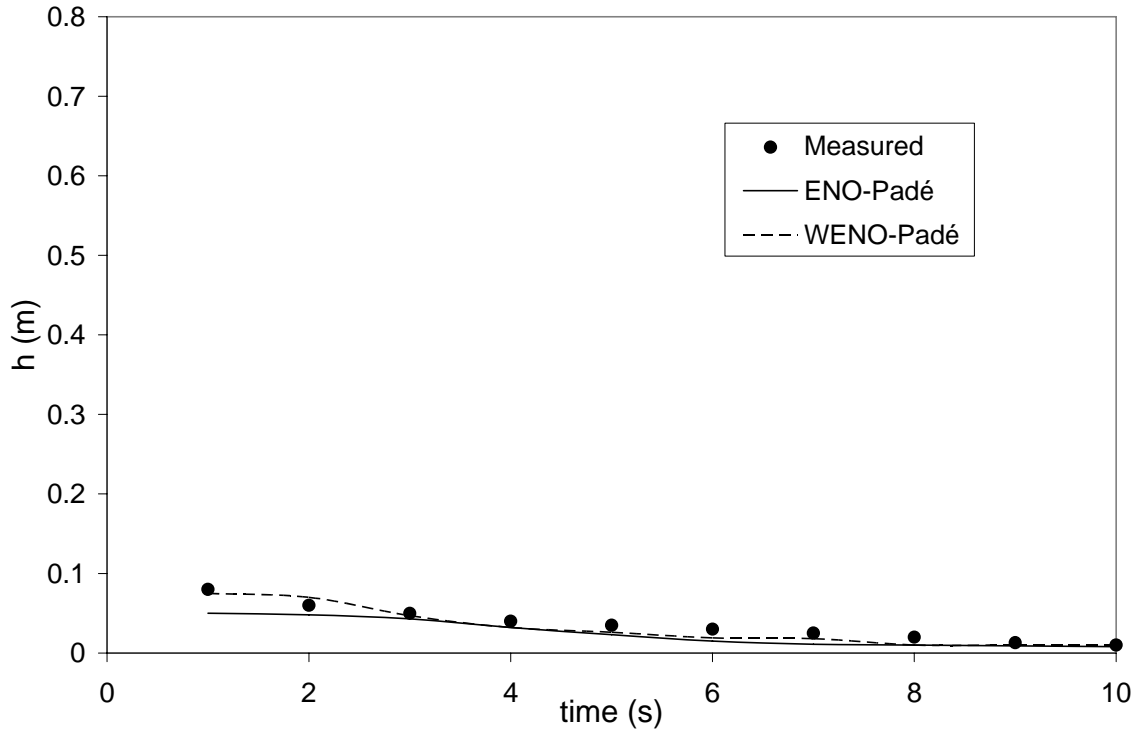


Figure 7-19. Comparison of stage hydrographs at gauge 8A

In summary, the schemes developed in Chapter 6 were tested in this chapter for one-dimensional and two-dimensional scalar equation and system equations. Numerical results indicate good shock transition without noticeable oscillations near the discontinuities and high accuracy in smooth regions for both schemes. Comparing these two schemes, the WENO-Padé scheme gives better overall performance for simulating shocks than the ENO-Padé scheme.

Chapter 8

Conclusions and Future Work

In this dissertation, a new family of high order finite difference scheme was developed to resolve the discontinuous phenomena in hyperbolic equations. The spatial discretization is based on a hybrid of high order compact central type Padé scheme with a weighted essentially non-oscillatory (WENO) reconstruction. The semi-implicit Crank Nicolson (CN) scheme is employed for the temporal discretization. Based on the one-dimensional framework, the scheme is extended to two dimensions using the Douglas-Gunn alternating direction implicit (ADI) method. The non-homogeneous problem is dealt with by the Strang splitting technique. In principle, an arbitrary order of accuracy in space can be constructed by the scheme developed in this dissertation. Third order is employed in the scheme implementation and numerical tests based on accuracy and efficiency consideration of the applications in this work.

Particularly, high order difference is constructed by performing a reconstruction of the variable from cell average and uses this reconstruction to approximate the point-wise values and the associated spatial derivative of the flux function. The essentially non-oscillatory (ENO) scheme and the weighted essentially non-oscillatory (WENO) scheme are employed to perform the reconstruction. These schemes are derived from the scalar wave equation and generalized to system equations. The generalizations are accompanied by approximate Riemann solvers. The approximate Riemann solver of Roe is used. The

ENO/WENO schemes use a local adaptive stencil to obtain information automatically from regions of smoothness when the solution contains discontinuities. As a result, approximations using these methods can obtain uniformly high order accuracy up to discontinuities while keeping a sharp, essentially non-oscillatory shock transition. Upwinding is achieved by the initial biased stencil. The Crank-Nicolson scheme is employed for time discretization to take the advantage of its unconditional stability.

The Douglas-Gunn ADI method is used to provide a way to solve multidimensional homogeneous problems. In dealing with the source terms, the Strang splitting technique decouples the source terms from the genetic homogeneous equations, thus the combined scheme is portable in solving any complex multi-dimensional non-homogeneous equations. To validate the accuracy and effectiveness of the schemes, various numerical tests were conducted. The tests include one- and two-dimensional scalar and system hyperbolic equations. For scalar cases, both linear and nonlinear problems are solved. For systems cases, homogeneous and non-homogeneous equations are solved. The numerical results are compared against the available analytical solutions and data from published results of laboratory and field measurements.

The numerical results reveal practical evidence of the good performance using the current developed approach. In terms of shock capturing, both schemes give equally good resolution of the leading shock. Further inspections show that results obtained by the WENO-Padé scheme are more accurate in approximating the rarefaction wave. For the

ENO-Padé scheme, the corners at the ending points of the rarefaction wave are usually rounded, showing a tendency to diffuse the solution.

Effectiveness and efficiency are two other issues also considered in this study. The two methods developed are based on the same underlying framework, i.e. spatial discretization and temporal integration. The difference between them lies in the technique for variable reconstruction of interfacial values. Of these two methods, the ENO scheme is conceptually straight forward. However, the searching for an optimal stencil is time consuming due to the comparison-selection procedure at each phase. Additionally, the ENO scheme sometimes places too tight criteria for choosing stencils which is prone to smearing the corners. The WENO scheme can completely remove the logical operations that appear in the ENO scheme, thus is easier to implement and is more efficient. Also, the WENO scheme maintains the high order characteristics of the ENO scheme but with less stringent requirement on the stencil, thus making the numerical flux smoother. It is expected that this smoothness allows larger time steps to be used in the time integration. On the whole, the hybrid WENO-Padé scheme shows better performance in capturing shocks and simplicity in coding. However, the derivation of WENO scheme needs more complex theoretical development. Considering the computational cost, the WENO-Padé scheme is faster compared to the ENO-Padé scheme, especially for two-dimensional problems. Usually the ENO-Padé scheme requires between 2 to 3 as much time as the WENO-Padé scheme. This is due to the expensive ENO interpolation in choosing the smoothest stencil.

The two schemes presented in this dissertation are applied on rectangular coordinates and uniform grid. It is possible to generalize these methods to other coordinate systems. However, a main restriction to this generalization is that conservative finite difference schemes can be achieved only on uniform rectangular or smooth curvilinear meshes.

From this work, it is found that there are several issues that need further investigations. One is the implementation of the numerical schemes on non-uniform grid. With the same interpolation idea of ENO/ WENO, the criteria have to be carefully designed for measuring smoothness to comply with automatic stencil shifting on a non-uniform grid. The scheme based on non-uniform grid could be far more complicated for multi-dimensional problems. It should be also pointed out that the study of multi-dimensional conservation laws on non-uniform grid is not mature.

Another issue is the usage of adaptive techniques for high order accuracy. Currently, the adaptive methods have gained wide attention. It is expected that by using this technique, the mesh density can be automatically modified such that special features of interest, such as the shocks in this study, can be easily captured in the refined portion of the mesh. Meanwhile, since the computation demands by the coarse part of the mesh are low, the overall computational expenses can be kept within a reasonable level.

Appendices

Appendix A

Some Numerical Flux Schemes and High Resolution Methods

Besides the Godunov scheme, another type of upwind scheme is the flux vector splitting schemes, in which the flux is split into two parts

$$F = F^+ + F^- \quad (\text{A.1})$$

where the components are defined as

$$F^- = (F - |F|)/2, \quad F^+ = (F + |F|)/2 \quad (\text{A.2})$$

Then the interface flux becomes

$$F_{i+\frac{1}{2}} = \frac{1}{2}(F_{i+1} + F_i) + \frac{1}{2}(|F|_{i+1} - |F|_i) \quad (\text{A.3})$$

One can see that the upwind direction is chosen automatically depending on the sign of the flux. This feature provides the advantage of no oscillation generation near a discontinuity.

For the second order schemes, a popular one is the Lax-Wendroff scheme. By retaining the first order terms, the scheme can be written as

$$F_{i+\frac{1}{2}} = \frac{1}{2}(F_{i+1} + F_i) - \frac{\Delta x}{2\Delta t} (A_{i+\frac{1}{2}}(Q_{i+1} - Q_i)) \quad (\text{A.4})$$

with

$$A_{i+\frac{1}{2}} = \frac{1}{2}(A_{i+1} + A_i) \quad (\text{A.5})$$

Another second order scheme is the McCormack scheme. In this scheme, a predictor-corrector procedure is involved:

$$Q_i^* = Q_i^n - \frac{\Delta t}{\Delta x}(F_{i+1}^n - F_i^n) \quad (\text{A.6})$$

$$Q_i^{n+1} = \frac{1}{2}(Q_i^n + Q_i^*) - \frac{\Delta t}{2\Delta x}(F_i^* - F_{i-1}^*) \quad (\text{A.7})$$

To develop high resolution methods, one approach is to add artificial diffusion to eliminate spurious oscillations. A typical example is the improved McCormack scheme, for which the added numerical viscosity reduces the oscillation by conducting the following predictor-corrector steps:

$$Q_i^* = Q_i^n - \frac{\Delta t}{\Delta x}(F_{i+1}^n - F_i^n) \quad (\text{A.8})$$

$$Q_i^{n+1} = Q_i^{Mac} + \varepsilon_{i+\frac{1}{2}}(Q_{i+1}^{Mac} - Q_i^{Mac}) - \varepsilon_{i-\frac{1}{2}}(Q_i^{Mac} - Q_{i-1}^{Mac}) \quad (\text{A.9})$$

Another approach of constructing high resolution methods is to apply limiters. This approach stems from the earliest attempt of the FCT scheme, which consists of anti-diffusion flux. With flux correction, the scheme is given by

$$F_{i+\frac{1}{2}} = F_{i+\frac{1}{2}}^{LW} + (F_{i+\frac{1}{2}}^{LW} - F_{i+\frac{1}{2}}^{HI}) \quad (\text{A.10})$$

where $F_{i+\frac{1}{2}}^{HI}$ is the flux calculated using a higher order scheme while $F_{i+\frac{1}{2}}^{LW}$ is the flux

calculated using a first order upwind scheme, and $F_{i+\frac{1}{2}}^{LW} - F_{i+\frac{1}{2}}^{HI}$ is the correction term.

Some limiters applied on the above modified flux include:

Yee's TVD limiter:

$$F_{i+\frac{1}{2}} = F_{i+\frac{1}{2}}^{HI} + \phi(\beta^+, \beta^-)(F_{i+\frac{1}{2}}^{LW} - F_{i+\frac{1}{2}}^{HI}) \quad (\text{A.11})$$

Here $\phi(\beta^+, \beta^-)$ is a limiter function. If the data is smooth, ϕ is close to 1, and if near large gradient, it is chosen near 0.

Minmod limiter

$$\phi(\beta^+, \beta^-) = \min \text{mod}(1, \beta^+, \beta^-) \quad (\text{A.12})$$

Superbee limiter

$$\phi(\beta^+, \beta^-) = \max(0, \min(1, 2\beta^-), \min(2, \beta^-)) + \max(0, \min(1, 2\beta^+), \min(2, \beta^+)) - 1 \quad (\text{A.13})$$

van Leer limiter

$$\phi(\beta^+, \beta^-) = \frac{\beta^+ + |\beta^+|^\omega}{1 + |\beta^+|^\omega} + \frac{\beta^- + |\beta^-|^\omega}{1 + |\beta^-|^\omega} - 1 \quad (\text{A.14})$$

when $\omega = 1$. The ratio β^\pm is a measure of the smoothness of the data near x_i . For smooth data $\beta^\pm \approx 1$, and for discontinuity $\beta^\pm \gg 1$.

Woodward limiter

$$\phi(\beta^+, \beta^-) = \max(0, \min(2, 2\beta^+, 2\beta^-, (\beta^+ + \beta^-)/2)) \quad (\text{A.15})$$

where

$$\beta^+ = \frac{\Delta_{i-\frac{1}{2}}}{\Delta_{i+\frac{1}{2}}}, \beta^- = \frac{\Delta_{i+\frac{3}{2}}}{\Delta_{i+\frac{1}{2}}}, \Delta_{i+\frac{1}{2}} = Q_{i+1} - Q_i \quad (\text{A.16})$$

Appendix B

Fourth Order WENO Scheme

For the fourth order WENO scheme, the interpolation candidate stencils include:

$$S_1 = (i, i+1, i+2, i+3) \quad (\text{B.1})$$

$$S_2 = (i-1, i, i+1, i+2) \quad (\text{B.2})$$

$$S_3 = (i-2, i-1, i, i+1) \quad (\text{B.3})$$

$$S_4 = (i-3, i-2, i-1, i) \quad (\text{B.4})$$

The corresponding smoothness indicators are given as:

$$\begin{aligned} \beta_1 = & 2107q_i^2 - 9402q_{i+1}q_i + 7042q_iq_{i+2} - 1854q_iq_{i+3} - 17246q_{i+1}q_{i+2} \\ & - 3882q_{i+2}q_{i+3} + 11003q_{i+1}^2 + 7043q_{i+2}^2 + 547q_{i+3}^2 + 4642q_{i+1}q_{i+3} \end{aligned} \quad (\text{B.5})$$

$$\begin{aligned} \beta_2 = & 267q_{i+2}^2 - 1642q_{i+2}q_{i+1} + 1602q_{i+2}q_i - 494q_{i+2}q_{i-1} - 2522q_iq_{i-1} \\ & + 3443q_i^2 + 547q_{i-1}^2 - 5966q_{i+1}q_i + 2843q_{i+1}^2 + 1922q_{i+1}q_{i-1} \end{aligned} \quad (\text{B.6})$$

$$\begin{aligned} \beta_3 = & 267q_{i-2}^2 - 494q_{i+1}q_{i-2} - 1642q_{i-1}q_{i-2} + 1602q_iq_{i-2} - 5966q_iq_{i-1} \\ & + 3443q_i^2 - 2522q_iq_{i+1} + 2843q_{i-1}^2 + 547q_{i+1}^2 + 1922q_{i+1}q_{i-1} \end{aligned} \quad (\text{B.7})$$

$$\begin{aligned} \beta_4 = & 2107q_i^2 + 7042q_iq_{i-2} - 1854q_iq_{i-3} - 9402q_{i-1}q_i - 17246q_{i-1}q_{i-2} \\ & - 3882q_{i-2}q_{i-3} + 11003q_{i-1}^2 + 7043q_{i-2}^2 + 547q_{i-3}^2 + 4642q_{i-1}q_{i-3} \end{aligned} \quad (\text{B.8})$$

The optimal weights d_i for the left extrapolated value $q_{i+\frac{1}{2}}^l$ at $x_{i+\frac{1}{2}}$ are given by

$$d_1 = \frac{4}{35}, d_2 = \frac{18}{35}, d_3 = \frac{12}{25}, d_4 = \frac{1}{35} \quad (\text{B.9})$$

and the left quantity $q_{i+\frac{1}{2}}^l$ is given by

$$\begin{aligned}
q_{i+\frac{1}{2}}^l &= \omega_1 \left[\frac{1}{4} q_i + \frac{13}{12} q_{i+1} - \frac{5}{12} q_{i+2} + \frac{1}{12} q_{i+3} \right] + \omega_2 \left[-\frac{1}{12} q_{i-1} + \frac{7}{12} q_i + \frac{7}{12} q_{i-1} - \frac{1}{12} q_{i-2} \right] \\
&+ \omega_3 \left[\frac{1}{12} q_{i-2} - \frac{5}{12} q_{i-1} + \frac{13}{12} q_i + \frac{1}{4} q_{i+1} \right] + \omega_4 \left[-\frac{1}{4} q_{i-3} + \frac{13}{12} q_{i-2} - \frac{23}{12} q_{i-1} + \frac{25}{12} q_i \right]
\end{aligned} \tag{B.10}$$

Similarly, the optimal weights d_i for the left extrapolated value $q_{i+\frac{1}{2}}^r$ at $x_{i+\frac{1}{2}}$ are given by

$$d_1 = \frac{1}{35}, d_2 = \frac{12}{25}, d_3 = \frac{18}{35}, d_4 = \frac{4}{35} \tag{B.11}$$

and $q_{i+\frac{1}{2}}^r$ is given by

$$\begin{aligned}
q_{i+\frac{1}{2}}^r &= \omega_1 \left[-\frac{1}{4} q_{i+3} + \frac{13}{12} q_{i+2} - \frac{23}{12} q_{i+1} + \frac{25}{12} q_i \right] + \omega_2 \left[\frac{1}{12} q_{i-2} - \frac{5}{12} q_{i+1} + \frac{13}{12} q_i + \frac{1}{4} q_{i-1} \right] \\
&+ \omega_3 \left[-\frac{1}{12} q_{i+1} + \frac{7}{12} q_i + \frac{7}{12} q_{i-1} - \frac{1}{12} q_{i-2} \right] + \omega_4 \left[\frac{1}{4} q_i + \frac{13}{12} q_{i-1} - \frac{5}{12} q_{i-2} + \frac{1}{12} q_{i-3} \right]
\end{aligned} \tag{B.12}$$

Appendix C

Optimal Weights for WENO Scheme

k	r	J=0	J=1	J=2	J=3	J=4	J=5	J=6
1	-1	1						
	0	1						
2	-1	3/2	-1/2					
	0	1/2	1/2					
	1	-1/2	3/2					
3	-1	11/6	-7/2	1/3				
	0	1/3	5/6	-1/6				
	1	-1/6	5/6	1/3				
	2	1/3	-7/6	11/6				
4	-1	25/12	-23/12	13/12	-1/4			
	0	1/	13/12	-5/12	1/12			
	1	-1/12	7/12	7/12	-1/12			
	2	1/12	-5/12	13/12	1/4			
	3	-1/4	13/12	-23/12	25/12			
5	-1	137/60	163/60	137/60	-21/20	1/5		
	0	1/5	77/60	-43/60	17/60	-1/20		
	1	-1/20	9/20	47/60	-13/60	1/30		
	2	1/30	-13/60	47/60	9/20	-1/20		
	3	-1/20	17/60	-43/60	77/60	1/5		
	4	1/5	-21/20	137/60	-163/60	137/60		
6	-1	49/20	-71/20	79/20	-163/60	-1/6		
	0	1/6	29/20	-21/20	37/60	1/30		
	1	-1/30	11/30	19/20	-23/60	-1/60		
	2	1/60	-2/15	37/60	37/60	1/60		
	3	-1/60	7/60	-23/60	19/20	-1/30		
	4	1/30	-13/60	37/60	-21/20	1/6		
	5	-1/6	31/30	-163/60	79/20	49/20		
7	-1	363/140	-617/140	853/140	-2341/420	667/210	-43/42	1/7
	0	1/7	223/140	-197/140	153/140	-241/420	37/210	-1/42
	1	-1/42	13/42	153/140	-241/420	109/420	-31/420	1/105
	2	1/105	-19/210	107/210	319/420	-101/420	5/84	-1/140
	3	-1/140	5/84	-101/420	13/42	107/210	-19/210	1/105
	4	1/105	-31/420	109/420	-241/420	153/140	13/42	-1/42
	5	-1/42	37/210	-241/420	153/140	-197/140	223/140	1/7
	6	1/7	-43/42	667/210	-2341/420	853/140	-617/140	363/140

References

- 1 Abgrall, R. (2001). “Toward the ultimate conservative scheme: following the quest.” *J. Comput. Phys.*, 167(2), 277-315.
- 2 Abgrall, R. and Mezone, M. (2003). “Construction of second order accurate monotone and stable residual distribution schemes for unsteady flow problems.” *J. Comput. Phys.*, 188(1), 16-55.
- 3 Adams, N.A. (1998). “Direct numerical simulation of turbulent compression corner flow.” *Theor. Comp. Fluid Dyn.*, 12, 109-129.
- 4 Adams, N.A., and Shariff, K. (1996). “A high-resolution hybrid compact-ENO scheme for shock-turbulence interaction problems.” *J. Comput. Phys.*, 127, 27-51.
- 5 Aslam, T.D. (2001). “A level-set algorithm for tracking discontinuities in hyperbolic conservation laws I. Scalar equations.” *J. Comput. Phys.*, 167, 413-438.
- 6 Baeza, A., and Mulet, P. (2004). “Adaptive mesh refinement techniques for high order shock capturing schemes for hyperbolic systems of conservation laws.” GrAN report 04-02.
- 7 Barash, D., and Kimmel, R. (2000). “An accurate operator splitting scheme for nonlinear diffusion filtering.” HP Laboratories, Israel, HPL-2000-48(R.1).
- 8 Beam, R.M., and Warming, R.F. (1978). “An Implicit Factored Scheme for the Incompressible NavierStokes Equations.” *AIAA Journal*, 16, 393-401.
- 9 Berger, R.C., and Stockstill, R.L. (1995). “Finite-element model for high-velocity channels.” *J. Hydraul. Eng.*, 121(10), 710–716.

- 10 Bermúdez, A. and Vázquez, M.E. (1994). “Upwind methods for hyperbolic conservation laws with source terms.” *Comp. & Fluids.*, 23, 1049-1071.
- 11 Billett, S.J., and Toro, E.F. (1997). “On WAF-type schemes for multidimensional hyperbolic conservation laws.” *J. Comput. Phys.*, 130, 1-24.
- 12 Boris, J.P., and Book, D.L. (1973). “Flux correct transport I. SHASTA, a fluid transport algorithm that works.” *J. Comput. Phys.*, 11, 38-69.
- 13 Bradford, S.F., and Sanders, B.F. (2002). “Finite-volume model for shallow water flooding of arbitrary topography.” *J. Hydraul. Eng.*, 128(3), 289-298.
- 14 Cao, Z.X., Pender, G., Wallis, S., and Carling, P. (2004). “Computational dam-break hydraulics over erodible sediment bed.” *J. Hydraul. Eng.*, 130(7), 689-703.
- 15 Chavent, G., and Salzano, G. (1982). “A finite element method for the 1D water flooding problem with gravity.” *J. Comput. Phys.*, 45, 307–344.
- 16 Cockburn, B. and Shu, C.W. (1994). “Nonlinearly stable compact schemes for shock calculation.” *J. Numer. Anal.* 31, 607-627.
- 17 Cockburn, B., and Shu, C.W. (1991). “The Runge–Kutta local projection P1-discontinuous Galerkin finite element method for scalar conservation laws.” *Math. Model. Numer. Anal.*, 25, 337–361.
- 18 Colella, P. (1985). “A direct Eulerian MUSCL scheme for gas dynamics.” *J. Sci. Statist. Comput.*, 6, 104–117.
- 19 Deconinck, H., Struijs, R., Bourgeois, G., and Roe, P.L. (1993). “Compact advection schemes on unstructured meshes.” *Computational Fluid Dynamics, VKI Lecture series 1993-04.*

- 20 Deng, X., and Maekawa, H. (1997). "Compact high-order accurate nonlinear schemes." *J. Comput. Phys.* 130, 77-91.
- 21 Deng, X., and Zhang, H. (2000). "Developing high-order weighted compact nonlinear schemes." *J. Comput. Phys.*, 165, 22-44.
- 22 Deng, X., Liu, X., Mao, M., and Zhang, H. (2005). "Investigation on weighted compact fifth-order nonlinear scheme and applications to complex flow." *17th AIAA Computational Fluid Dynamics Conference*, Toronto, Canada.
- 23 Douglas, J. Jr., and Gunn, J.E. (1964). "A general formulation of alternating direction methods. I. Parabolic and hyperbolic problems." *Numer. Math.*, 6, 428-453.
- 24 Douglas, J. Jr., and Kim, S. (2001). "Improved accuracy for locally one-dimensional methods for parabolic equations." *Math. Mod. Meth. Appl. S.*, 11, 1563-1579.
- 25 Engquist, B., and Osher, S. (1981). "One sided difference approximations for nonlinear conservation laws." *Math. Comput.*, 36(154), 321-351.
- 26 Engquist, B., and Sjögreen, B. (1998). "The convergence of finite difference schemes in the presence of shock." *J. Numer. Anal.*, 35(6), 2464-2485.
- 27 Fennema, R.J., and Chaudhry, H.M. (1987). "Simulation of one-dimensional dam-break flows." *J. Hydraul. Res.*, 25(1), 41-51.
- 28 Fennema, R.J., and Chaudhry, M.H. (1990). "Explicit methods for 2-D transient free-surface flows." *J. Hydraul. Eng.*, 116(8), 1013-1034.
- 29 Fraccarollo, L., and Toro, E.F. (1995). "Experimental and numerical assessment of the shallow water model for two-dimensional dam-break type problems." *J. Hydraul. Res.*, 33(6), 843-864.

- 30 Francesco, M., Morelli, M.A., and Assunta, M. (2003). “Practical aspects in comparing shock-capturing schemes for dam break problems.” *J. Hydraul. Eng.*, 129(3), 187-196.
- 31 Garcia-Navarro, P., and Vazquez-Cendon, M.E. (2000). “On numerical treatment of the source terms in the shallow water equations.” *Comp. & Fluids.*, 29, 951-979.
- 32 Godnov, S. K. (1959). “Finite difference methods for the computation of discontinuous solutions for the equations of fluid dynamics.” *Mat. Sb.*, 47, 271-306.
- 33 Gottardi, G., and Venutelli, M. (2003). “Central schemes for open-channel flow.” *Int. J. Numer. Meth. Fl.*, 41(8), 841 – 861.
- 34 Gottardi, G., and Venutelli, M. (2004). “Central scheme for two-dimensional dam-break flow simulation.” *Adv. Water Resour.*, 27(3), 259-268.
- 35 Grasso, F., and Pirozzoli, S. (2000). “Shock wave - thermal in-homogeneity interactions: analysis and numerical simulations of sound generation.” *Phys. Fluids*, 12 (1), 205–219.
- 36 Harten, A. (1983). “High resolution schemes for hyperbolic conservation laws.” *J. Comput. Phys.*, 49, 357-393.
- 37 Harten, A., Lax, P.D., and van Leer, B. (1983). “On upstream differencing and Godunov-type schemes for hyperbolic conservation laws.” *SIAM Rev.*, 25(1), 35-61.
- 38 Harten, A., Osher, S., Engquist, B., and Chakravarthy, S.R. (1986). “Some results on uniformly high-order accurate essentially nonoscillatory schemes.” *Appl. Numer. Math.*, 2, 347-376.
- 39 Harten, A., Enquist, B., Osher, S., and Chakravarthy, S. (1987). “Uniformly high order essentially non-oscillatory schemes III.” *J. Comput. Phys.*, 71, 231-303.

- 40 Henderson, F.M. (1966). *Open Channel Flow*, Prentice-Hall, New Jersey.
- 41 Hoffman, J.D. (1992). *Numerical Methods for Engineers and Scientists*, McGraw-Hill, Inc.
- 42 Hou, T., and LeFloch, P. (1994). “Why non-conservative schemes converge to the wrong solutions: Error analysis.” *Math. Comput.*, 62, 497-530.
- 43 Hsu, C.T., and Yeh, K.C. (2002). “Iterative explicit simulation of 1D surges and dam-break flows.” *Int. J. Numer. Meth. Fl.*, 38(7), 647-675.
- 44 Hubbard, M.E., and Garcia-Navarro, P. (2000). “Flux difference splitting and the balancing of source terms and flux gradient.” *J. Comput. Phys.*, 165, 89-125.
- 45 Jha, A.K., Akiyama, J., and Ura, M. (1995). “First and second-order flux difference splitting schemes for dam-break problem.” *J. Hydraul. Eng.*, 121(12), 877-884.
- 46 Jha, A.K., Akiyama, J., and Ura, M. (2000). “Flux-difference splitting schemes for 2D flood flows.” *J. Hydraul. Eng.*, 126(1), 33-42.
- 47 Jiang, G.S., and Shu, C.W. (1996). “Efficient implementation of weighted ENO schemes.” *J. Comput. Phys.*, 126, 202-228.
- 48 Jiang, L., Shan, H., and Liu, C. (2001). “Weighted compact schemes for shock capturing,” *Int. J. Comput. Fluid D.*, 15, 147-155.
- 49 Kim, D.H., Cho, Y.S., and Kim, W.G. (2004). “Weighted averaged flux-type scheme for shallow-water equations with fractional step method.” *J. Engr. Mech.*, 130(2), 152-160.
- 50 Lax, P.D., and Wendroff, B. (1960). “Systems of conservation laws.” *Commun. Pur. Appl. Math.*, 13, 217-237.

- 51 Lele, S.K. (1992). "Compact finite difference schemes with spectral-like resolution." *J. Comput. Phys.*, 103, 16-42.
- 52 LeVeque, R.J. (1999). *Numerical methods for conservation laws*, Birkhuser Verlag, Basel.
- 53 LeVeque, R.J. (2002). *Finite volume methods for hyperbolic problems*, Cambridge University Press, Cambridge, England.
- 54 Levy, D., Puppo, G., and Russo, G. (1999). "Central WENO schemes for hyperbolic systems of conservation laws." *Math. Model. Numer. Anal.*, 33 (3), 547-571.
- 55 Levy, D., Puppo, G., and Russo, G. (2002). "A fourth order central WENO scheme for multidimensional hyperbolic systems of conservation laws." *J. Sci. Comput.*, 22, 480-506.
- 56 Li, S.T. (1998). "Adaptive mesh methods and software for time-dependent partial differential equations." Ph.D thesis, University of Minnesota.
- 57 Liu, X.D., Osher, S., and Chan, T. (1994). "Weighted essentially non-oscillatory schemes." *J. Comput. Phys.*, 115, 200-212.
- 58 Mitchell, A.R., and Griffiths, D.F. (1980). *The finite-difference method in partial differential equations*, John Wiley & Sons.
- 59 Nujic, M. (1995). "Efficient implementation of non-oscillatory schemes for the computation of free-surface flows." *J. Hydraul. Res.* 33(1), 101-111.
- 60 Peaceman, D., and Rachford, H. (1955). "The numerical solution for parabolic and elliptic equation." *J. Soc. Ind. Appl. Math.*, 3, 28-41.
- 61 Pirozzoli, S. (2002). "Conservative hybrid compact-WENO schemes for shock turbulence interaction." *J. Comput. Phys.*, 178, 81-117.

- 62 Puppo, G., and Russo, G. (2004). "Staggered finite difference schemes for conservation Laws." (http://calvino.polito.it/ricerca/2004/pdf/36_2004.pdf).
- 63 Qiu, J., and Shu, C.W. (2002). "On the construction, comparison, and local characteristic decomposition for high order central WENO schemes." *J. Comp. Phys.*, 183, 187-209.
- 64 Reed, W.H., and Hill, T.R. (1973). "Triangular mesh methods for the neutron transport equation." Los Alamos Scientific Laboratory Report, LA-UR-73-479.
- 65 Ren, Y.X., Liu, M., and Zhang, H.X. (2003). "A characteristic-wise hybrid compact-WENO scheme for solving hyperbolic conservation laws." *J. Comput Phys.*, 192, 365-386.
- 66 Roe, P.L. (1981). "Approximate Riemann solvers, parameter vectors, and difference schemes." *J. Comput. Phys.*, 43, 357-372.
- 67 Roe, P.L. (1985). "Some contributions to the modeling of discontinuous flows." *Lecture Notes in Applied Mathematics*, 22, 163-193.
- 68 Roe, P.L., and Pike, J. (1984). "Efficient construction and utilization of approximate Riemann solutions." *Comput. Methods Appl. Sci. Engrg.*, 449-518.
- 69 Sanders, B.F. (2001). "High-resolution and non-oscillatory solution of the St. Venant equations in non-rectangular and non-prismatic channels." *J. Hydraul. Res.*, 39(3), 321-330.
- 70 Schwanenberg, D., and Harms, M. (2004). "Discontinuous Galerkin finite-element method for transcritical two-dimensional shallow water flows." *J. Hydraul. Eng.*, 130(5), 412-421.

- 71 Sengupta, T.K., Jain, R., and Dipankar, A. (2005). "A new flux–vector splitting compact finite volume scheme." *J. Comput. Phys.*, 207, 261-281.
- 72 Shu, C.W., and Osher, S. (1988). "Efficient implementation of essentially non-oscillatory shock-capturing schemes." *J. Comput. Phys.*, 77, 439-471.
- 73 Shu, C.W., and Osher, S. (1989). "Efficient implementation of essentially non-oscillatory shock-capturing schemes II." *J. Comput. Phys.*, 83, 32-78.
- 74 Steger, J.L., and Warming, R.F. (1981). "Flux vector splitting of the inviscid gas dynamic equations with application to finite-difference methods." *J. Comput. Phys.*, 40(2), 263-292.
- 75 Stoker, J.J. (1957). *Water waves: the mathematical theory with applications*, Interscience, London.
- 76 Titarev, V.A., and Toro, E.F. (2004). "Finite-volume WENO schemes for three-dimensional conservation laws." *J. Comput. Phys.*, 201, 238-260.
- 77 Tolstykh, A.I., and Lipavskii, M.V. (1998). "On performance of methods with third- and fifth-order compact upwind differencing." *J. Comput. Phys.*, 140, 205-232.
- 78 Toro, E.F., Spruce, M., and Spares, W. (1994). "Restoration of the contact surface in the HLL-Riemann solver." *Shock Waves*, 4(1), 25-34.
- 79 Toro, E.F. (1999). *Riemann solvers and numerical methods for fluid dynamics, a practical introduction*, Springer-Verlag, Berlin, Germany, second edition.
- 80 Toro, E.F. (2001). *Shock-capturing methods for free-surface shallow flows*, Wiley, Chichester, England.
- 81 Tseng, M.H. (1999). "Explicit finite-volume non-oscillatory schemes for 2D transient free-surface flows." *Int. J. Numer. Meth. Fl.*, 30, 831-843.

- 82 Tseng, M.H. (1999). "Verification of 1-D transcritical flow model in channels." *Proceedings of National Science Council, ROC (A) 23 (5)*, 654-664.
- 83 van Leer, B. (1977). "Towards the ultimate conservative difference scheme. IV A new approach to numerical convection." *J. Comput. Phys.*, 23(3), 276-298.
- 84 van Leer, B. (1979). "Towards the ultimate conservative difference scheme V. A second order sequel to Godunov's scheme." *J. Comput. Phys.*, 32,101-136.
- 85 Wang, J.S., He, Y.S., and Ni, H.G. (2003). "Free surface flow in branch channels by a finite-volume TVD scheme." *Adv. Water Resour.*, 26, 623-632.
- 86 Wang, J.W., and Liu, R.X. (2001). "The composite finite-volume method on unstructured meshes for the 2-dimensional shallow-water equations." *Int. J. Numer. Meth. Fl.*, 37(8), 933-949.
- 87 Wang, Z.P. (2002). "An essentially non-oscillatory high order Padé-type (ENO-Padé) scheme." Ph.D dissertation, University of Kentucky.
- 88 Wang, Z.J., and Chen, R.F. (2001). "Optimized weighted essentially non-Oscillatory schemes for computational aeroacoustics." AIAA Paper, 2001-1101.
- 89 Waterways Experiment Station (WES). (1960). "Floods resulting from suddenly breached dams." Miscellaneous Paper No. 2-374, *U.S. Army Corps of Engineers, Rep. 1: Conditions of minimum resistance*, Vicksburg, Miss.
- 90 Weirs, V.G., and Candler, G.V. (1997). "Optimization of weighed ENO schemes for DNS of compressible turbulence." AIAA Paper, 97-1940.
- 91 Wesseling, P. (2000). *Principle of Computational Fluid Dynamics*, Springer.
- 92 Whitham, G. (1974). *Linear and Nonlinear Waves*, Wiley, New York.

- 93 Yang, J.Y., Hsu, C.A., and Chang, S. H. (1993). "Computations of free surface flows part 1: One dimensional dam-break flow." *J. Hydraul. Res.*, 31(1), 19-34.
- 94 Yee, H.C. (1987). "Construction of explicit and implicit symmetric TVD schemes and their applications." *J. Comput Phys.*, 68(1), 151-179.
- 95 Ying, X., Wang, S. SY., and Khan, A.A. (2003). "Numerical simulation of flood inundation due to dam and levee breach." *World Water & Environmental Resources Congress*, ASCE, Philadelphia.
- 96 Yost, S.A., and Rao, P. (1998). "Non-Oscillatory Scheme for Open Channel Flows." *Adv. Water Resour.*, 22(2), 133-143.
- 97 Yost, S.A., and Rao, P. (1999). "Flux Corrected Transport Technique for Open Channel Flow." *Int. J. Numer. Meth. Fl.*, 29, 951-973.
- 98 Zhao, D.H., Shen, H.W., Tabios, G. Q., Lai, J. S., and Tan, W. Y. (1994). "Finite-volume two dimensional unsteady-flow model for river basins." *J. Hydraul. Eng.*, 120(7), 863-882.
- 99 Zhao, D.H., Shen, H.W., Tabios, G.Q., and Lai, J.S. (1996). "Approximate Riemann solvers in FVM for 2D hydraulic shock wave modeling." *J. Hydraul. Eng.*, 122(12), 692-702.
- 100 Zhuang, M., and Cheng, R.F. (1998). "Optimized upwind dispersion-relation-preserving finite difference schemes for computational aeroacoustics." *AIAA Journal*, 36(11), 2146-2148.
- 101 Zoppou, C., and Roberts, S. (1999). "Catastrophic collapse of water-supply reservoirs in urban areas." *J. Hydraul. Eng.*, 125(7), 686-695.
- 102 Zoppou, C., and Roberts, S. (2003). "Explicit schemes for dam-break simulations." *J.*

Hydraul. Eng., 129(11), 11–34.

Vita

Chunfang Chen

Date of Birth: 05/09/1974

Place of Birth: Tianjin, P. R. China

Education

Ph.D. Civil Engineering, University of Kentucky, KY, expected, 2006

M.S. Civil Engineering, University of Kentucky, KY, 2004

M.S. Civil Engineering, Tianjin University, P.R. China, 2000

B.S. Civil Engineering, Tianjin University, P.R. China, 1997

B.S. Engineering Management, Tianjin University, P.R. China, 1997

Professional Experience

Research Associate, Center for Louisiana Inland Water Studies, Civil Engineering, University of Louisiana at Lafayette, 05/2005-present

Research and Teaching Assistant, Civil Engineering, University of Kentucky, 08/2000-05/2005

Research Assistant, Civil Engineering, Tianjin University, China, 09/1997-03/2000

Publications

Meselhe, E., Griborio, A., Chen, C., McCorquodale, J. A., and Stronach, J. (2005). "Multi-dimensional modeling of the Lower Mississippi River." *The proceedings of 9th International Conference on Estuarine and Coastal Modeling*, ASCE, Charleston, SC (to appear).

Chen, C., and Yost, S.A. (2005). "An Algebraic Multigrid (AMG) Strategy for Convection-Diffusion Equations." *The proceedings of the Conference on Mechanics and Materials*, ASME/ASCE/SES, Baton Rouge, LA.

Chen, C., Yost, S.A., and Kim, S. (2004). "PADE-ENO-CN Scheme for One-Dimensional Open Channel Flow." *The proceedings of 17th Engineering Mechanics Conference*, ASCE, Delaware, DE.

Chen, C., and Yost, S.A. (2003), "CN-PADE-ENO Shock Capturing Scheme for 1-D Hyperbolic Equation." *The proceedings of 16th Engineering Mechanics Conference*, ASCE, Seattle, WA.

Chen, C., Yost, S.A., and Shao, Z. (2003). "High Performance Programming of the 3-D Finite Element Hydrodynamic Model – QUODDY." *The proceedings of 8th International Conference on Estuarine and Coastal Modeling*, ASCE, Monterey, CA.

Chen, C., Zhao, X. (2000), *Study on Water Distribution Network Reliability*, China Water & Wastewater, Vol.16, No.1.

Zhang, H., Tan, X., and Chen, C. (1999). "Research on Optimal Operation of Water Treatment System." *Transaction of Tianjin University*, Vol.4, No.10.

Honors and Awards

Oliver H. Raymond Fellowship, University of Kentucky, 2000-2005

Graduate travel support, the 17th Engineering Mechanics Conference, ASCE, DE, 2004

Finalist, Provost's Awards for Outstanding Teaching, University of Kentucky, 2004

First Prize, Scholarship of Outstanding Undergraduates, Tianjin University, China, 1994 & 1996

First Prize, Kechang Wang Scholarship, Tianjin University, China, 1995

First Prize, Scholarship of Outstanding Graduates, Tianjin University, China, 1998-1999

Professional Activities

Member, American Society of Civil Engineer (ASCE)

Reviewer, Journal of Hydraulic Research, the International Association of Hydraulic Research (IAHR), 2005